Technische Universität Berlin
Fakultät I - Geisteswissenschaften
Fachgebiet Audiokommunikation und -technologie

Master of Science

Analytical and numerical approaches for optimising the curving of touring line source arrays

David Albanés Bonillo
[redacted]

Advisors:
Prof. Dr. Stefan Weinzierl
Dipl.-Ing. Florian Straube

December 2017

Zusammenfassung

Line Source Arrays (LSAs) werden zur Beschallung großer Publikumsflächen eingesetzt und zielen auf die Synthese von homogenen Schallfeldern im gesamten hörbaren Frequenzbereich ab. Die verwendeten Lautsprecherboxen werden mit unterschiedlichen Neigungswinkeln positioniert und / oder elektronisch gesteuert, um die beabsichtigte Abdeckung der Zuschauerzonen zu gewährleisten und Abstrahlung in Richtung Decken, reflektierenden Wänden oder Wohnbereichen zu vermeiden. Diese Masterarbeit zielt darauf ab, einen bestehenden analytischen Optimierungsansatz in Übereinstimmung mit den Beschränkungen kommerziell verfügbarer Line-Source-Array-Systeme für diskrete Neigungswinkel nach dem Stand der Technik anzupassen. Eine Untersuchung verschiedener kommerziell erhältlicher LSA-Systeme wird durchgeführt, um einen geeigneten Satz von Winkeln zu bestimmen, die als Optimierungsziele verwendet werden können, gefolgt von der Diskretisierung der resultierenden Neigungswinkel des Algorithmus. Als ein alternativer Ansatz wird eine numerische Optimierung basierend auf der Goal-Attainment-Methode auf die Neigungswinkel angewendet. Die Ergebnisse der verschiedenen Optimierungsansätze werden mit Hilfe von technischen Qualitätsmaßnahmen verglichen.

Abstract

Line Source Arrays (LSAs) are used for large-scale sound reinforcement aiming at the synthesis of homogenous sound fields for the whole audio bandwidth. The deployed loudspeaker cabinets are rigged with different tilt angles and/or electronically controlled to provide the intended coverage of the audience zones and to avoid radiation towards the ceiling, reflective walls or residential areas. This thesis intends to adapt an existing analytical optimisation approach for sets of discrete tilt angles in accordance to the restrictions of commercially available state of the art Line Source Array (LSA) systems. A research into various commercially available LSA systems will be carried out to determine a suitable set of angles to use as optimisation targets, followed by the discretisation of the algorithm's resulting tilt angles. As an alternative approach, a numerical optimisation based on the goal attainment method will be applied to the tilt angles. The results of the different optimisation approaches will be compared with the help of technical quality measures.

Contents

List of Figures

List of Tables

Fakultät |
Geisteswissenschaften

Prüfungsausschüsse

Studiendekan und Vorsitzender

Prof. Dr. Friedrich Steinle

Eidesstattliche Erklärung

Ist jeder an der TU Berlin verfassten schriftlichen Arbeit eigenhändig unterzeichnet beizufügen!

Hiermit erkläre ich an Eides statt gegenüber der Fakultät I der Technischen Universität Berlin, dass die vorliegende, dieser Erklärung angefügte Arbeit selbstständig und nur unter Zuhilfenahme der im Literaturverzeichnis genannten Quellen und Hilfsmittel angefertigt wurde. Alle Stellen der Arbeit, die anderen Werken dem Wortlaut oder dem Sinn nach entnommen wurden, sind kenntlich gemacht. Ich reiche die Arbeit erstmals als Prüfungsleistung ein. Ich versichere, dass diese Arbeit oder wesentliche Teile dieser Arbeit nicht bereits dem Leistungserwerb in einer anderen Lehrveranstaltung zugrunde lagen.

Titel der schriftlichen Arbeit

VerfasserIn/VerfasserInnen*

Name Vorname Matr.-Nr.

Betreuende/r DozentIn

Name Vorname

Mit meiner Unterschrift bestätige ich, dass ich über fachübliche Zitierregeln unterrichtet worden bin und verstanden habe. Die im betroffenen Fachgebiet üblichen Zitiervorschriften sind eingehalten worden.

Eine Überprüfung der Arbeit auf Plagiate mithilfe elektronischer Hilfsmittel darf vorgenommen werden.

Ort, Datum Unterschrift**

*Bei Gruppenarbeiten sind die Unterschriften aller VerfasserInnen erforderlich.
**Durch die Unterschrift bürgen Sie für den vollumfänglichen Inhalt der Endversion dieser schriftlichen Arbeit.

1 Introduction

1.1 Line Source Array systems

Loudspeaker arrays, especially line arrays, have found widespread use in both sound system installations as well as live sound applications. Their ability to focus and to direct sound at a much higher level than available with conventional sources allows, e.g., for more homogeneous sound fields, increased speech intelligibility in acoustically difficult spaces and higher SPL in open-air scenarios where long distances must be covered. Due to the complexity of this technology and the challenges of configuring line arrays properly, the use of prediction tools such as EASE Software or CAPS Aiming Software has become a standard approach in planning and commissioning portable line arrays as well as digitally steered column loudspeakers. Increasingly, acoustic modelling tools offer optimisation functions in order to shape the radiated sound field based on the requirements given by the user instead of a time-consuming trial-and-error approach. The two most popular approaches to shape the sound field of line source arrays are the optimisation of the curving i.e. the tilt angles between cabinets (Thompson, 2006), and the optimisation of the driving functions for the loudspeakers, also known as electronic control (van Beuningen, 2000; Thompson, 2009; Feistel et al., 2013). In order to set up such a system, the operator relies upon pre-calculated and in situ configuration data compiled using the manufacturer's unique and proprietary processes, as well as adjusting the pre-EQ, high pass filtering, array gain, etc.

The curving and electronic control of line arrays for improved sound reinforcement for large audience surfaces lacks a standard procedure. Both pure geometric and pure electronic wave front shaping as well as combinations thereof are realised. As the process for mixed geometric-electronic optimisations typically starts with the LSA curving, the numerical optimisation is preceded by the optimisation of the cabinet tilt angles. This could be taken as a primary stage for the optimisation of the loudspeakers driving functions, i.e. for the calculation of the FIR filter coefficients, or could also be applied for uniformly driven line arrays without further computation. The geometric optimisation takes several factors into account, such as the LSA setup, venue geometry and curving scheme, which can be numerically or analytically optimised. There are several approaches for the optimisation of LSA tilt angles based on numerical (Thompson, 2006; Thompson, 2008) as well as analytical methods (Straube et al. 2017). These algorithms result in a series of tilt angles that provide the desired sound field.

Unfortunately, due to structural reasons, there is a limited number of realisable tilt angles for most LSA cabinets, the value of which depends on the brand of the system used. In this thesis, an analysis of the tilt angles used by several different commercially available state of the art LSA systems will be presented, followed by an adaptation of the PALC algorithm used by Straube et al. (2017) to generate the best possible set of tilt angles including the possibility of applying the multi objective goal-attainment method, first described by Gembicki et al. (1975), for the optimisation of the tilt angles.

1.2 State of the art

Scheirman, D. (2015) presents a comprehensive analysis of the advancements carried out in the field of large scale loudspeaker arrays throughout the years until the present. For example, during the 1980's, as portable large-scale sound reinforcement systems became more powerful and prevalent, they were considered to be more useful if the directivity was electronically adjustable by varying the signals applied to its discrete elements. Meyer, D. (1982) observed that the directivity of an array of loudspeakers could be controlled digitally by means of varying the amplitude and group delay as a function of frequency, and varying the gain of the composite elemental signal. Already in 1994 at the AES 13th Conference (Computer-Controlled Sound Systems) a hypothetical future "smart" loudspeaker array system was discussed. This loudspeaker array system would require advances in different areas of research and development such as control network, digital audio transport and software user interface. In order to design such a system, developers should understand how groups of multiple identical enclosures perform when assembled into large-scale arrays, as well as having purpose-built on-board electronic modules available for processing and feeding power to each transducer. He identifies three basic system electronics formats for the assembly of LSAs which are still in use today: traditional with centralised DSP, networked intelligent amplifiers driving passive loudspeakers, and DSP-enabled powered loudspeakers. The latter systems are best equipped for the most intuitive control and acoustical performance resolution, due to the electronics' close proximity to the individual transducers. Also at the AES 13th Conference, Forsythe, K. et al. (1994) introduced the "beam steering" technique within individual enclosures, by means of applying differing amounts of delay to drivers covering the same frequencies. The interaction of these signals allow variances of coverage angle and major axis of the output of the device.

The creation of system-specific algorithms broadened the horizon in terms of sound field control. Based upon actual LSA measurements and then modified and incrementally improved from data gathered during field operation, adaptive algorithms can be applied to all types of filter circuits useful in audio circuit applications (Avalos, J. et al., 2011).

Scheirman, D. (2015) writes as a conclusion to his analysis of the history of LSA research: "Over the past years, the ever-increasing power of digital signal processing has resulted in on-board electronics suitable for use in highly sophisticated loudspeaker arrays with venue-adaptive control and configuration elements. Along with modular amplification, computer control and networked audio technologies, this now enables the design and use of "smart" loudspeaker arrays, designed to self-configure for each acoustic environment in which they are used. With discrete enclosures able to alter their electroacoustical output in coordination with other identical, adjacent modules in the array, a new discipline of speaker array design that incorporates electronic beam-steering has been established for top-tier use in professional portable system deployments".

Keele, D.B. (2000) applies the broadband Constant Bandwidth Transducer (CBT) theory, originally applied to underwater transducers by the military, in order to improve the sound field uniformity and directivity of LSAs. Here, the transducer is a continuous Legendre-shaded spherical cap and the applied Legendre shading is independent of frequency. The CBT provides nearly perfect polar behaviour with extremely low side-lobes and constant directivity over a very wide frequency range above a certain cutoff frequency. In Keele, D.B. (2002) he describes a method of designing CBT systems that are based on straight-line and flat-surface array configurations, rather than the required circular arcs and curved surfaces. This is achieved by means of processing each channel with different signal delays and power amplifiers.

The directional characteristics of the J and progressive LSA systems are analysed

in Ureda, M.S. (2001) by derivation of their directivity functions and polar responses. Other types of spiral arrays are proposed in this publication, for instance a geometric rate of curvature instead of the arithmetic spiral presented. This analysis is more thoroughly carried out in Ureda, M.S. (2004), where in-depth mathematical models are provided to estimate the polar response, on-axis pressure response, and pressure fields of straight, curved (arc), J, and progressive LSAs. In this paper, Ureda, M.S. proves how J and progressive LSAs have asymmetrical polar responses in the vertical plane, which is useful in many venues. Furthermore he shows how progressive arrays produce vertical polar response that is exceptionally constant with frequency over a very wide bandwidth. He also provides a model showing the effect of gaps in LSAs introduced by the thickness of the loudspeaker enclosure construction material, proving that at high frequencies the side-lobe structure changes materially with the gap length. Finally, modelled results are compared to measured polar response data for two different LSAs, showing that the models produce very good estimates of actual performance for a wide variety of array types across an extended frequency range of interest.
Studies such as Feistel et al. (2013) show how based on acoustic simulation, numerical optimisation of the LSA configuration, particularly of FIR filters, achieves substantial improvements in sound field uniformity and output SPL adding a new level of flexibility. New radiation characteristics can be established, which improve sound field homogeneity and output SPL. Feistel tackles the spatial resolution of driven sources, the number of FIR coefficients and the quality of loudspeaker data by presenting real-world case studies based on measurements and simulations.

To this day, many LSA systems with computer control, network connectivity, a comprehensive software user interface, and beam steering capabilities are commercially available. Each one of these systems can alter its directivity (and therefore its coverage pattern) by electronic means. Some achieve this through a combination of variable inter-cabinet splay angles and beam steering once the array is mechanically configured. Others do so through purely electronic means, without adjusting the individual loudspeaker cabinets. In one of the first attempts to automatise the optimisation of LSA splay angles, Thompson (2006) proposes a pattern search algorithm as described in Audet, C. et al. (2000) and Dennis, J.E. et al. (1994), which uses the target SPL along the audience plane section as objective function for the algorithm, i.e. a measure of performance. A target shape is set by choosing a "mix" position and the levels relative to this position at the extremes of coverage on the Polygonal Audience Line (PAL). Between each extreme point and the mix position the target pressure has a constant gradient, typically dropping progressively in amplitude with increasing distance from the array. The major setback of this method is the radiation model, only reliable at frequencies between 200 Hz and 12,5 kHz. This is improved in Thompson (2008), including complex transfer functions as targets in the optimisation algorithm, which improve the control of the response throughout the audience. Thompson introduces here a software solution in the form of a Java application using an exported library of MATLAB functions, which would later become Martin Audio's Display software. This method offers good results over a wide bandwidth, with the disadvantages of adding a high computational load and once again not taking into account environmental factors like wind or temperature gradients. Other manufacturers have also developed commercially available software based on algorithms applied to both LSA tilt angle and FIR filter optimisation, e.g., d&b's ArrayCalc, AFMG's FIRmaker or EAW's Resolution 2. The specific algorithms used by these software applications remain undocumented by the manufacturers.

Further studies like Feistel et al. (2013) and Thompson et al. (2011) focus more on electronic beam steering by means of a numerical optimisation of the loudspeakers' driving functions. These studies do not go into detail as in how a certain target output in the audience is achieved, for example a constant SPL or a level gradient along the

audience line, as it would naturally occur when increasing the distance of the source.

The Polygonal Audience Line Curving algorithm by Straube et al. (2017) offers an analytical approach for the optimisation of LSA tilt angles based on the geometry of the receiver area and the intended coverage, aiming at improved sound field homogeneity and target-oriented radiation. This algorithm proves to be faster and more efficient than the numerical approaches. The resulting tilt angles take an infinite number of values that make them unsuitable in terms of its application to commercially available LSAs, which due to structural reasons, only accept a limited amount of discrete tilt angles. Therefore, a research into the splay angles used by standard, commercially available LSAs and the extension of the algorithm to seek only among this set of angles becomes relevant and will be tackled in this thesis.

2 PALC algorithm

2.1 Requirements

The Polygonal Audience Line Curving algorithm can be used with different objectives, such as a constant interaction between adjacent cabinets with respect to the receiver geometry or by additionally considering amplitude attenuation. Acoustic simulations based on the complex-directivity point source (CDPS) model (van Beuningen, 2000, 10-12) including far-field radiation patterns of baffled line and circular pistons provide the data for an evaluation of the introduced approach. In this thesis, four different LSA systems are analysed for four concert venues. The analytical optimisation of the tilt angles used by this algorithm is tackled in the following subsections.

2.2 Calculation model

When modelling multi-way cabinets, the total sound pressure is composed of the sound pressures of the different frequency bands, i.e.

$$P(m,\omega) = P_{\mathrm{LF}}(m,\omega) + P_{\mathrm{MF}}(m,\omega) + P_{\mathrm{HF}}(m,\omega). \tag{1}$$

Since the calculations are performed separately for each frequency band with a subsequent summation, the frequency band indices (LF, MF, HF) are omitted for generalisation in the following equations. The sound field prediction is based on a CDPS model of baffled piston far-field radiation patterns. Its fundamental equation [Meyer, D.G. (1984), Eq. (5)], [van Beuningen et al., Eq. (3-5)], [Meyer, P. (2003), Sec. 1.1], [Feistel et al. (2009), Eq. (11)] reads

$$P(m,\omega) = \sum_{i=1}^{LN} G(m,i,\omega) D(i,\omega). \tag{2}$$

$P(m,\omega)$ denotes the sound pressure spectrum at the receiver position $\mathbf{x_m}$ with $[P(m,\omega)] = 1\,\mathrm{Pa/Hz}$. $G(m,i,\omega)$ terms the acoustic transfer function (ATF) from the i-th source to the m-th receiver position. The complex driving function spectrum $D(i,\omega)$ with $[D(i,\omega)] = 1\,\mathrm{Pa/Hz}$ of the i-th source is directly proportional to the source's velocity spectrum.

Eq. (2) is modified including a loudspeaker sensitivity standardisation in order to obtain realistic absolute sound pressure levels (SPLs). Therefore $G(m,i,\omega)$ is considered as a scaled ATF

$$G(m,i,\omega) = H_{\mathrm{post}}(\beta(m,i),\omega) \cdot \frac{e^{-\mathrm{j}\frac{\omega}{c}|\mathbf{x_m}-\mathbf{x_{0,i}}|}}{(\frac{|\mathbf{x_m}-\mathbf{x_{0,i}}|}{\mathrm{m}})} \cdot (\frac{p_0}{\mathrm{Pa}}) \cdot 10^{\frac{1}{20}\left(\frac{S_{\mathrm{dB}}(i,\omega)}{\mathrm{dB_{\frac{SPL\,m}{W}}}}\right)} \tag{3}$$

being composed of a specific far-field radiation pattern $H_{\mathrm{post}}(\beta(m,i),\omega)$, the 4π-discarded free-field 3D Green's function $\frac{e^{-\mathrm{j}\frac{\omega}{c}|\mathbf{x_m}-\mathbf{x_{0,i}}|}}{|\mathbf{x_m}-\mathbf{x_{0,i}}|}$ (i.e the ideal point source), the reference sound pressure p_0 that commonly amounts to $2 \cdot 10^{-5}$ Pa in air, and the loudspeaker sensitivity $S_{\mathrm{dB}}(i,\omega)$ specifying the SPL in 1 m distance for an electrical input power of 1 W. The sensitivity is assumed to be constant for all drivers and all frequencies per frequency band, i.e. $S_{\mathrm{dB}}(i,\omega) = S_{\mathrm{dB}}$. The driving function $D(i,\omega)$ consists of the signal input spectrum $D_{\mathrm{in}}(i,\omega)$ with $[D_{\mathrm{in}}(i,\omega)] = 1\,\mathrm{Pa/Hz}$, the complex optimised filter $D_{\mathrm{opt}}(i,\omega)$ with $[D_{\mathrm{opt}}(i,\omega)] = 1$ and the complex frequency band crossover as well as high-/lowpass filter $D_{\mathrm{xo}}(\omega)$ with $[D_{\mathrm{xo}}(\omega)] = 1$, thus

$$D(i,\omega) = D_{\mathrm{in}}(i.\omega) D_{\mathrm{opt}}(i,\omega) D_{\mathrm{xo}}(\omega). \tag{4}$$

As this thesis is exclusively focused on the curving of the LSA cabinets, only uniformly driven sources are considered, i.e.

$$D_{\mathrm{opt}}(i,\omega) = 1 \qquad \forall i \text{ and } \forall \omega. \tag{5}$$

The far-field radiation pattern of the baffled circular piston with a constant surface velocity is [Skudrzyk, E. (1971), Eq. (26.42)]

$$H_{\mathrm{post,circ}}(\beta,\omega) = \frac{2J_1(\frac{\omega}{c}R\sin\beta)}{\frac{\omega}{c}R\sin\beta}, \tag{6}$$

denoting the cylindrical Bessel function of 1st kind of 1st order as $J_1(\cdot)$ [Olver, F.W.J. et al., Eq. (10.2.2)]. The line piston models an ideal waveguide for the HF band and its far-field radiation pattern can be written as [Skudrzyk, E. (1971), Eq. (26.44)]

$$H_{\mathrm{post,line}}(\beta,\omega) = \frac{\sin(\frac{\omega}{c}\frac{\Lambda_y}{2}\sin\beta)}{\frac{\omega}{c}\frac{\Lambda_y}{2}\sin\beta}. \tag{7}$$

Note that these patterns exhibit main lobe unity gain (i.e. 0 dB for $\beta = 0$) in order to control the energy radiated by the pistons via the assumed sensitivities. In line with this modelling, air absorption is neglected, a constant velocity of sound ($c = 343$ m/s) and for the modelled sources infinite, straight baffles and a constant surface velocity are assumed. The sound field predictions are performed for a logarithmically spaced frequency vector with $f_{\mathrm{start}} = 200$ Hz, $f_{\mathrm{stop}} = 20$ kHz and $1/36$ octave resolution.

2.3 Geometric setup

Fig. 1 represents the PAL with K sections $[k = 0, 1, 2, ..., K]$. These line sections are covered by N LSA cabinets with $n = 1, 2, ..., N$. The polygonal audience line is therefore divided into N segments that represent the main radiation area of the LSA cabinets. Γ_n denotes the length of the n-th segment with the distance $\Gamma_{n,1}$ from the top to the centre position and $\Gamma_{n,2}$ from the centre to the bottom position of the segment, i.e. $\Gamma_n = \Gamma_{n,1} + \Gamma_{n,2}$. the total length of the covered audience line sections can be concluded from

$$\Gamma = \sum_{n=1}^{n=N} \Gamma_n. \tag{8}$$

The positioning of the cabinets will consider the distances of the different positions from the sources and the desired sound field. Thus, the product of the coverage angles ψ_n and the distances from the source to the receiver positions must be constant. It seems to be reasonable to either specify the coverage angles ψ_n and to modify the number of the applied LSA cabinets depending on the covered length Γ of the polygonal audience line or to specify the actual length Γ and to determine the appropriate (constant) coverage angles ψ_n. Note that for the tilt angles of commercially available LSAs only discrete values can typically be set. This analytical approach will be further improved by adding weights for the different audience positions according to the distance and the desired sound field. The different audience areas are indexed from the bottommost/nearest to the topmost/ farthest audience positions. In order to compute the position and the tilt (γ_n) of each LSA cabinet, it is necessary to start with the uppermost cabinet and compute iteratively from top to bottom.

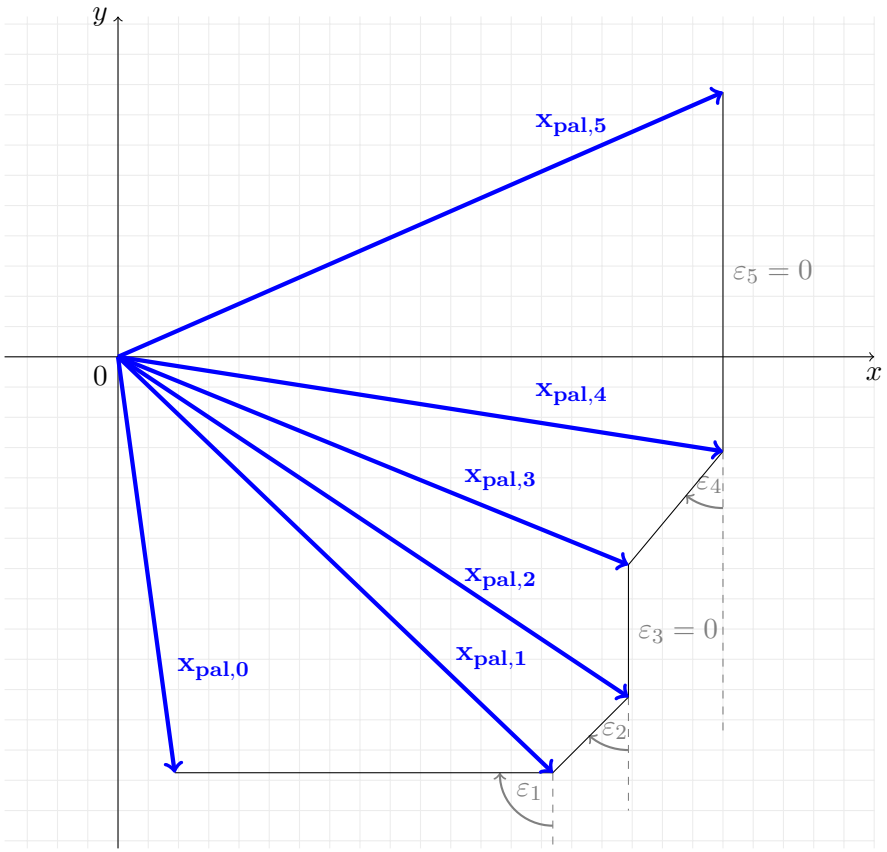

Figure 1: PAL with K sections (in this case: $K = 5$). The start position of the k-th line section is specified by the vector $\mathbf{x_{pal,k-1}}$ and the stop position is given by the vector $\mathbf{x_{pal,k}}$. ε_k denotes the tilt angle of the k-th line section.

2.4 LSA setup

The LSA setup and the geometry under discussion is schematically depicted in Fig. 2. A total number of $N = 16$ LSA cabinets with $n = 1, 2, ..., N$ is used. The front grille's height $\Lambda_{y,\mathrm{LSA}}$ of a single LSA cabinet is set to 0.372 m resulting in an overall LSA length of ca. 5.96 m. The front grille top and bottom coordinates $(x_\mathrm{t}, y_\mathrm{t})$ and $(x_\mathrm{b}, y_\mathrm{b})$ respectively of the individual cabinets are given as

$$\begin{pmatrix} x_{\mathrm{t},n} \\ y_{\mathrm{t},n} \end{pmatrix} = \begin{pmatrix} x_\mathrm{H} \\ y_\mathrm{H} \end{pmatrix} - \sum_{\mu=1}^{\mu=n-1} \Lambda_{y,\mathrm{LSA}} \begin{pmatrix} \sin\gamma_\mu \\ \cos\gamma_\mu \end{pmatrix} \tag{9}$$

$$\begin{pmatrix} x_{\mathrm{b},n} \\ y_{\mathrm{b},n} \end{pmatrix} = \begin{pmatrix} x_\mathrm{H} \\ y_\mathrm{H} \end{pmatrix} - \sum_{\mu=1}^{\mu=n} \Lambda_{y,\mathrm{LSA}} \begin{pmatrix} \sin\gamma_\mu \\ \cos\gamma_\mu \end{pmatrix} \tag{10}$$

using x_H and y_H as the initial front grille top position of the top LSA cabinet ($n = 1$) and the individual tilting angles γ_n. Detailed information on the geometric configuration can be found in Straube et al. (2015a) and Straube et al. (2015b).

The LSA is built from multi-way cabinets, each modelled with L_LF, L_MF, L_HF vertically stacked, individually controlled drivers for the low, mid and high frequency band (LF, MF, HF). With (9) and (10) the front grille centre position of the i-th LSA driver is given as

$$\mathbf{x_{0,i}} = \begin{pmatrix} x_{0,i} \\ y_{0,i} \end{pmatrix} = \begin{pmatrix} x_{\mathrm{t},n} \\ y_{\mathrm{t},n} \end{pmatrix} + \frac{l - 0.5}{L} \begin{pmatrix} x_{\mathrm{b},n} - x_{\mathrm{t},n} \\ y_{\mathrm{b},n} - y_{\mathrm{t},n} \end{pmatrix}, \tag{11}$$

using $l = 1, 2, ..., L$ and $i = (n-1) \cdot L + l$ for $L = \{L_\mathrm{LF}, L_\mathrm{MF}, L_\mathrm{HF}\}$ with respect to the different frequency bands.

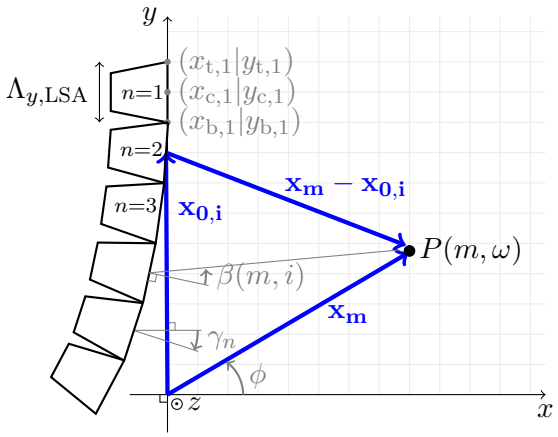

Figure 2: Sketch of the LSA setup under discussion. A total of N LSA cabinets of the height $\Lambda_{y,\mathrm{LSA}}$ is used.

The Active Radiating Factor (ARF) is used to specify the piston dimensions – i.e. the circular piston radius R and the line piston length Λ_y – related to the fixed distance between adjacent piston centres

$$\Delta y = \frac{\Lambda_{y,\mathrm{LSA}}}{L}. \tag{12}$$

The ARF of a line piston reads

$$\mathrm{ARF}_{\mathrm{line}} = \alpha = \frac{\Lambda_y}{\Delta y} \qquad 0 \leq \alpha \leq 1, \tag{13}$$

and the ARF for a circular piston can be written as

$$\mathrm{ARF}_{\mathrm{circ}} = \frac{\pi}{4}\,\alpha^2 = \frac{\pi}{4}\left(\frac{2R}{\Delta y}\right)^2 \qquad 0 \leq \alpha \leq 1. \tag{14}$$

Note that $\mathrm{ARF}_{\mathrm{circ}}$ is in fact a ratio of surface areas ($\mathrm{ARF}_{\mathrm{circ}} \neq \alpha$), whereas a ratio of line lengths is defined for the line piston ($\mathrm{ARF}_{\mathrm{line}} = \alpha$). Different LSA systems in the market use different amounts of pistons for each cabinet with different circular piston radiuses and line piston lengths. Furthermore, the distance between adjacent piston centres also varies, thus the value of these ARFs are subject to variation.

2.5 Venue geometry

Two multi-stand arenas, one of them taken from Thompson et al. (2011, Sec. 6.1), one open-air amphitheater as presented by Schultz, F. (2016, Sec. 4.2.2) and a simple outdoor audience surface with audience and non-audience sections, i.e. zones to be covered and zones to be avoided, are modelled by two dimensional slice representations. The first multi-stand arena slice representation consists of four audience lines with different tilt angles, the second multi-stand arena resembles the new Calderón football stadium in Madrid and consists of six audience lines with different tilt angles. Both of these venues typify a rather complex source-receiver configuration. The open-air amphitheater resembles the Waldbuehne in Berlin and is composed of two audience lines with different tilt angles for the sake of simplicity. The second outdoor venue consists of one horizontal audience line only and resembles a generic outdoor music festival situation. Both of these venues conform to extreme long-throw applications. In this thesis, near-fills, side-fills and delayed arrays that are routine in practical realisations are not considered. Only the xy-plane is considered for vertical radiation,

cf. Fig. 7. This is a common approach for optimisation schemes of the loudspeakers driving functions as the horizontal radiation is assumed to be convenient anyway.

There are $M_{\mathrm{v1}} = 297$, $M_{\mathrm{v2}} = 466$, $M_{\mathrm{v3}} = 402$ and $M_{\mathrm{v4}} = 397$ receiver positions of which $m = 1, 2, ..., M$ are taken into account for venues 1 to 4 respectively. This corresponds to a distance of 0.5 m between the receiver positions. The receiver positions are composed of M_{a} audience positions from the set $\mathscr{M}_{\mathrm{a}}$ and M_{na} non-audience positions from the set $\mathscr{M}_{\mathrm{na}}$ with $M = M_{\mathrm{a}} + M_{\mathrm{na}}$. They are characterised by the position vectors $\mathbf{x_m} = (x_m, y_m, 0)^{\mathrm{T}}$ and are numbered counterclockwise starting from the position under the LSA that is closest to the LSA (index 1, cf. Fig. 7). The venue slice coordinates are documented in Tab. 3 to 6 for venues 1 to 4 in the Appendix.

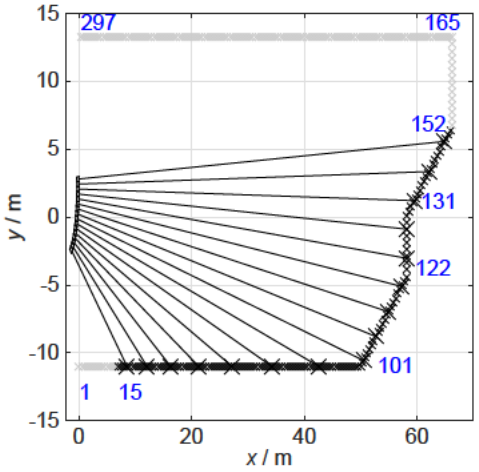

Figure 3: Venue 1

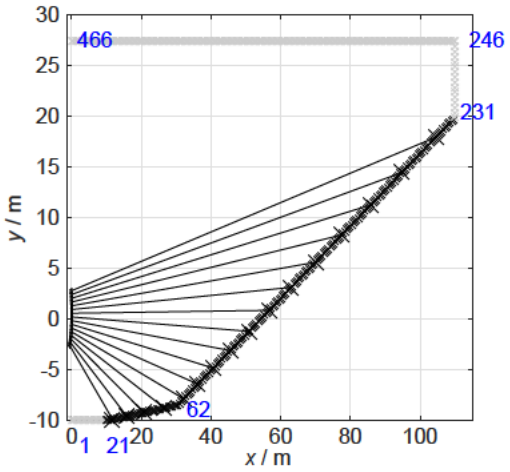

Figure 4: Venue 2

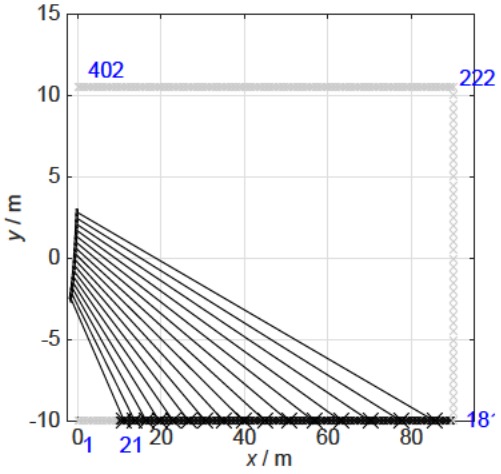

Figure 5: Venue 3

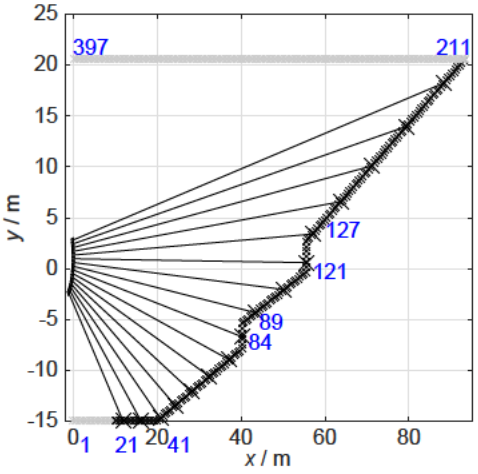

Figure 6: Venue 4

Figure 7: Venue slices within the xy-plane with audience (black) as well as non-audience/avoid (gray) zones and selected index numbers (change of audience/avoid zone and/or polygonal line's segment angle) from M receiver positions

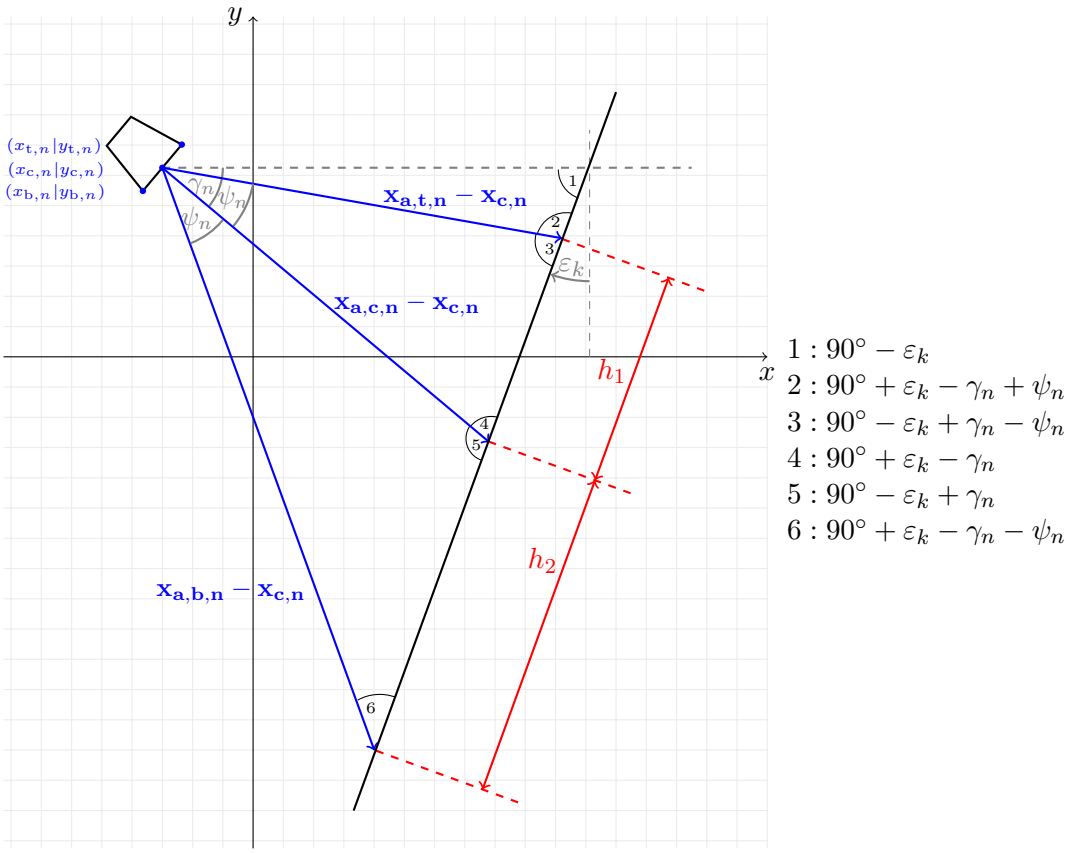

Figure 8: Sketch of one section of the polygonal audience line with the n-th segment including only one section. The line section is not changed.

2.6 One section in Polygonal Audience Line

The length h_1 can be geometrically calculated by, cf. Fig. 8,

$$h_1 = |\mathbf{x_{a,t,n}} - \mathbf{x_{c,n}}| \frac{\sin\psi_n}{\sin(90° + \varepsilon_k - \gamma_n)} = |\mathbf{x_{a,t,n}} - \mathbf{x_{c,n}}| \frac{\sin\psi_n}{\cos(\varepsilon_k - \gamma_n)}. \tag{15}$$

The centre position of the current segment is therefore

$$\mathbf{x_{a,c,n}} = \mathbf{x_{a,t,n}} + h_1 \begin{pmatrix} \cos\varepsilon_k \\ \sin\varepsilon_k \end{pmatrix} \tag{16}$$

and hence the segment's half length

$$\Gamma_{n,1} = h_1. \tag{17}$$

h_2 can be written as

$$h_2 = |\mathbf{x_{a,c,n}} - \mathbf{x_{c,n}}| \frac{\sin\psi_n}{\sin(90° + \varepsilon_k - \gamma_n - \psi_n)} = |\mathbf{x_{a,c,n}} - \mathbf{x_{c,n}}| \frac{\sin\psi_n}{\cos(\varepsilon_k - \gamma_n - \psi_n)}. \tag{18}$$

The bottom position of the current segment is therefore

$$\mathbf{x_{a,b,n}} = \mathbf{x_{a,c,n}} + h_2 \begin{pmatrix} \cos\varepsilon_k \\ \sin\varepsilon_k \end{pmatrix} \tag{19}$$

and hence the segment's half length

$$\Gamma_{n,2} = h_2. \tag{20}$$

2.7 Multiple sections in Polygonal Audience Line

2.7.1 Centre position on current section

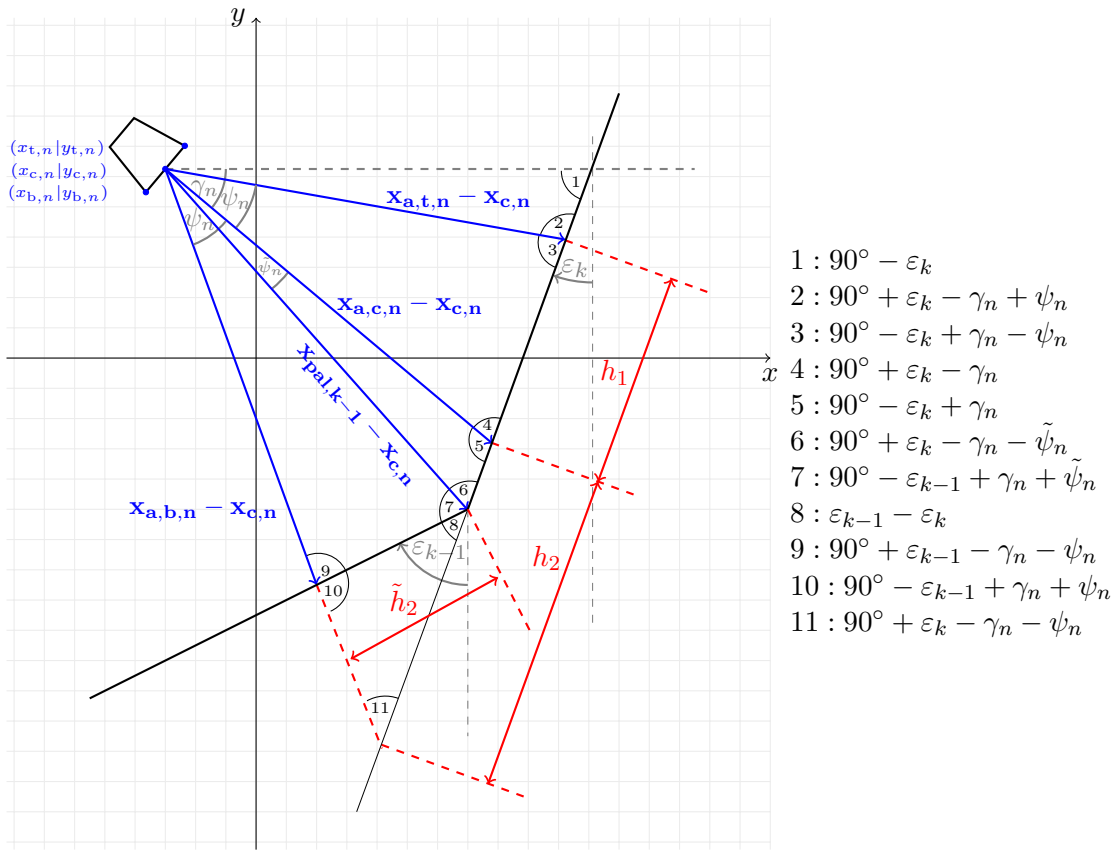

Figure 9: Sketch of two sections of the polygonal audience line with the n-th segment including both sections. The line section is changed between the centre and the bottom position of the segment, case (a) in 3) and 5).

The condition

$$h_1 \leq |\mathbf{x_{a,t,n}} - \mathbf{x_{pal,k-1}}| \tag{21}$$

holds, i.e. the section of the polygonal audience line is not changed. The centre position of the current segment can be calculated with

$$\mathbf{x_{a,c,n}} = \mathbf{x_{a,t,n}} + h_1 \begin{pmatrix} \cos\varepsilon_k \\ \sin\varepsilon_k \end{pmatrix} \tag{22}$$

and hence the segment's half length

$$\Gamma_{n,1} = h_1. \tag{23}$$

On the other hand, equation

$$h_2 > |\mathbf{x_{a,c,n}} - \mathbf{x_{pal,k-1}}| \tag{24}$$

is valid. The segment angle $\tilde{\psi}_n$ has to be calculated with

$$\frac{|\mathbf{x_{a,c,n}} - \mathbf{x_{pal,k-1}}|}{|\mathbf{x_{a,c,n}} - \mathbf{x_{c,n}}|} = \frac{\sin\tilde{\psi}_n}{\cos(\varepsilon_k - \gamma_n - \tilde{\psi}_n)}. \tag{25}$$

The length $\tilde{h}_2$ of the segment is

$$\tilde{h}_2 = |\mathbf{x_{pal,k-1}} - \mathbf{x_{c,n}}| \frac{\sin(\psi_n - \tilde{\psi}_n)}{\cos(\varepsilon_{k-1} - \gamma_n - \psi_n)}, \tag{26}$$

and the bottom position of the current segment can be written as

$$\mathbf{x_{a,b,n}} = \mathbf{x_{pal,k-1}} + \tilde{h}_2 \begin{pmatrix} \cos\varepsilon_{k-1} \\ \sin\varepsilon_{k-1} \end{pmatrix}, \tag{27}$$

and hence the segment's half length

$$\Gamma_{n,2} = |\mathbf{x_{a,c,n}} - \mathbf{x_{pal,k-1}}| + \tilde{h}_2. \tag{28}$$

2.7.2 Centre position on next section

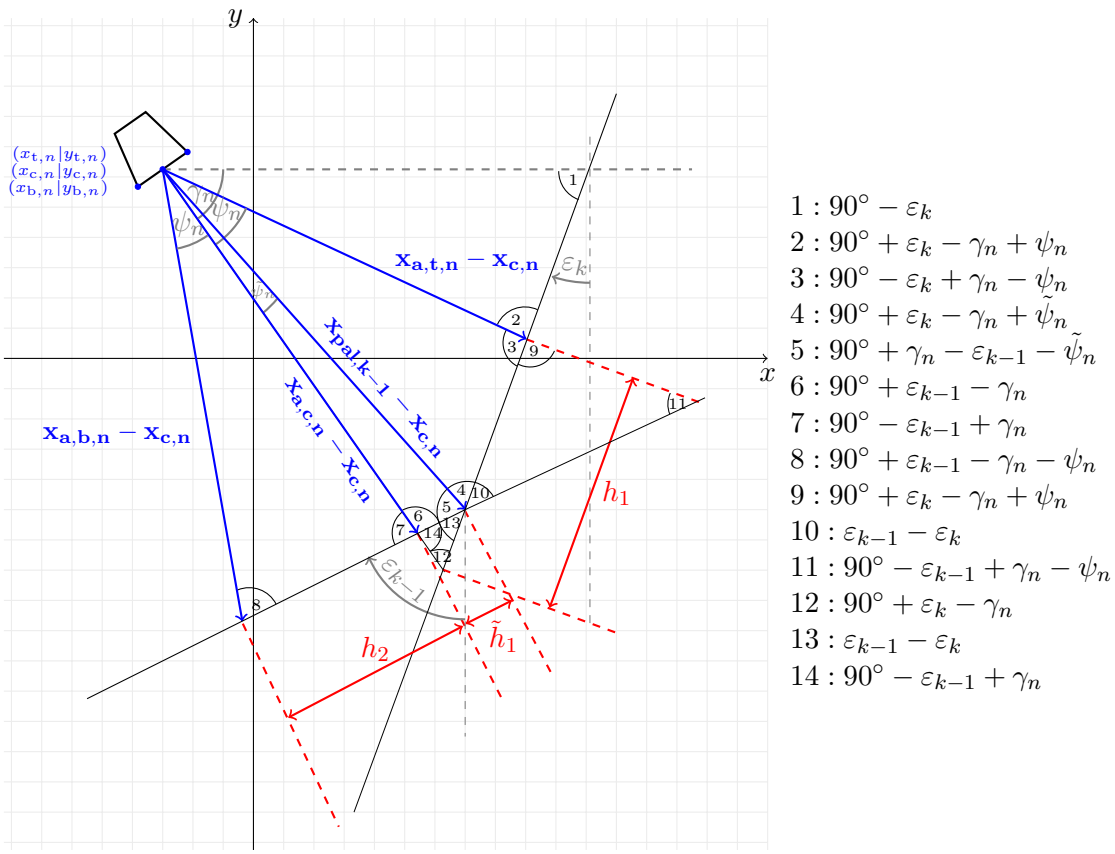

Figure 10: Sketch of two sections of the polygonal audience line with the n-th segment including both sections. The line section is changed between the top and the centre position of the segment, case (b) in 3) and 5).

The condition

$$h_1 > |\mathbf{x_{a,t,n}} - \mathbf{x_{pal,k-1}}| \tag{29}$$

holds, i.e. the section of the polygonal audience line is changed. The segment angle $\tilde{\psi}_n$ has to be calculated with

$$\frac{|\mathbf{x_{a,t,n}} - \mathbf{x_{pal,k-1}}|}{|\mathbf{x_{a,t,n}} - \mathbf{x_{c,n}}|} = \frac{\sin(\psi_n - \tilde{\psi}_n)}{\cos(\varepsilon_k - \gamma_n + \tilde{\psi}_n)}. \tag{30}$$

The length $\tilde{h}_1$ of the segment is

$$\tilde{h}_1 = |\mathbf{x_{pal,k-1}} - \mathbf{x_{c,n}}| \frac{\sin \tilde{\psi}_n}{\cos(\varepsilon_{k-1} - \gamma_n)} \tag{31}$$

and the centre position of the current segment can be written as

$$\mathbf{x_{a,c,n}} = \mathbf{x_{pal,k-1}} + \tilde{h}_1 \begin{pmatrix} \cos \varepsilon_{k-1} \\ \sin \varepsilon_{k-1} \end{pmatrix} \tag{32}$$

and hence the segment's half length

$$\Gamma_{n,1} = |\mathbf{x_{a,t,n}} - \mathbf{x_{pal,k-1}}| + \tilde{h}_1. \tag{33}$$

On the other hand, equation

$$h_2 \leq |\mathbf{x_{a,c,n}} - \mathbf{x_{pal,k-1}}| \tag{34}$$

holds as well. The bottom position of the current segment can be calculated with

$$\mathbf{x_{a,b,n}} = \mathbf{x_{a,c,n}} + h_2 \begin{pmatrix} \cos \varepsilon_k \\ \sin \varepsilon_k \end{pmatrix}, \tag{35}$$

and hence the segment's half length

$$\Gamma_{n,2} = h_2. \tag{36}$$

2.8 Calculation of the tilt angles

Starting with $n = 1$ and $k = K$. n is increased, k is decreased.

1. Compute the tilt angle γ_n of the n-th LSA cabinet from the slope

   $$\tan(-\gamma_n + \psi_n) = \frac{y_{\mathrm{a,t},n} - y_{\mathrm{c},n}}{x_{\mathrm{a,t},n} - x_{\mathrm{c},n}} \tag{37}$$

   with

   $$\mathbf{x_{c,n}} = \begin{pmatrix} x_{\mathrm{c},n} \\ y_{\mathrm{c},n} \end{pmatrix} = \begin{pmatrix} x_{\mathrm{t},n} \\ y_{\mathrm{t},n} \end{pmatrix} - \frac{\Lambda_{y,\mathrm{LSA}}}{2} \begin{pmatrix} \sin \gamma_n \\ \cos \gamma_n \end{pmatrix} \tag{38}$$

   and

   $$\begin{pmatrix} x_{\mathrm{t},1} \\ y_{\mathrm{t},1} \end{pmatrix} = \begin{pmatrix} x_{\mathrm{H}} \\ y_{\mathrm{H}} \end{pmatrix} \tag{39}$$

   and

   $$\mathbf{x_{a,t,1}} = \mathbf{x_{pal,K}} \tag{40}$$

   with the front grille's height $\Lambda_{\mathrm{y,LSA}}$ of an LSA cabinet, the mounting positions x_{H} and y_{H} of the topmost LSA cabinet and the top position of the K-th (topmost) audience section.

2. Compute the centre position $\mathbf{x_{c,n}}$ $[n = 1, 2, ..., N]$ of every LSA cabinet with eq. 38.

3. Compute the length h_1 with

   $$h_1 = |\mathbf{x_{a,t,n}} - \mathbf{x_{c,n}}| \frac{\sin \psi_n}{\cos(\varepsilon_k - \gamma_n)}. \tag{41}$$

   We consider two cases:

(a) Equation

$$h_1 \leq |\mathbf{x_{a,t,n}} - \mathbf{x_{pal,k-1}}| \tag{42}$$

holds, i.e. the section of the polygonal audience line is not changed, cf. Sec. 2.7.1 and Fig. 9. The centre position of the current segment can be calculated with

$$\mathbf{x_{a,c,n}} = \mathbf{x_{a,t,n}} + h_1 \begin{pmatrix} \cos\varepsilon_k \\ \sin\varepsilon_k \end{pmatrix} \tag{43}$$

and hence the segment's half length

$$\Gamma_{n,1} = h_1. \tag{44}$$

(b) Equation

$$h_1 > |\mathbf{x_{a,t,n}} - \mathbf{x_{pal,k-1}}| \tag{45}$$

holds, i.e. the section of the polygonal audience line is changed, cf. Sec. 2.7.2 and Fig. 10. The segment angle $\tilde{\psi}_n$ has to be calculated with

$$\frac{|\mathbf{x_{a,t,n}} - \mathbf{x_{pal,k-1}}|}{|\mathbf{x_{a,t,n}} - \mathbf{x_{c,n}}|} = \frac{\sin(\psi_n - \tilde{\psi}_n)}{\cos(\varepsilon_k - \gamma_n + \tilde{\psi}_n)}. \tag{46}$$

The length $\tilde{h}_1$ of the segment is

$$\tilde{h}_1 = |\mathbf{x_{pal,k-1}} - \mathbf{x_{c,n}}| \frac{\sin\tilde{\psi}_n}{\cos(\varepsilon_{k-1} - \gamma_n)} \tag{47}$$

and the centre position of the current segment can be written as

$$\mathbf{x_{a,c,n}} = \mathbf{x_{pal,k-1}} + \tilde{h}_1 \begin{pmatrix} \cos\varepsilon_{k-1} \\ \sin\varepsilon_{k-1} \end{pmatrix} \tag{48}$$

and hence the segment's half length

$$\Gamma_{n,1} = |\mathbf{x_{a,t,n}} - \mathbf{x_{pal,k-1}}| + \tilde{h}_1. \tag{49}$$

4. Update k, i.e. k is not changed if the section of the polygonal audience line was not changed (3, case (a)). k has to be decreased by 1 if the section of the polygonal audience line was changed (3, case (b)).

5. Compute the length h_2 with

$$h_2 = |\mathbf{x_{a,c,n}} - \mathbf{x_{c,n}}| \frac{\sin\psi_n}{\cos(\varepsilon_k - \gamma_n - \psi_n)} \tag{50}$$

we again consider two cases:

(a) Equation

$$h_2 > |\mathbf{x_{a,c,n}} - \mathbf{x_{pal,k-1}}| \tag{51}$$

holds, i.e. the section of the polygonal audience line is changed, cf. Sec. 2.7.1 and Fig. 9. The segment angle $\tilde{\psi}_n$ has to be calculated with

$$\frac{|\mathbf{x_{a,c,n}} - \mathbf{x_{pal,k-1}}|}{|\mathbf{x_{a,c,n}} - \mathbf{x_{c,n}}|} = \frac{\sin\tilde{\psi}_n}{\cos(\varepsilon_k - \gamma_n - \tilde{\psi}_n)}. \tag{52}$$

The length $\tilde{h}_2$ of the segment is

$$\tilde{h}_2 = |\mathbf{x_{pal,k-1}} - \mathbf{x_{c,n}}| \frac{\sin(\psi_n - \tilde{\psi}_n)}{\cos(\varepsilon_{k-1} - \gamma_n - \psi_n)} \tag{53}$$

and the bottom position of the current segment can be written as

$$\mathbf{x_{a,b,n}} = \mathbf{x_{pal,k-1}} + \tilde{h}_2 \begin{pmatrix} \cos\varepsilon_{k-1} \\ \sin\varepsilon_{k-1} \end{pmatrix} \tag{54}$$

and hence the segment's half length

$$\Gamma_{n,2} = |\mathbf{x_{a,c,n}} - \mathbf{x_{pal,k-1}}| + \tilde{h}_2. \tag{55}$$

(b) Equation

$$h_2 \leq |\mathbf{x_{a,c,n}} - \mathbf{x_{pal,k-1}}| \tag{56}$$

is valid, i.e. the section of the polygonal audience line is not changed, cf. Sec. 2.7.2 and Fig. 10. The bottom position of the current segment can be calculated with

$$\mathbf{x_{a,b,n}} = \mathbf{x_{a,c,n}} + h_2 \begin{pmatrix} \cos\varepsilon_k \\ \sin\varepsilon_k \end{pmatrix} \tag{57}$$

and hence the segment's half length

$$\Gamma_{n,2} = h_2. \tag{58}$$

6. Update k, i.e. k is not changed if the section of the polygonal audience line was not changed (5, case (b)). k has to be decreased by 1 if the section of the polygonal audience line was changed (5, case (a)).

3 Modification of the PALC algorithm

3.1 Discretisation of the inter-cabinet angles

The purpose of this chapter is to present the modification of the PALC algorithm for its application on commercially available LSA systems. The first step is to research the market and come up with a representative selection of LSA systems; the systems are chosen focusing on having the most varied set of inter-cabinet angles possible available. In order to adapt the PALC algorithm to use only inter-cabinet angles provided by the selection of LSAs available, the LSA models and their inter-cabinet angles are entered in the algorithm. A rounding algorithm is added to the code in order to round the inter-cabinet angle values resulting from the PALC algorithm to the possible values offered by each of the LSAs. There are three basic rounding methods that can be applied to the resulting inter-cabinet angles:

Round: round to nearest inter-cabinet angle

Floor: round to nearest inter-cabinet angle that is smaller than the value

Ceil: round to nearest inter-cabinet angle that is larger than the value

In order to find an optimal solution, not only should the different LSA systems be compared with one another, it should also be tested which rounding method works best with which system. Thus, the results of the algorithm will be evaluated using each of the LSA systems in combination with each of the rounding methods presented for each of the four venues shown in Fig. 7.

LSA System	**Inter cabinet angles**
Martin Audio MLA	0, 0.5, 1, 2, 3, 4, 5, 6, 7.5
DB J-Series	0, 1, 2, 3, 4, 5, 6, 7
Meyer LEO	0, 0.5, 1, 1.5, 2, 2.5, 3, 4, 5
Meyer LYON	0, 0.5, 1, 1.5, 2, 3, 4, 5, 7, 9
Adam Hall LD VA 8	0, 1, 2, 3, 4, 5, 6
Adamson E12	0, 0.5, 1, 2, 3, 4.5, 6.3, 8
Adamson E15	0, 0.3, 0.6, 1.3, 2, 3.1, 4.4, 6
Alcons LR28	0, 0.1, 0.15, 0.24, 0.38, 0.6, 0.95, 1.5, 2.4, 3.8, 6
Alcons LR18	0, 0.5, 0.7, 1, 1.4, 1.9, 2.7, 3.7, 5.2, 7.2, 10
JBL V25 11	1, 2, 3, 4, 5, 6, 7, 8, 9, 10
Yamaha NEXO STM M46	0.2, 0.5, 1.2, 2.5, 5, 7, 10
L'Acoustics K1	0, 0.5, 1, 1.5, 2, 2.5, 3, 4, 5
General set	0, 0.5, 1, 2, 3, 4, 5, 6

Table 1: Every possible inter cabinet angle offered by several standard LSA system models.

The table above shows how the number of possible inter-cabinet angles is limited to a minimum of 7 and a maximum of 11 different angles per model for the systems ADAM HALL LD VA 8 and ALCONS LR28 respectively. As mentioned before, the discretisation of the LSA inter-cabinet angles is carried out for practical purposes, thus allowing the PALC algorithm to be conveniently applied to most industry standard LSA systems.

Straube et al. (2017) evaluates the PALC algorithm for two goals:

PALC1 incorporates the goal of an invariant interaction between adjacent cabinets so that the radiated sound of the different sources overlap at a constant coverage angle ϕ in the far-field of the individual sources. This constraint simply reads

$$\phi_1 = \phi_2 = \phi_3 = \text{const.} \tag{59}$$

PALC1 is similar to an arc array but the goal does not refer to the array itself, i.e. constant splay angles between all cabinets, but it refers to the shape of the receiver geometry.

PALC2 considers the distances of the different positions from the sources and the desired sound field. It demands a constant product of the coverage angle ϕ and the distance from the source to the receiver positions, i.e.

$$\tan\phi_1 \cdot |\mathbf{x_{a,c,1}} - \mathbf{x_{c,1}}| = \tan\phi_2 \cdot |\mathbf{x_{a,c,2}} - \mathbf{x_{c,2}}| = ... = \text{const.} \tag{60}$$

For small ϕ_n, (60) arises from a simplification of attaining a constant length Γ_n for all n segments. The PALC2 constraint should not be confused with the Wavefront Sculpture Technology criterion #4 (Urban, M. et al., 2003, p. 929).

The discretisation of the inter-cabinet angles will be evaluated under the condition PALC2, i.e. considering the distance from the source to the receiver positions, as it is proven in Straube et al. (2017) that this condition yields more appropriate results than PALC1. The discretisation and rounding of inter-cabinet angles is carried out with the tilt angle of the first (uppermost) cabinet as the reference. The tilt angle of the first cabinet can be specified at will by the mounting technician and the following cabinets are tilted according to the possible inter-cabinet angles offered by each LSA system.

3.2 Optimisation of the curving of LSAs by means of the goal attainment method

The purpose of this chapter is to present a method for optimising the curving of LSA systems, namely a numerical optimisation, as an alternative method to the analytical optimisation described by Straube et al (2017). In the context of this thesis, the numerical optimisation can be applied either after the discretisation of the LSA's inter-cabinet angles or as an alternative method to further optimise the curving of the LSA.

3.2.1 Multiobjective optimisation

Multiobjective optimisation (also called multiobjective programming, multi criteria optimisation, multi attribute optimisation or Pareto optimisation) belongs to the field of multiple criteria decision making, which deals with mathematical optimisation problems that involve multiple objective functions to be optimised at the same time. More specifically, multiobjective optimisation is applied in situations where trade-offs between two or more conflicting objectives exist. This method reflects real life problems more adequately, in which there is often a vector of objective functions $F(x) = [F_1(x), F_2(x), ..., F_m(x)]$ that needs to be traded off in some way. The purpose of multiobjective optimisation is to minimise a vector of objectives $F(x)$ which can be the subject of a number of constraints. This is expressed, in mathematical terms, as follows:

minimise $F(x)$

$x \in \Re^n$

$$\begin{aligned} G_i(x) &= 0, \qquad i = 1, ..., m_e \\ G_i(x) &\leq 0, \qquad i = m_e + 1, ..., m \\ x_l &\leq x \leq x_u \end{aligned} \tag{61}$$

It is important to note that if any of the elements of $F(x)$ are competing, then there are multiple solutions to the problem. In this case, the concept of Pareto optimality or non-inferiority must be used in order to characterise the objectives: non-inferiority refers to solutions where an improvement in one of the objectives requires a degradation of the other. Consequently, for any solution that is not non-inferior there is a possibility of improvement in all the objectives. This means that such a solution has no value for the process. Therefore, the process of multiobjective optimisation is only concerned with the generation and selection of non-inferior solutions, for which there are several different techniques found in the literature. In this thesis, the chosen technique is the goal attainment method, first utilised by Gembicki et al. (1975) for solving technical optimisation problems.

3.2.2 Goal attainment method

Numerical optimisation by means of the goal attainment method has already been applied, among others, by Thompson et al. (2011) for optimising the LSA's cabinets driving functions. The purpose of this section is to test the goal attainment method in the context of geometric optimisation of LSAs.

In the goal attainment method, a set of design goals $F^* = [F_1^*, F_2^*, ..., F_m^*]$ is defined and associated with a set of objectives, $F(x) = [F_1(x), F_2(x), ..., F_m(x)]$. The fact that it is possible for the objectives to be under- or overachieved allows the designer a relative freedom when defining the initial design goals. The under- or overachievement of the goals is controlled by a vector of weighting coefficients, $w = [w_1, w_2, ..., w_m]$. The optimisation problem is formulated as follows:

$$\begin{aligned} &\textbf{minimise } \gamma \\ &\gamma \in \Re, x \in \Omega \\ &\text{such that } \; F_i(x) - w_i\gamma \leq F_i^* \qquad i = 1, ..., m \end{aligned} \tag{62}$$

The term $w_i\gamma$ means that the goals of the problem don't necessarily have to be rigidly met. Instead, the weighting vector, w, makes it possible to express a measure of the relative tradeoffs between the objectives. This means the designer can incorporate particular constraints into the design. For example, setting one weighting factor to zero(i.e. $w_i = 0$) will incorporate a hard constraint on the design. On a hypothetical two dimensional plane, specification of the goals $[F_1^*, F_2^*]$ defines the goal point, P. The weights define the direction of search from P to the feasible function space, $\Lambda(\gamma)$. During the optimisation γ is varied, changing the size of the feasible region, while the constraint boundaries converge to the unique solution point.

Thus, in the present problem, two of the technical quality measures used by Straube et al. (2017) are assigned as objective functions for the optimisation, namely the acoustic contrast $L_{p,\mathrm{a,na}}(\omega)$ and the sound field homogeneity $H1(\omega)$. One goal value is assigned to each of the objective functions making a total of two goal values, which can be arbitrarily set. During the optimisation the vector of resulting LSA cabinet tilt angles from the PALC algorithm is varied until a unique solution point is found with the help of weighting factors assigned to $L_{p,\mathrm{a,na}}(\omega)$ and $H1(\omega)$. According to this algorithm, if the optimisation is carried out for each frequency band separately, then

one set of tilt angles is obtained for each frequency band. This is obviously not in our interest, since it is only possible to have one unique geometry for each LSA system at any given point in time for all frequencies. Hence, in order to obtain one valid set of tilt angles, the optimisation must be performed for all frequencies at once. However, knowing which tilt angles work best for each frequency band can be helpful in order to find a set of tilt angles which deliver better results than the ones obtained from the optimisation over all frequencies at once.

4 Evaluation

4.1 Discretisation of the inter-cabinet angles

Before the results of the discretisation of inter-cabinet angles are evaluated it is important to mention that this discretisation has a direct effect on the resulting sound field, especially on the interaction between adjacent cabinets. After several test runs of the algorithm with different LSAs and rounding methods, the results show that for all tested LSA systems, the radiation area of several cabinets either overlap with one another in the PAL or fails to fully cover the PAL. This is an expected consequence, since the algorithm is not able to choose an inter-cabinet angle at will anymore, but is limited to those angles offered by the LSA system used. There were modifications carried out in the PALC algorithm in order to be able to obtain the following results. The algorithm uses an iterative method that compares the difference between the total length of the PAL and the length of the PAL which has been successfully covered by the LSA cabinets ($h_1 + h_2$ in Fig. 8) with a constant quantity, namely 0.1 meters. This is the error tolerance permitted by the algorithm and is labelled as Γ_{aud} (cf. (8)). Thus, the iterations do not stop until a value of $\Gamma_{\text{aud}} < 0.1$ is reached.

Once the algorithm was modified and the inter-cabinet angles are discretised, the accuracy of the PAL coverage decreases. This means that the algorithm cannot fulfil the condition $\Gamma_{\text{aud}} < 0.1$ in every case. This happens for certain LSA systems as well as for certain rounding types more than for others. For this reason, the value of Γ_{aud} was increased in some cases to meet the requirements of the new inter-cabinet angles.

The quantitative evaluation is based on two technical quality measures. On the one hand, the frequency dependent relation of the obtained average SPLs of the audience and the non audience zone

$$L_{p,\text{a,na}}(\omega) = 10 \log_{10} \left(\frac{\frac{1}{M_{\text{a}}} ||\mathbf{p}_{m \in \mathscr{M}_{\text{a}}}(\omega)||_2^2}{\frac{1}{M_{\text{na}}} ||\mathbf{p}_{m \in \mathscr{M}_{\text{na}}}(\omega)||_2^2} \right) \tag{63}$$

(Straube, F. et al. (2015b), Eq. (18)) is evaluated. This measure is depicted, for example, in Fig. 14b, 14d, 14f and 14h and corresponds to the acoustic contrast (Choi, J.W. et al. (2002), Eq. (16)), (Coleman, P. et al. (2014a), Eq. (2)), (Coleman, P. et al. (2014b), Eq. (2)) established in the field of multi-zone sound field synthesis (MZSFS). On the other hand, the homogeneity of the generated sound field, meaning the frequency dependent standard deviation of the distance compensated SPLs of all audience positions

$$H1(\omega) = \underset{m \in \mathscr{M}}{\sigma} \left[20 \log_{10} \left(\frac{|P(m,\omega)|}{p_0} \sqrt{\frac{|\mathbf{x_m} - \mathbf{x_s}|}{|\mathbf{x_{min(m)}} - \mathbf{x_s}|}} \right) \right], \tag{64}$$

cf. (Feistel, S. et al. (2013), e.g. Fig. 6, Fig. 8) is also evaluated. It is depicted, for example, in Fig. 14a, 14c, 14e and 14g.

In the following paragraphs, the results will be evaluated for each one of the four venues separately.

VENUE 1

The first venue is a multi-stand arena with several amphitheater levels taken from Thompson et al. (2011, Sec. 6.1). The cases that required an increase of the allowed Γ_{aud} error value in order to achieve a result are shown in Table 2; for all the other cases, the Γ_{aud} error value did not have to be modified.

After applying three different types of rounding to the discretisation of the tilt angles for four of the systems (Martin Audio MLA, Alcons LR28 ,Yamaha NEXO STM

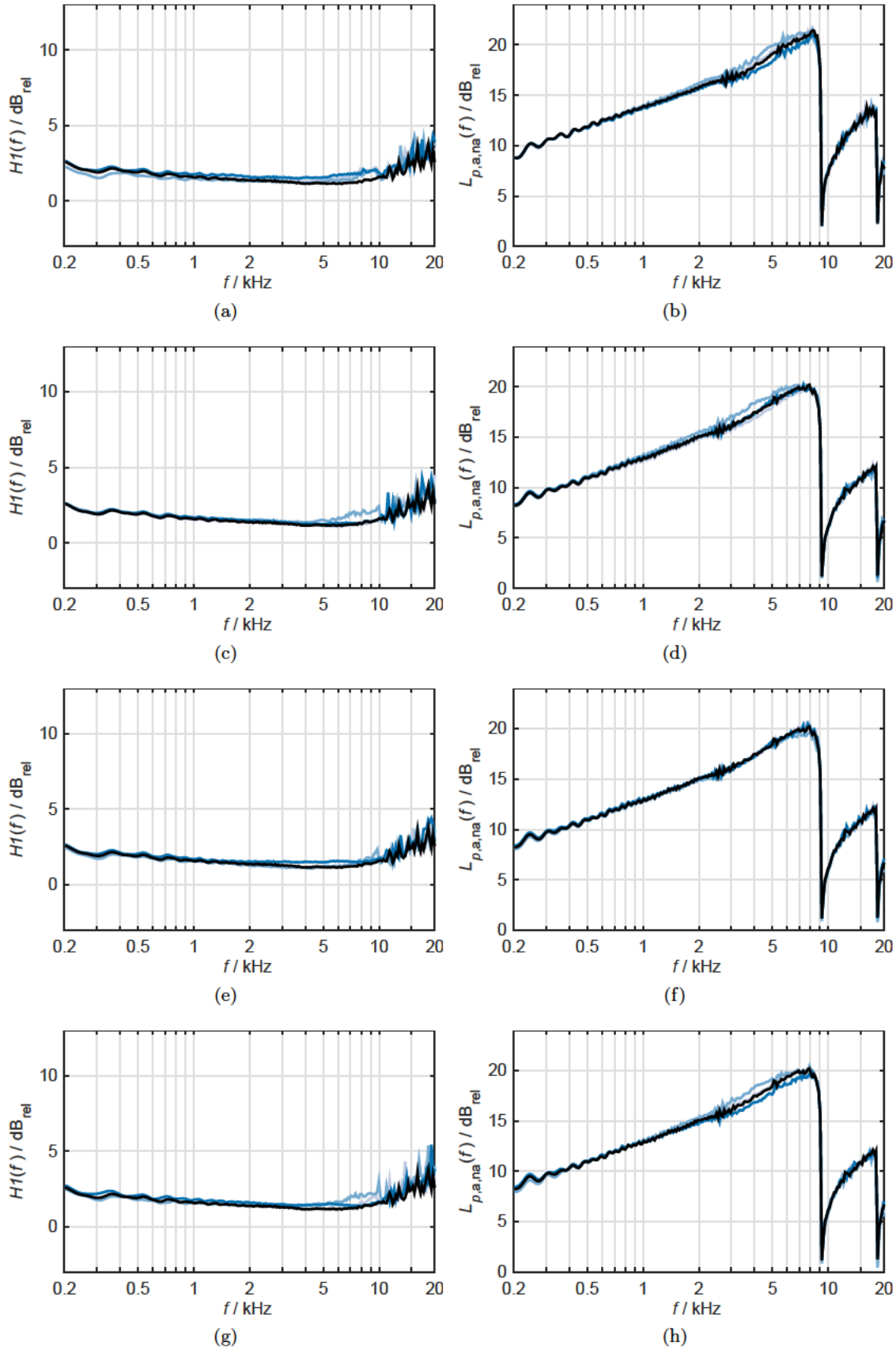

Figure 11: Technical quality measures $H1$ (left column) and $L_{p,\mathrm{a,na}}$ (right column): (a) (b) Alcons LR28, (c) (d) Meyer LYON, (e) (f) Martin Audio MLA and (g) (h) Yamaha NEXO STM (M46) for all analysed rounding types for venue 1 (cf. Fig. 3 a)

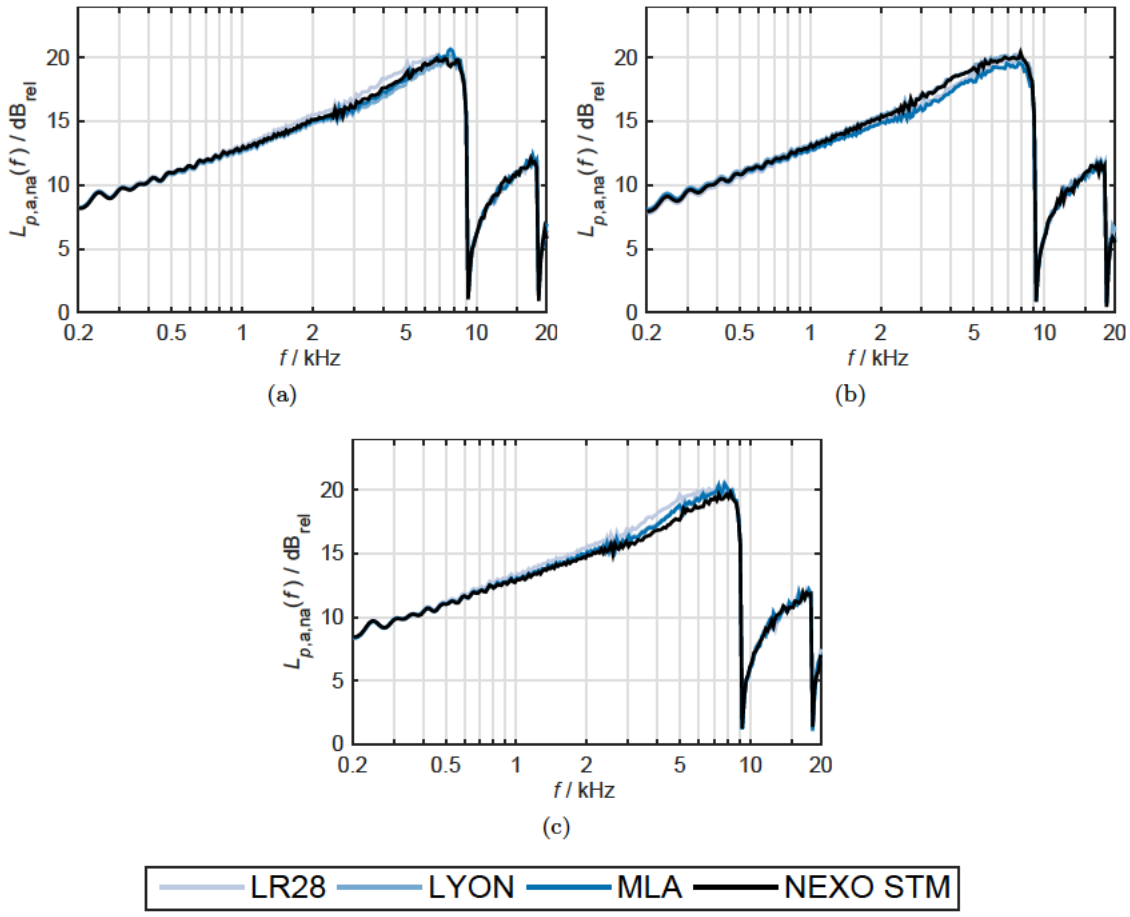

Figure 12: $L_{p,\mathrm{a,na}}$ for every LSA system used in venue 1: (a) "round", (b) "floor" and (c) "ceil" rounding methods.

	floor	**round**	**ceil**
Martin Audio MLA	0.1	0.1	0.14
Alcons LR28	0.1	0.24	0.1
Yamaha NEXO STM	0.13	0.1	0.18

Table 2: Modifications on the allowed Γ_{aud} error on venue 1. The left column consists of LSA models, and the top row consists of the three types of rounding applied to the tilt angles.

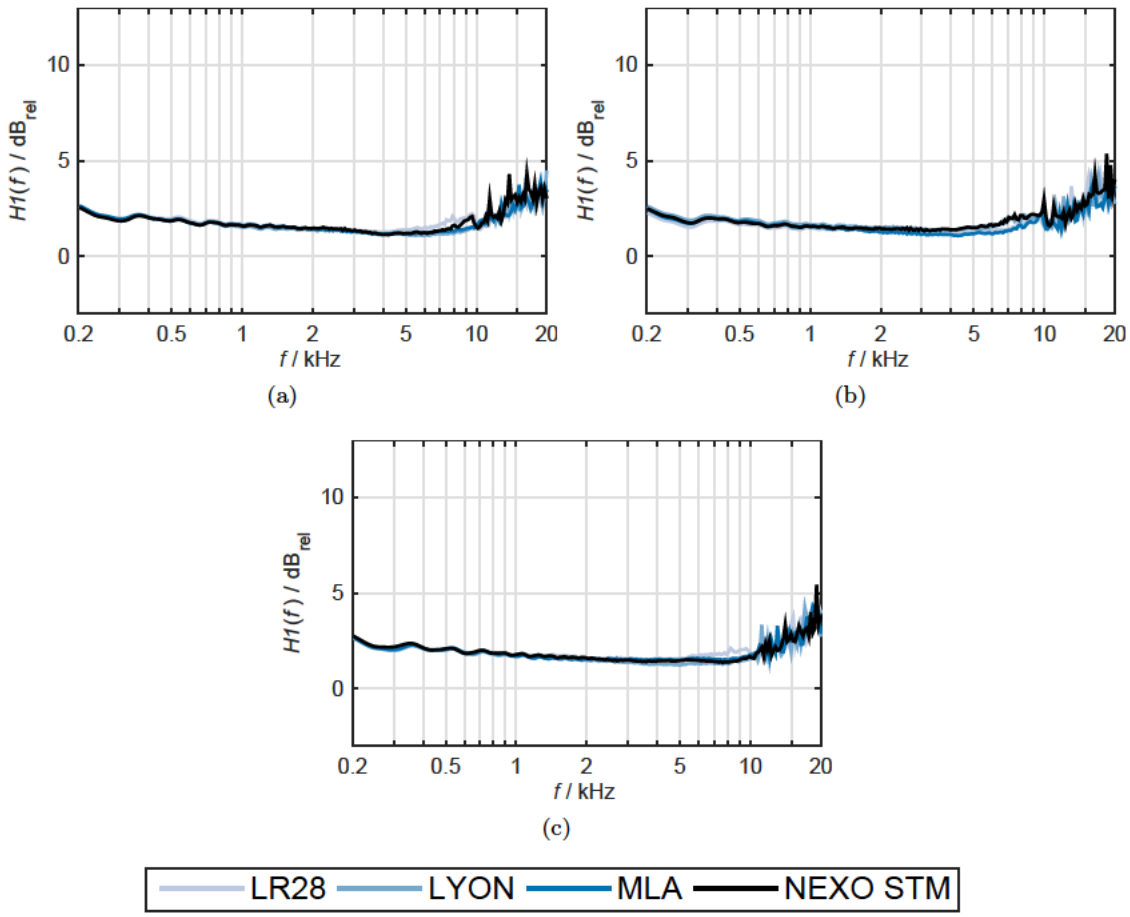

Figure 13: $H1$ for every LSA system used in venue 1: (a) "round", (b) "floor" and (c) "ceil" rounding methods.

M46 and Meyer LYON), the results show that in venue 1 the rounding type “round" offers a slightly more homogeneous sound field than the two other rounding types for the LSA models Alcons LR28, Meyer Lyon and Martin Audio MLA, as can be seen with the technical quality measure $H1(\omega)$ in Fig. 11c, 11e and 11g. The Yamaha Nexo STM system achieves better results with the “ceil" rounding, especially in frequencies higher than 7 kHz.

The ratio of energy radiated into the audience versus the non-audience zones is very similar for all rounding types, but slightly better for the “floor" rounding type when using the Alcons LR28, which outperforms the non-discretised PALC algorithm at frequencies lower than 8 kHz, as can be seen in Fig. 11b. For the Meyer Lyon and the Yamaha Nexo STM less energy is radiated into the non-audience zones compared to the audience zones when using the “floor" rounding, the latter outperforming the non-discretised PALC algorithm between 1 and 7 kHz, as seen in Fig. 11d and 11h. Finally, there is no noticeable improvement for the Martin Audio MLA in terms of acoustic contrast between the audience and non-audience zones, as seen in Fig. 11f.

Regarding the question of which LSA system works best with each of the rounding methods, Fig. 12a shows that for the “round” method, the Alcons LR28 delivers both the highest ratio of acoustic energy in the audience versus the non-audience areas for frequencies up to 7 kHz, and the most homogeneous sound field for frequencies up to 11 kHz (Fig. 13a). For frequencies higher than 11 kHz, the Yamaha NEXO outperforms the Alcons LR28 in sound field homogeneity. In Fig. 12b and 13b respectively, we see how the Meyer LYON performs slightly better than all other systems both in terms of acoustic contrast between audience and non audience zones and sound field homogeneity when using the “floor” rounding method. However, for frequencies higher than 3.5 kHz the Yamaha NEXO delivers a more homogeneous sound field. Regarding the “ceil” rounding method, the Alcons LR28 delivers once more the best results both in terms of acoustic contrast between the audience and non-audience areas and sound field homogeneity (Fig. 12c and 13c respectively).

VENUE 2

The second venue is an open air amphitheater and resembles the Waldbuehne in Berlin, composed of two audience lines with different tilt angles. For the “floor” rounding when using the ALCONS LR28 system, the error was increased to 0.13 to obtain a result. For all the other cases, the Γ_{aud} error did not have to be modified.

In venue 2 the rounding type “floor" offers a slightly more homogeneous sound field for frequencies lower than 5 kHz when using the Meyer Lyon, Martin Audio MLA and Alcons LR28 systems, as can be seen with the homogeneity measure $H1(\omega)$ in Fig. 14a, 14c and 14e. On the other hand, the rounding type “ceil" offers a more homogeneous sound field when using the Yamaha Nexo STM as seen in Fig. 14g.

The ratio of the energy radiated into the audience versus the non-audience zones is very similar for all rounding types, but slightly better for the “floor" rounding type in al LSA systems used, outperforming the non-discretised PALC algorithm at frequencies between 1 and 8 kHz, as seen in Fig. 14b, 14d and 14h.

In terms of which LSA system works best with which rounding method, Fig. 15a shows that for the “round” method, the Alcons LR28 delivers the best results regarding the acoustic contrast between the audience and non-audience areas. Concerning the sound field homogenity, the Yamaha NEXO delivers the best result. When using the “floor” rounding method, the Alcons LR28 provides both the best acoustic contrast and sound homogeneity as seen in Fig. 15b and 16b respectively. Regarding the “ceil” rounding method, the Yamaha NEXO performs best in the lower frequency range (up

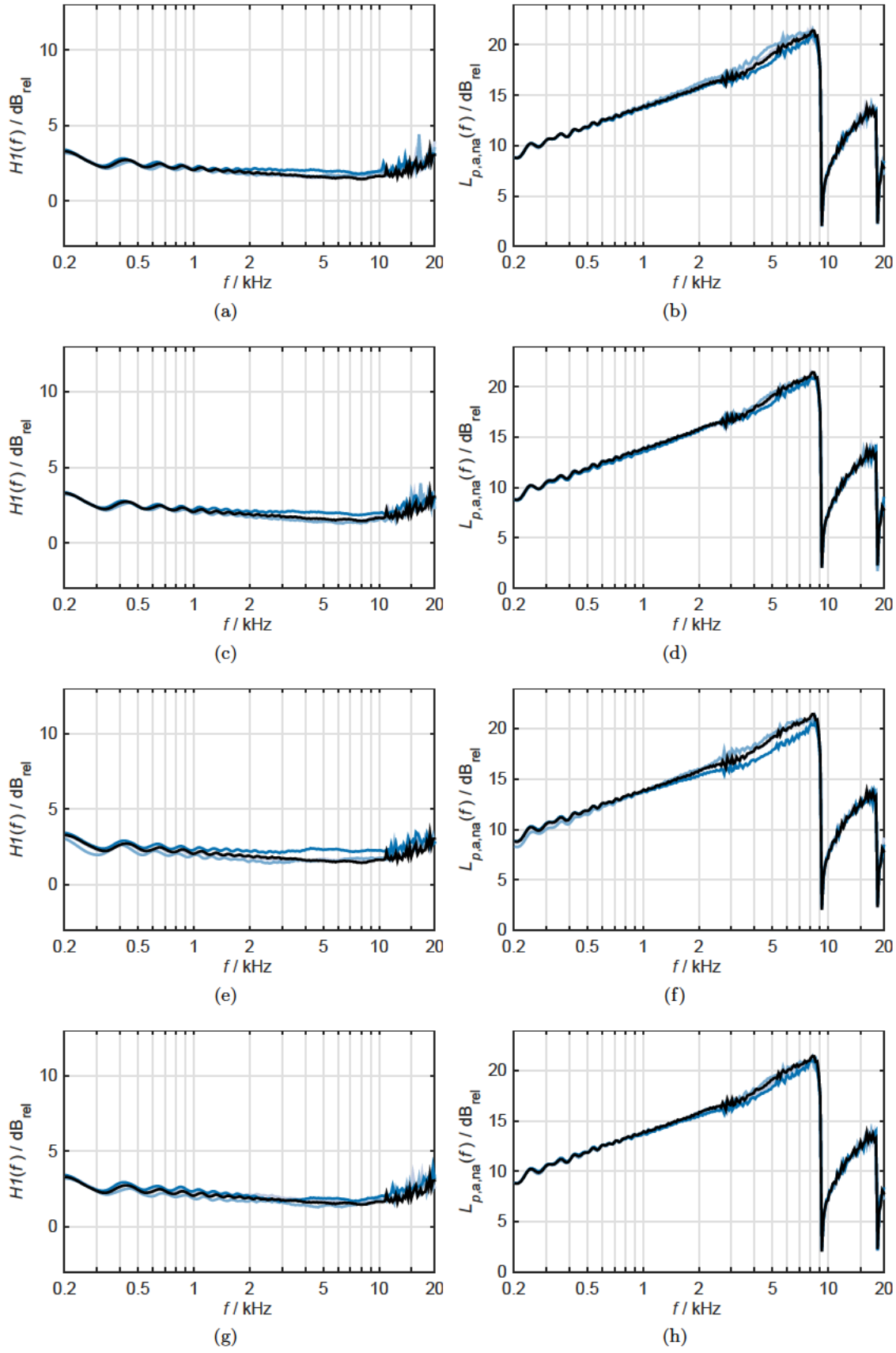

Figure 14: Technical quality measures $H1$ (left column) and $L_{p,\mathrm{a,na}}$ (right column): (a) (b) Alcons LR28, (c) (d) Meyer LYON, (e) (f) Martin Audio MLA and (g) (h) Yamaha NEXO STM (M46) for all analysed rounding types for venue 2 from Fig. 3 b)

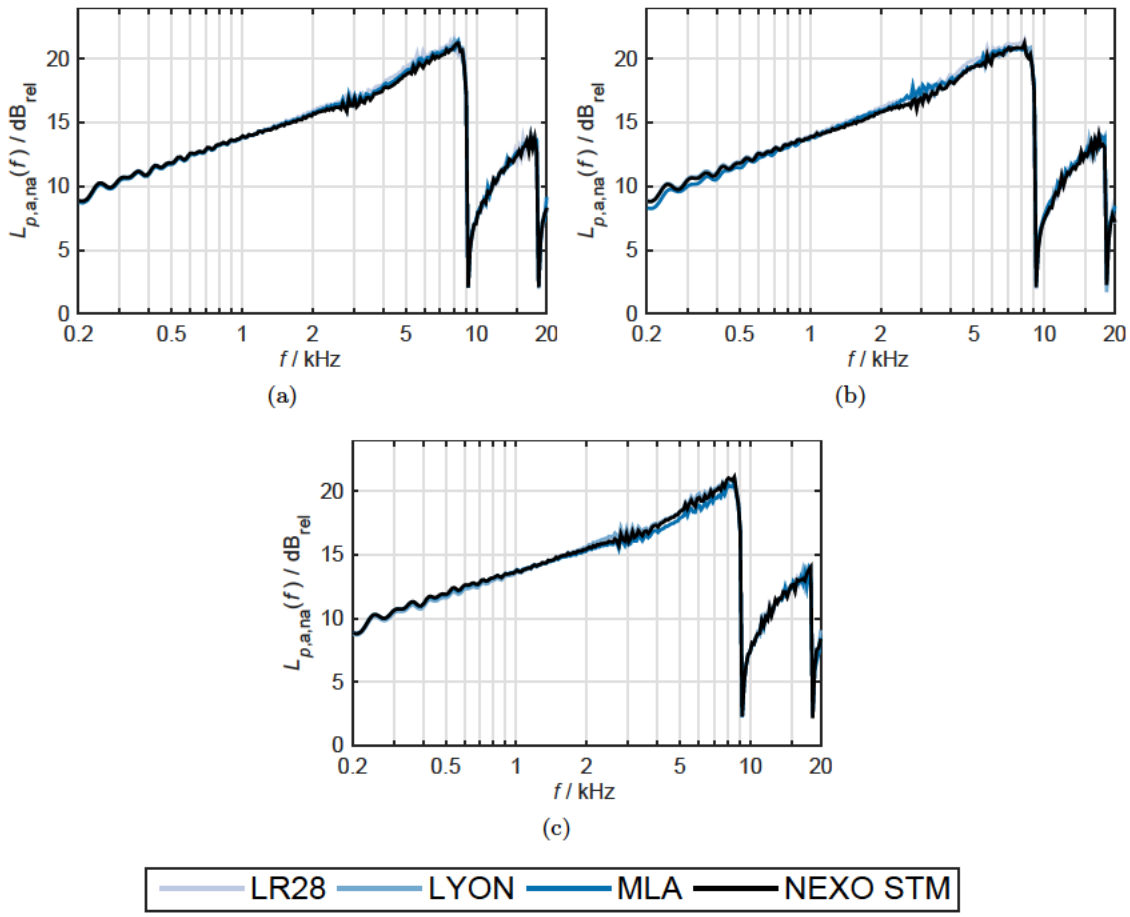

Figure 15: $L_{p,\mathrm{a,na}}$ for every LSA system used in venue 2: (a) "round", (b) "floor" and (c) "ceil" rounding methods.

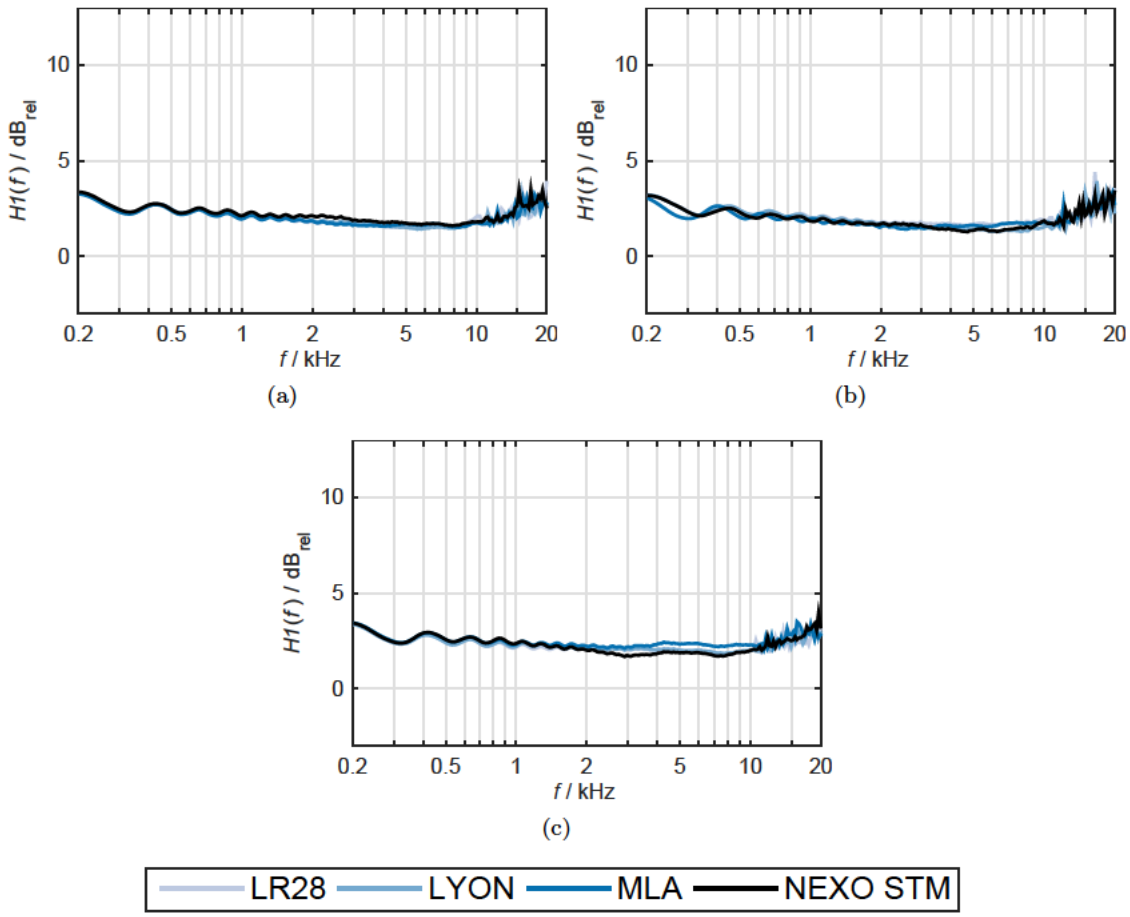

Figure 16: $H1$ for every LSA system used in venue 2: (a) "round", (b) "floor" and (c) "ceil" rounding methods.

to 1.5 kHz) and the Meyer LYON outperforms all other systems at frequencies higher than 1.5 kHz (Fig. 15c). In terms of sound homogeneity, the Martin Audio MLA provides the best results as seen in Fig. 16c.

VENUE 3

The third venue consists of one horizontal audience line only and resembles a generic outdoor music festival situation. For the "ceil" rounding type with the MEYER LYON system the Γ_{aud} error was increased to a value of 0.31. For all the other cases, the Γ_{aud} error did not have to be modified.

Using the Meyer LYON system in venue 3, the rounding types "round" and "floor" offer a slightly more homogeneous sound field than the "ceil" rounding as can be seen with the technical quality measure $H1(\omega)$ in Fig. 17c. In this case, the "floor" rounding works better for lower frequencies up to 7 kHz, and the "round" type achieves higher homogeneity from 7 kHz and up. The ratio of the energy radiated into the audience versus the non-audience zones is very similar for all rounding types, but slightly better for the "ceil" rounding type at frequencies higher than 1.5 kHz, outperforming the non-discretised PALC algorithm. At frequencies lower than 1.5 kHz the "floor" and "round" rounding achieve better results, as seen in Fig. 17d.

Using the Martin Audio MLA LSA the rounding type "floor" offers a slightly more homogeneous sound field for frequencies under 7 kHz, as can be seen with the quality measure H1(w) in figure Fig. 17e. The ratio of the energy radiated into the audience versus the non-audience zones is very similar for all rounding types, but slightly better for the "floor" and "round" rounding types, as seen in Fig. 17f.

Using the Yamaha Nexo STM system, the "floor" rounding offers a slightly more homogeneous sound field at low frequencies under 2.5 kHz, as can be seen with the quality measure $H1(\omega)$ in Fig. 17g. The ratio of energy radiated into the audience versus the non-audience zones is higher for the "floor" rounding type for this system, as seen in Fig. 17h.

Using the Alcons LR28 LSA the rounding type "floor" offers a slightly more homogeneous sound field throughout all the frequency range, as can be seen with the quality measure H1(w) in figure Fig. 17a. A higher ratio of energy radiated into the audience versus the non-audience zones is achieved by the "floor" rounding type for frequencies lower than 3 k Hz (Fig. 17b)

Regarding the question of which LSA system works best with each of the rounding methods, Fig. 18a shows that for the "round" method, the Yamaha NEXO clearly delivers the highest ratio of acoustic energy in the audience versus the non-audience areas throughout the whole frequency spectrum as well as the most homogeneous sound field (Fig. 19a). In Fig. 18b and 19b we see the same results when using the "floor" rounding method. Regarding the "ceil" rounding method, the Meyer LYON delivers the best results in terms of acoustic contrast between the audience and non-audience areas followed closely by the Yamaha NEXO, especially in mid-high frequencies. In the lower spectrum, the Alcons LR28 performs slightly better (Fig. 18c). In terms of sound field homogeneity, the Yamaha NEXO provides the best results one more time (Fig. 19c)

VENUE 4

The fourth venue resembles the new Calderón football stadium in Madrid and consists of six audience lines with different tilt angles. For the "floor" rounding type

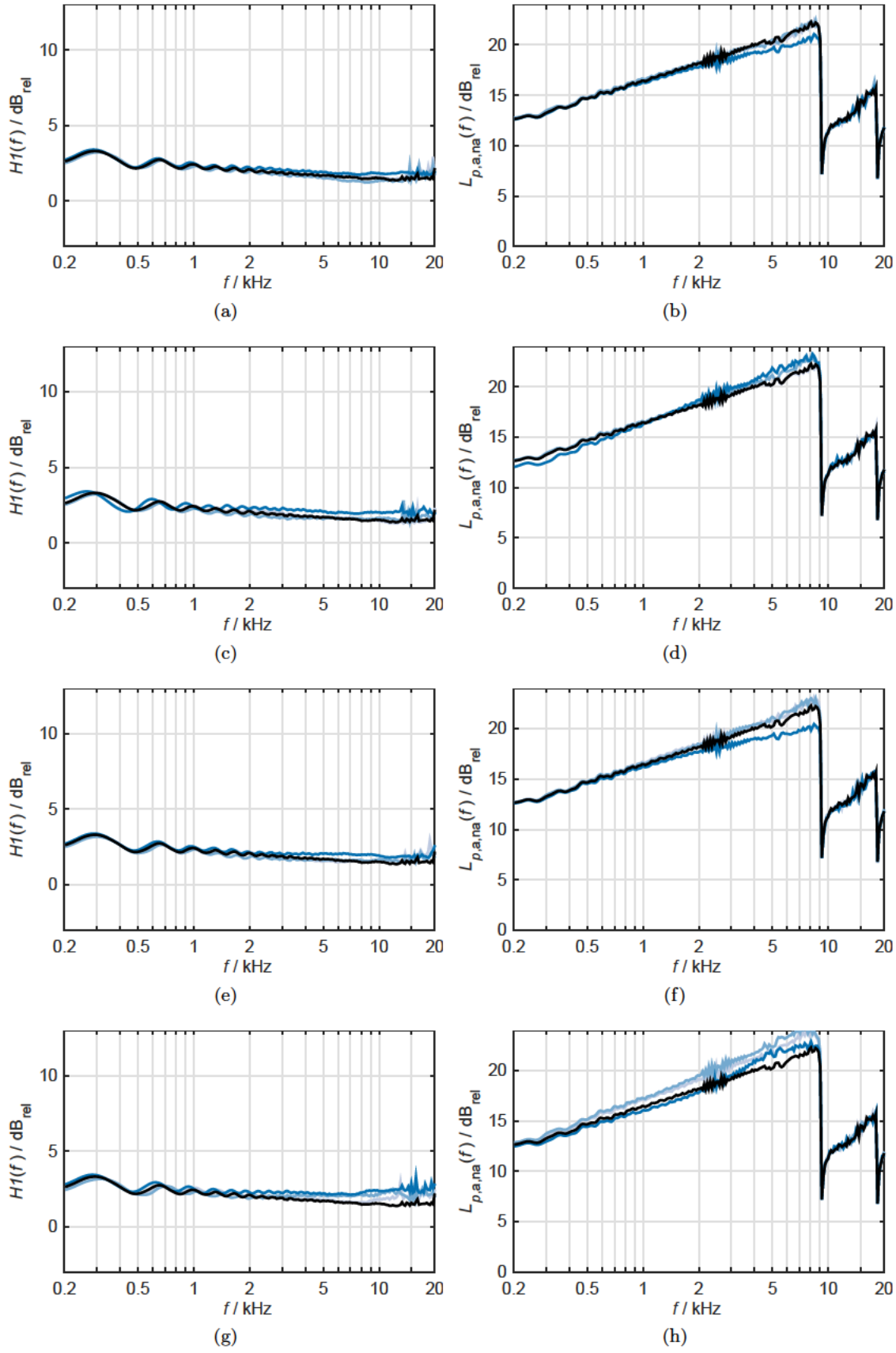

Figure 17: Technical quality measures $H1$ (left column) and $L_{p,\mathrm{a,na}}$ (right column): (a) (b) Alcons LR28, (c) (d) Meyer LYON, (e) (f) Martin Audio MLA and (g) (h) Yamaha NEXO STM (M46) for all analysed rounding types for venue 3 from Fig. 3 c)

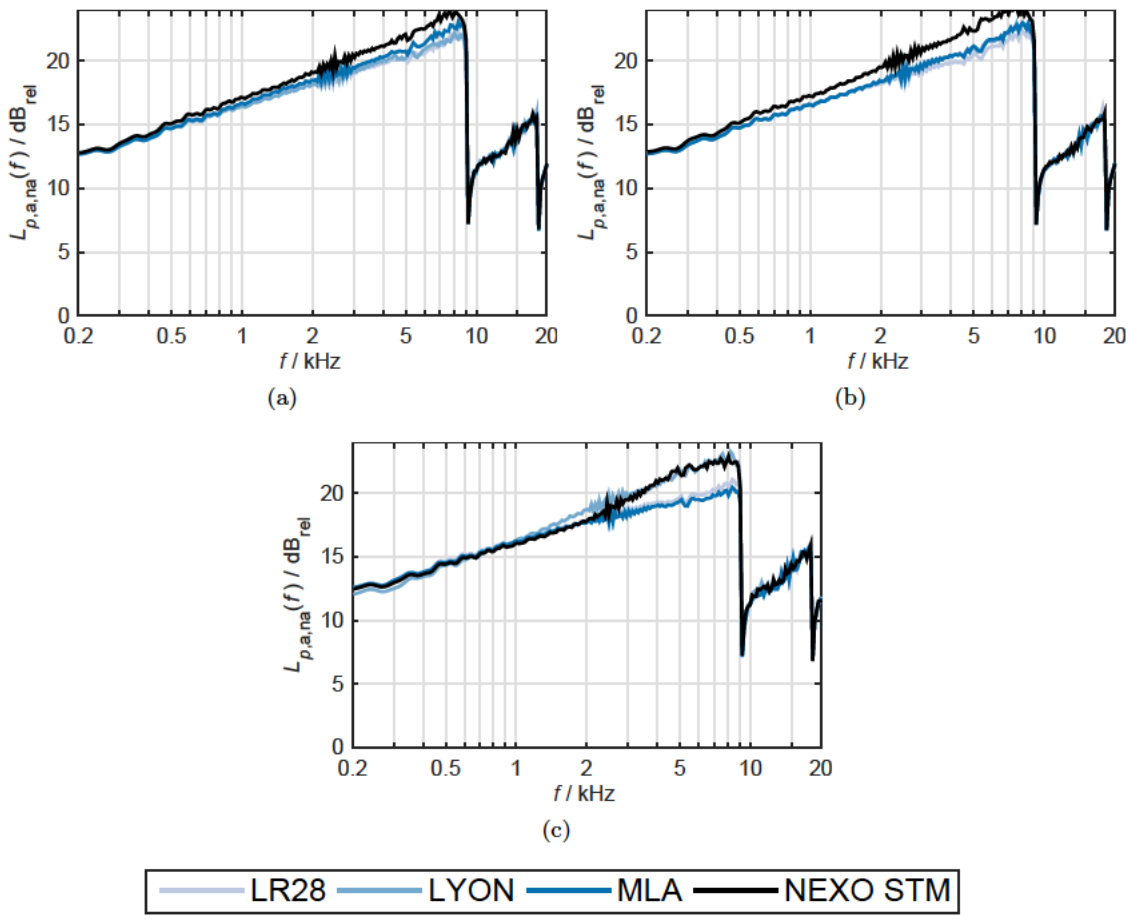

Figure 18: $L_{p,\mathrm{a,na}}$ for every LSA system used in venue 3: (a) "round", (b) "floor" and (c) "ceil" rounding methods.

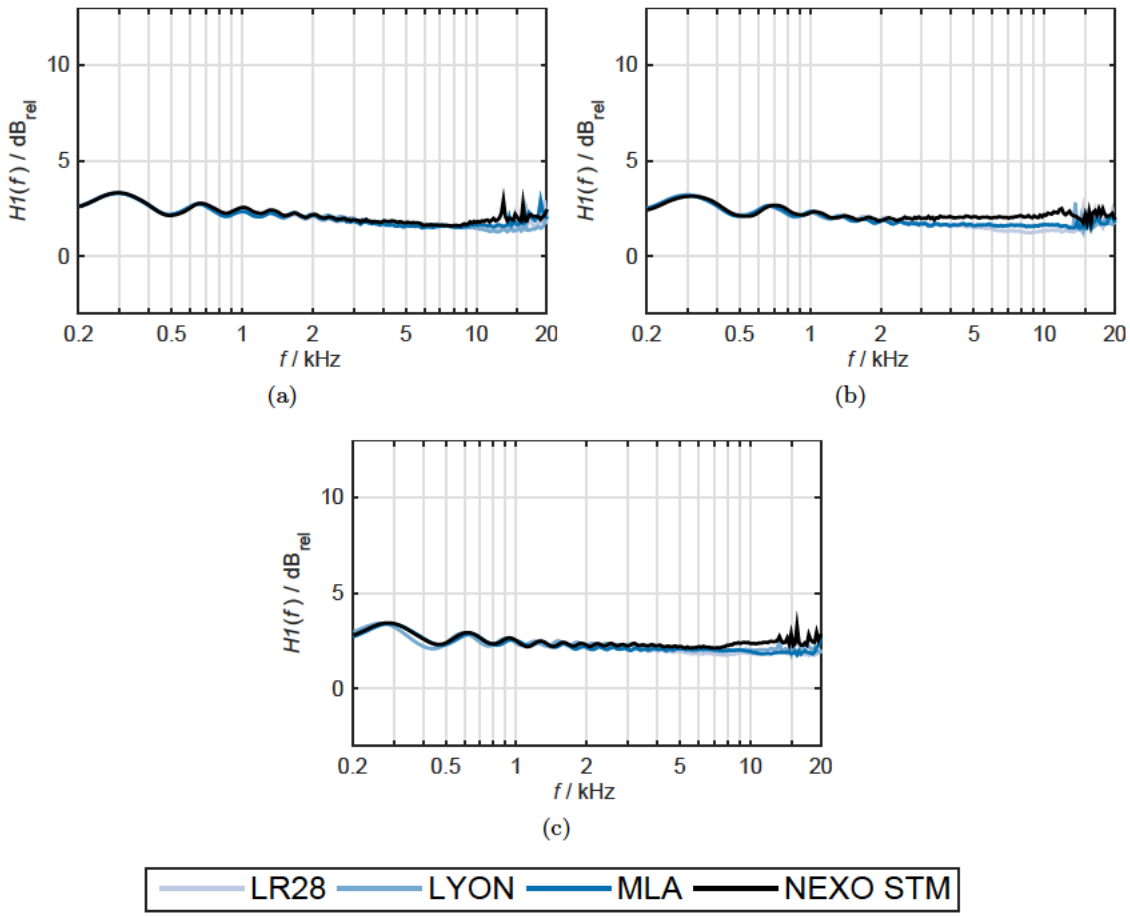

Figure 19: $H1$ for every LSA model used in venue 3: (a) "round", (b) "floor" and (c) "ceil" rounding methods.

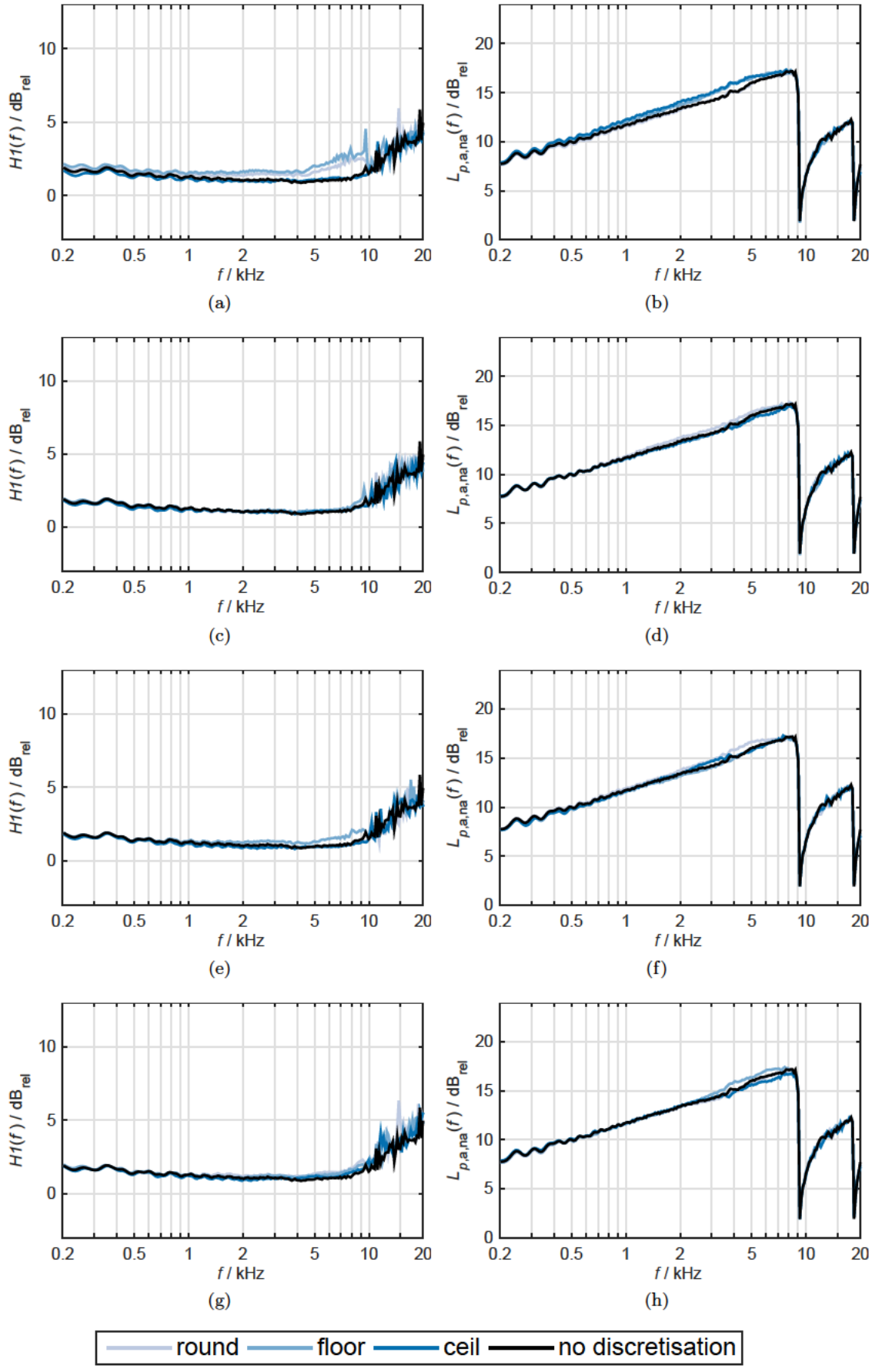

Figure 20: Technical quality measures $H1$ (left column) and $L_{p,\mathrm{a,na}}$ (right column): (a) (b) Alcons LR28, (c) (d) Meyer LYON, (e) (f) Martin Audio MLA and (g) (h) Yamaha NEXO STM (M46) for all analysed rounding types for venue 4 from Fig. 3 d)

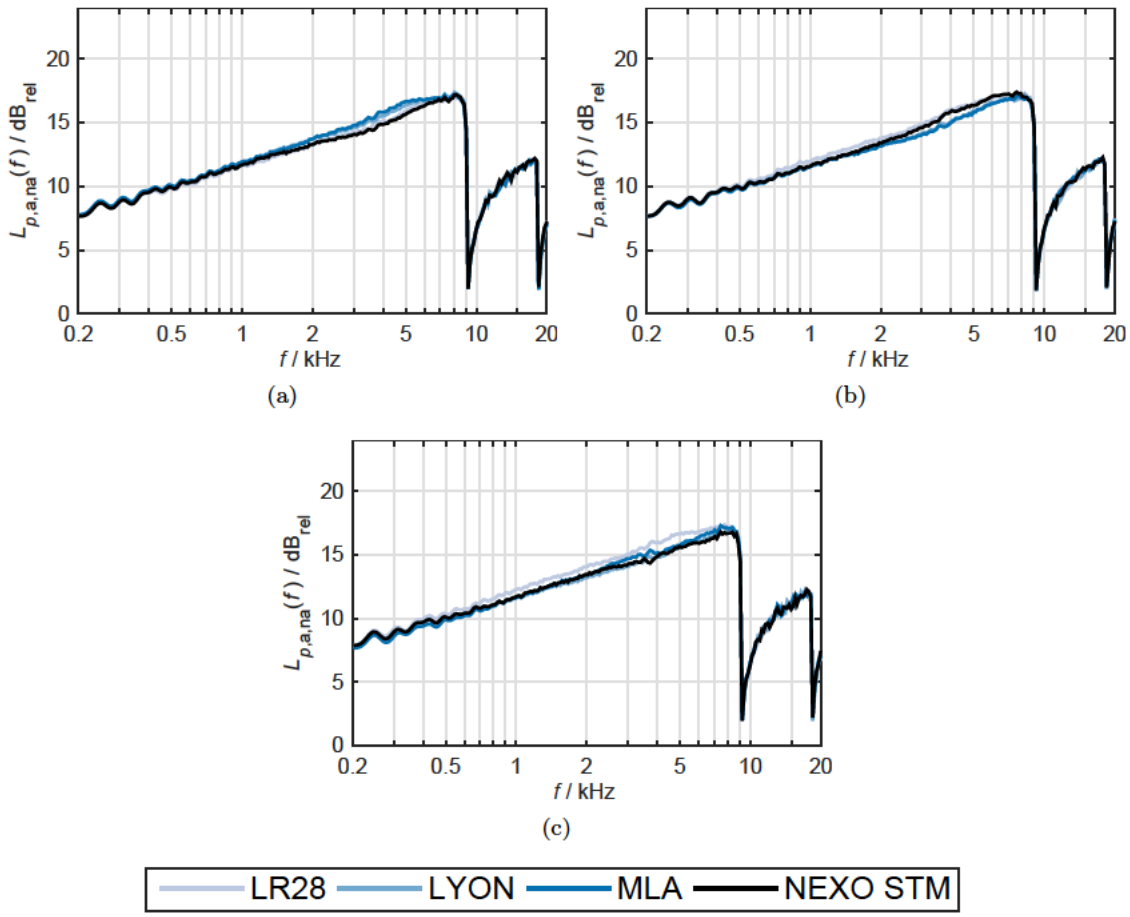

Figure 21: $L_{p,\mathrm{a,na}}$ for every LSA system used in venue 4: (a) "round", (b) "floor" and (c) "ceil" rounding methods.

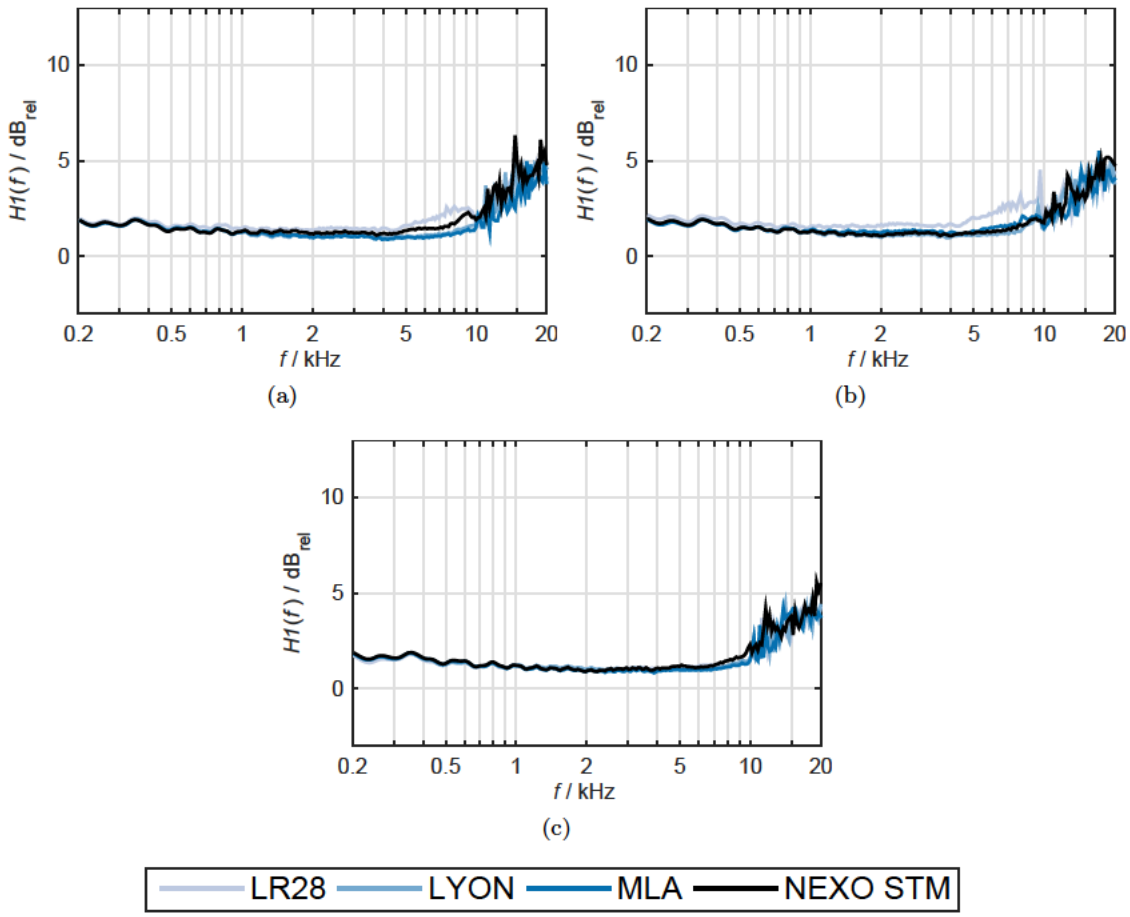

Figure 22: $H1$ for every LSA system used in venue 4: (a) "round", (b) "floor" and (c) "ceil" rounding methods.

with the NEXO STM system the Γ_{aud} error was increased to a value of 0.11. For all the other cases, the Γ_{aud} error did not have to be modified.

Using the Meyer Lyon, Yamaha Nexo STM and Alcons LR28 systems in venue 4, all rounding types offer a very similar sound field homogeneity, but the “ceil" rounding offers better results especially in frequencies lower than 10 kHz as seen in Fig. 20a, 20c and 20g. On the other hand, when using the Martin Audio MLA LSA the rounding type “round” offers a slightly more homogeneous sound field, as can be seen with the quality measure $H1(\omega)$ in Fig. 20e.

The ratio of energy radiated into the audience versus the non-audience zones is very similar for all rounding types, but slightly better for the “ceil" rounding type for the Alcons LR28 system, as seen in Fig. 20b. Fig. 20d and 20f show how the “round” rounding method delivers slightly better results with the Lyon and Martin Audio MLA systems. and finally in Fig. 20h, the “floor” rounding achieves the best results especially between 2 and 8 kHz.

In terms of which LSA system works best with which rounding method, Fig. 21a shows that for the “round” method, the Martin Audio MLA delivers slightly better results in terms of acoustic contrast between the audience and non-audience areas than all other systems, while the Alcons LR28 system stands out providing the most homogeneous sound field for frequencies as high as 10 kHz (Fig. 22a). The Alcons LR28 system provides a higher acoustic contrast between audience and non-audience zones than the other systems up to 6 kHz when using the “floor” rounding method as seen in Fig. 21b. For frequencies over 6 kHz, the best results are achieved with the Yamaha NEXO and the Martin Audio MLA, while the Alcons LR28 stands out once more providing the most homogeneous sound field for frequencies as high as 10 kHz (Fig. 22b). Regarding the “ceil” rounding method concerning the acoustic contrast, the Alcons LR28 performs best throughout most of the frequency range (Fig. 21c). In terms of sound field homogeneity, the Yamaha NEXO delivers the best results throughout the whole frequency spectrum (Fig. 22c).

4.2 Optimisation of the curving of LSAs by means of the goal attainment method

For the evaluation of the geometrical optimisation of the LSAs by means of the goal attainment method, the octave resolution of the frequency vector has been reduced from 1/36 to 1/12, in order to reduce the processing time.

Initially, the optimisation process is applied directly to the angles that result from the PALC algorithm, i.e. non discretised tilt angles, for the four venues. In order to obtain an overall impression of the performance of the goal attainment method, the first step is to carry out the optimisation process for the whole frequency range. In this manner, the algorithm yields a new set of tilt angles which is used to compute the technical quality measures. After a repetitive process of trial and error, three combinations of goal values are selected so as to demonstrate the direct effect that these different optimisation parameters have on the technical quality measures. The results from these combinations of goal values are then graphically compared to the quality measures obtained by the PALC algorithm.

Subsequently, in order to improve the results obtained so far, the optimisation process will be carried out for each frequency band independently and with the same goal values. With this approach, the intention is for the algorithm to find the optimal tilt angles in each venue for each individual frequency band without considering the rest. Each one of the 79 resulting sets of tilt angles contains 16 different angles from

which the inter-cabinet angles will be computed. These angles will be graphically displayed for each venue in order to find a pattern that could assist in the process of optimisation. Naturally, the optimal inter-cabinet angles vary significantly as the frequency increases. At low frequencies, a repetition of inter-cabinet angles along several cabinets is observed; this phenomenon is inversely proportional to the frequency value: as the frequency value increases, each one of the cabinets ends up taking a different tilt angle. Now, it is possible to choose any set of tilt angles belonging to a reference frequency band, and evaluate how the LSA will perform across all frequencies with the chosen set of tilt angles. The variety of the chosen venue geometries and optimisation parameters causes the chosen reference frequency values for the evaluation of the tilt angles to vary significantly among venues and sometimes even among different goal value combinations in the same venue. In some cases, the quality measures resulting from a reference frequency used for one venue and/or goal value combination deliver much worse results for another, therefore other frequencies must be found which yield better results. This does not affect the consistency of the research, since the aim of this thesis is to find the tilt angles that yield the best possible quality measures. The reference frequencies used are situated between 0.5 and 9 kHz.

As a reminder to the reader, ideally the values of acoustic contrast ($L_{p,\mathrm{a,na}}(\omega)$) should be as high as possible and the values of sound field homogeneity ($H1(\omega)$) should be as low as possible through all frequency bands. It is also relevant to mention the considerable computing time necessary for each of these optimisation routines. When executing the PALC algorithm, the computing times are between five and ten minutes, whereas for the goal attainment method, the computing times ascend exponentially to approximately six to eleven hours for each simulation. For lack of better equipment, the simulations and evaluations have been carried out on a standard, inexpensive personal laptop computer.

The results of the evaluation are presented individually for each of the four venues:

VENUE 1

When carrying out the optimisation of the tilt angles for the complete frequency range at once with the goal value combinations 17/0.1, 20/0.1 and 20/0.1, it is observed in Fig. 23a how for the goal value combination 17/0.1, the sound field homogeneity resulting from the goal attainment method is very similar to that of the PALC algorithm, except for some minor deterioration in frequencies higher than 6 kHz. The sound field homogeneity visibly deteriorates in most frequencies when using the two other goal value combinations, namely 20/0.1 and 22/0.1 (Fig. 23c and 23e). On the other hand, the acoustic contrast yields very similar yet slightly improved results when using the goal values 17/0.1 (Fig. 23b), 20/0.1 (Fig. 23d) and 22/0.1 (Fig. 23f).

After evaluating the goal attainment method for all frequencies at the same time, the optimisation is carried out for each frequency band individually, yielding one set of tilt angles each. The chosen goal values are the same three combinations used when optimising for all frequencies. In Fig. 23 we can see the 79 sets of inter-cabinet angles across all frequency bands for every one of the three goal value combinations. Each of the LSA cabinets is represented with a single line ranging from light to dark blue, from the uppermost to the bottom LSA cabinet respectively. It is observed how between 4 and 9 kHz, all angles remain relatively constant, whereas in other frequency bands the variation is more notable. Also worth noting is the fact that as the difference between goal values increases, the value of inter-cabinet angles decreases throughout all frequencies.

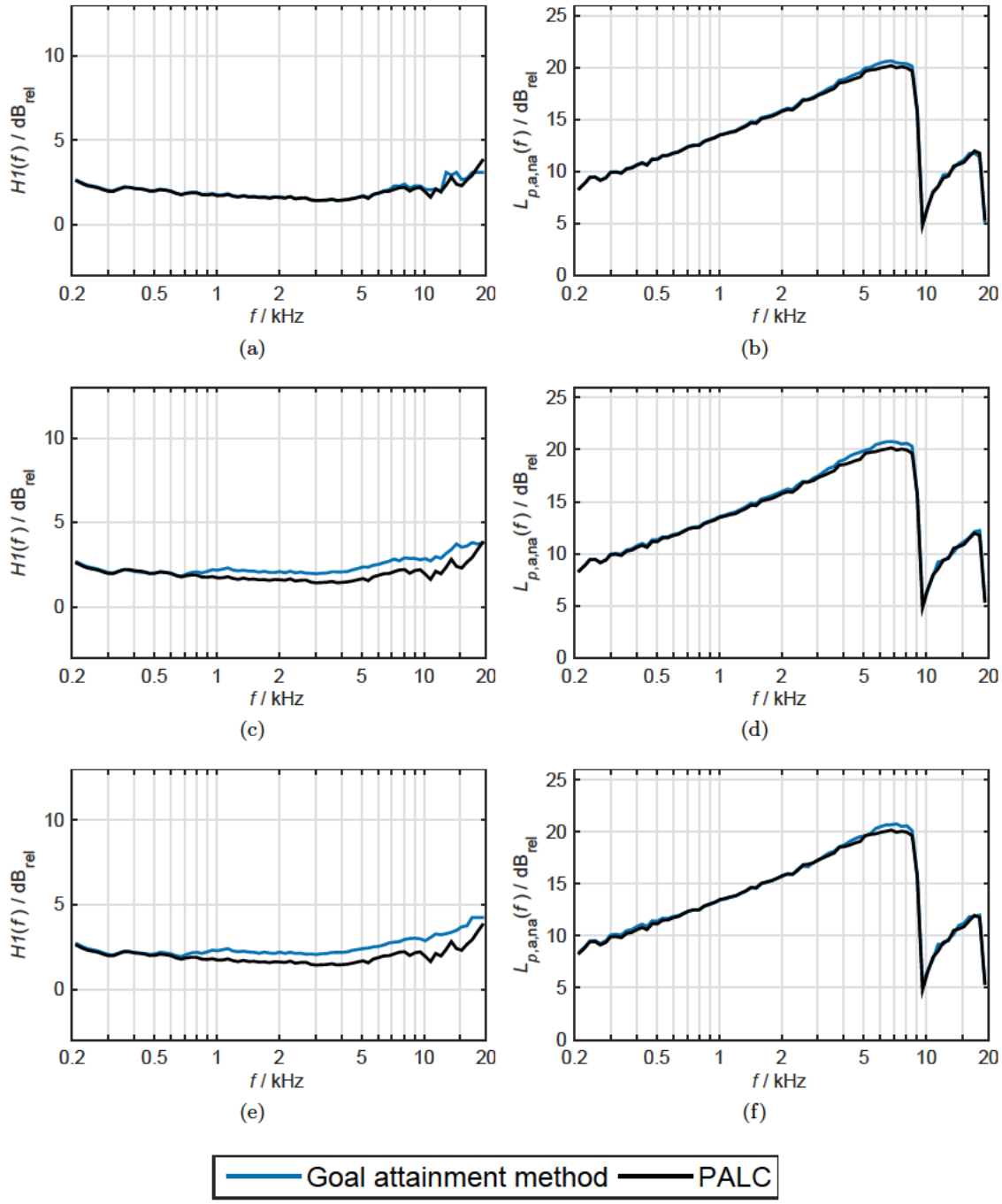

Figure 23: Technical quality measures $H1$ (left column) and $L_{p,\mathrm{a,na}}$ (right column) for goal values 17/0.1 (a) (b), 20/0.1 (c) (d), and 22/0.1 (e) (f) in venue 1.

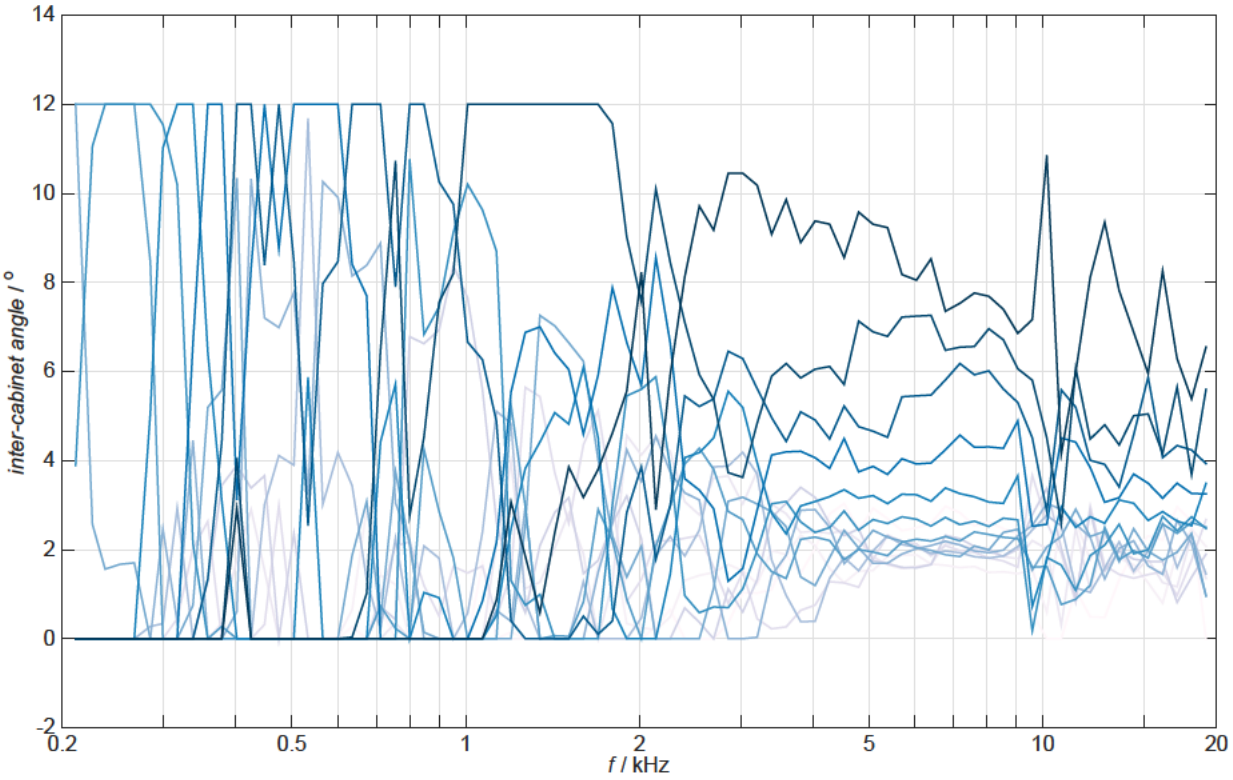
inter-cabinet angle / °
14
12
10
8
6
4
2
0
-2
0.2
0.5
1
2
5
10
20
f / kHz

(a)

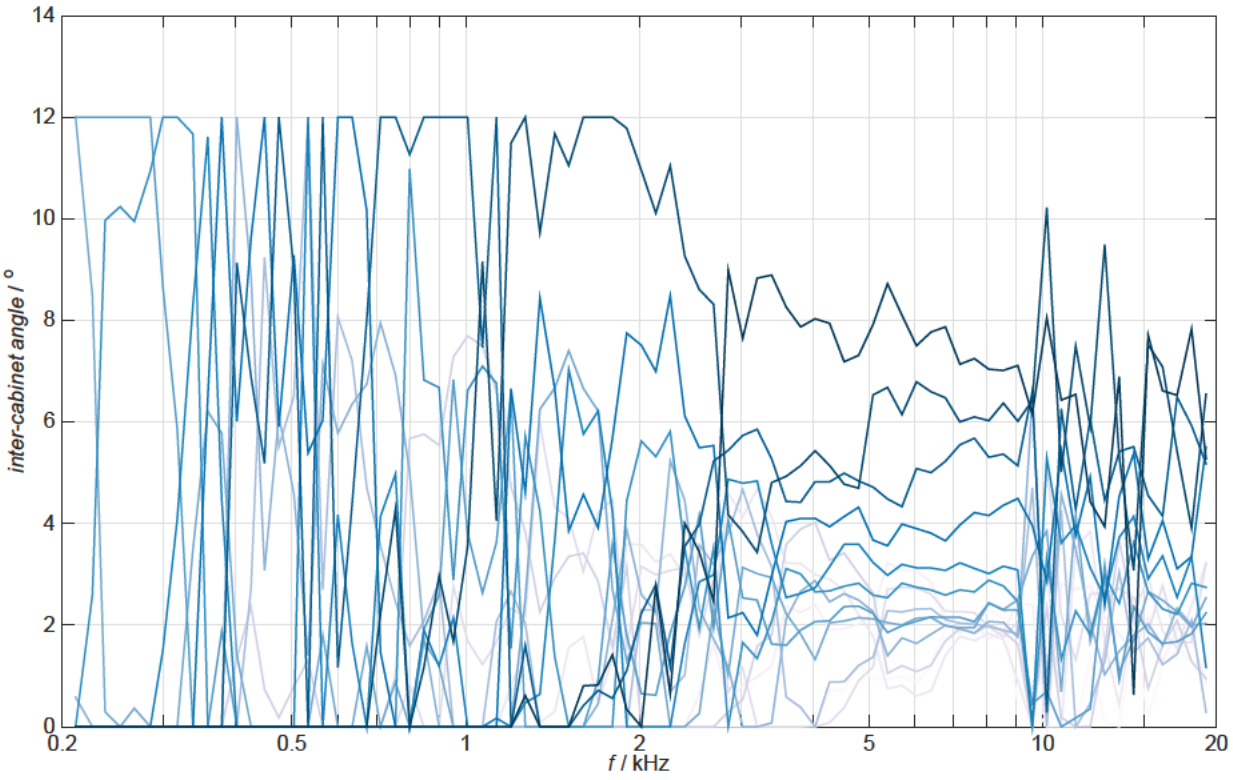
inter-cabinet angle / °
14
12
10
8
6
4
2
0
0.2
0.5
1
2
5
10
20
f / kHz

(b)

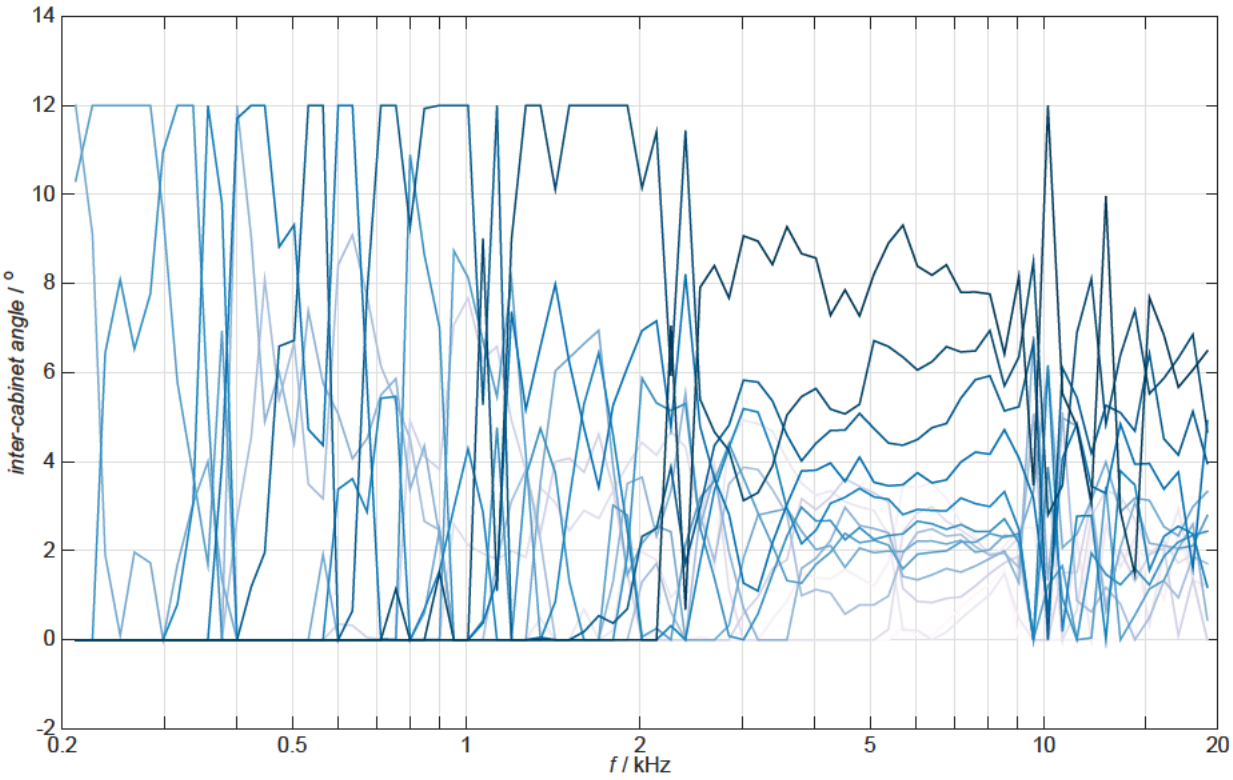

(c)

Figure 23: Tilt angles for all frequency bands when optimising with goal values (a), (b) 20 / 0.1 and (c) 22 / 0.1 for venue 1.

Three frequency bands centred around 0.5, 1 and 4 kHz are chosen as references for further evaluating the performance of the goal attainment method in venue 1. The resulting sets of tilt angles from the optimisation carried out for each single reference frequency are used to obtain the quality measures throughout the whole frequency range, and are then compared to the quality measures obtained using the PALC algorithm.

Regarding the sound field homogeneity, Fig. 24a shows how for reference frequencies 0.5 and 1 kHz a deterioration is observed for all frequencies higher than 0.7 and 1.4 kHz respectively. When the chosen reference frequency is 4 kHz, an improvement in the sound field homogeneity is observed for frequencies below 12 kHz followed by a slight deterioration in higher frequencies. As the difference between goal values increases, so does the deterioration of the sound field homogeneity, which extends down to 0.65, 1.2 and 10 kHz for the goal values 20/0.1 (Fig. 24c) and dominates the whole frequency range for reference frequencies 0.5 and 1 kHz, while for the reference frequency 4 kHz extends down to 8 kHz for the goal values 22/0.1 (Fig. 24e).

On the other hand, as seen in Fig. 24b, 24d and 24f the improvement of one quality measure comes at the expense of the other, demonstrating clearly the principle of non-inferiority. There are notable improvements observed in the acoustic contrast: for the goal values 17/0.1 (Fig. 24b), the goal attainment method yields better results for all frequencies over 0.4 and 1 kHz when optimising for 0.5 and 1 kHz, whereas for the 4 kHz reference frequency it is deteriorated throughout the whole frequency range. For the goal value combination 20/0.1 (Fig. 24d the results are slightly better, showing improvement throughout all frequencies when optimising for 500 Hz, for all frequencies

over 550 Hz when optimising for 1 kHz, and a subtle deterioration for all frequencies when optimising for 4 kHz. For the goal value combination 22/0.1 24f), the results are improved, yielding a better acoustic contrast throughout the whole frequency range except when optimising for the 4 kHz reference frequency, where a slight deterioration takes place mostly below 5.5 kHz.

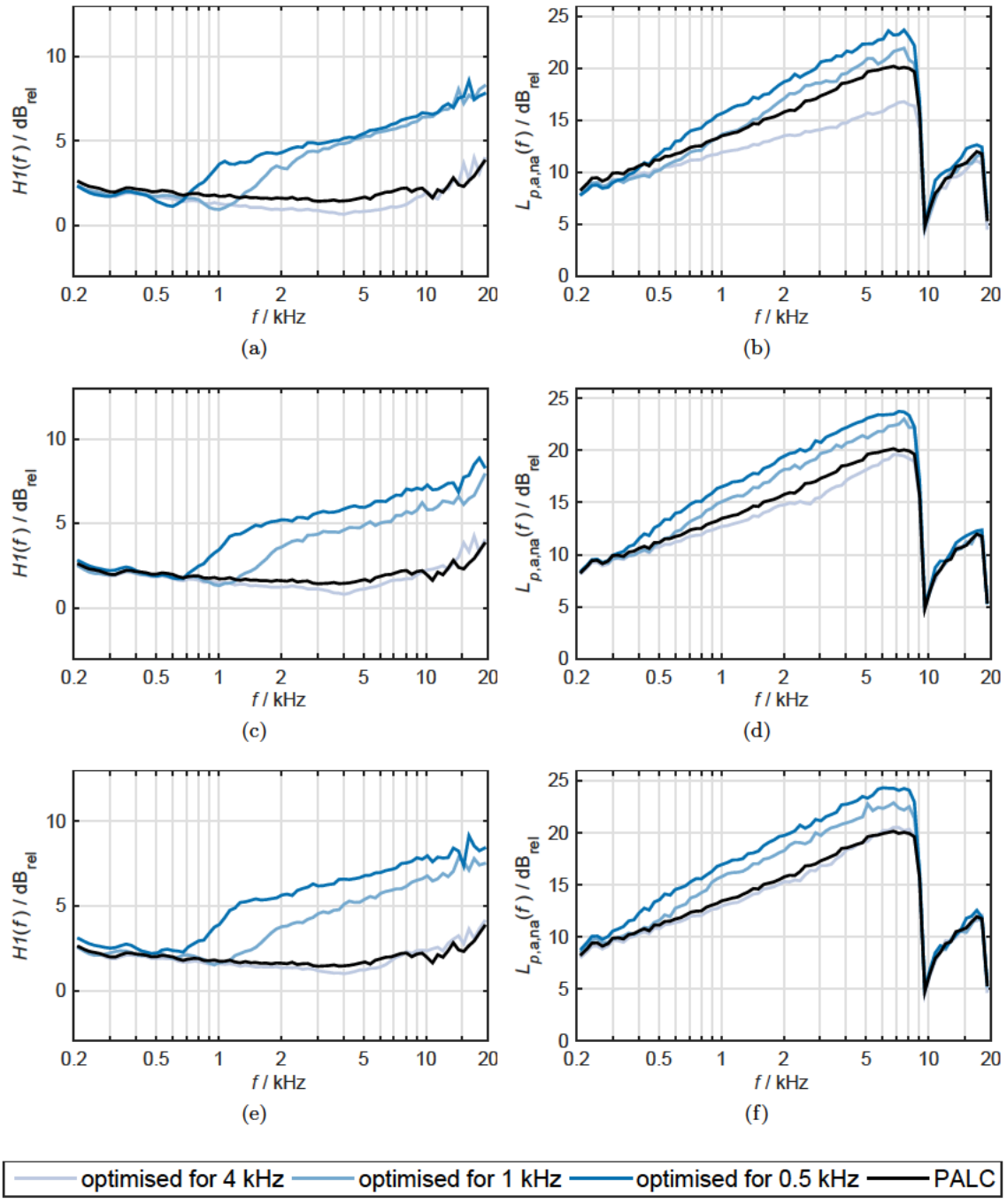

Figure 24: Technical quality measures $H1$ (left column) and $L_{p,\mathrm{a,na}}$ (right column) for goal values 17/0.1 (a) (b), 20/0.1 (c) (d), and 22/0.1 (e) (f) in venue 1.

VENUE 2

When carrying out the optimisation of the tilt angles for the complete frequency range at once with the goal value combinations 17/0.1, 20/0.1 and 20/0.1, it is observed in Fig. 25a how for the goal value combination 17/0.1, the sound field homogeneity resulting from the goal attainment method has improved in comparison to the PALC algorithm, except for some deterioration in frequencies higher than 5 kHz. This deterioration extends to lower frequencies as the difference between goal values increases, namely 20/0.1 and 22/0.1 (Fig. 25c and 25e). In the latter, the deterioration extends to all frequencies over 400 Hz. On the other hand, the acoustic contrast yields also similar yet slightly deteriorated results in comparison to the PALC algorithm when using the goal values 17/0.1 (Fig. 25b). For the goal values 20/0.1 (Fig. 25d), the acoustic contrast is almost identical to that of the PALC algorithm except for some minor deterioration, and for goal values 22/0.1 (Fig. 25f), the acoustic contrast shows visible improvement throughout the whole frequency range.

After evaluating the goal attainment method for all frequencies at the same time, the optimisation is carried out for each frequency band individually, yielding one set of tilt angles each. The chosen goal values are the same three combinations used when optimising for all frequencies. In Fig. 25 we can see the 79 sets of inter-cabinet angles across all frequency bands for every one of the three goal value combinations. Each of the LSA cabinets is represented with a single line ranging from light to dark blue, from the uppermost to the bottom LSA cabinet respectively. It is observed how between 3 and 9 kHz, all angles remain relatively constant, whereas in other frequency bands the variation is more notable. Also worth noting is the fact that as the difference between goal values increases, the value of inter-cabinet angles decreases throughout all frequencies.

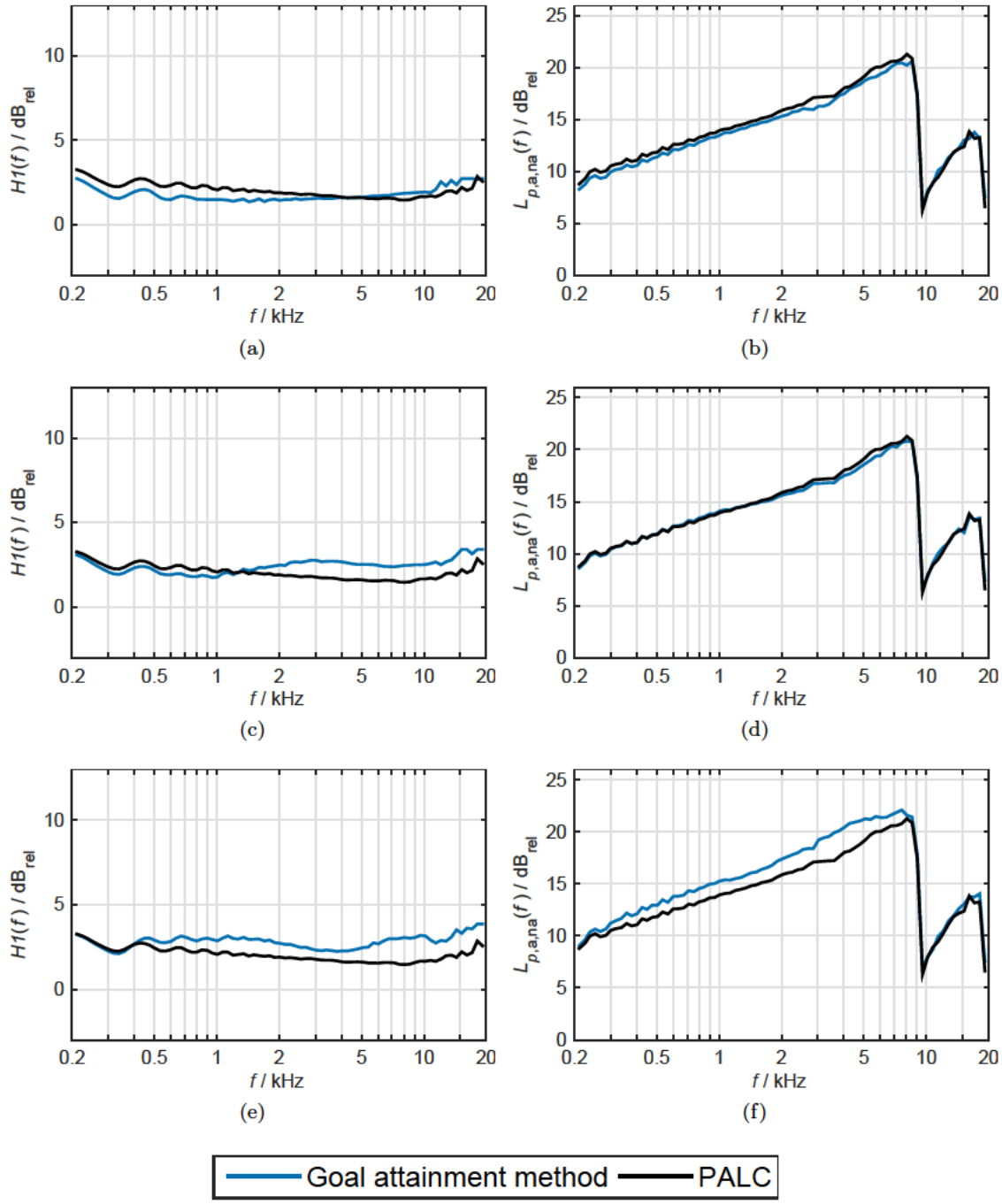

Figure 25: Technical quality measures $H1$ (left column) and $L_{p,\mathrm{a,na}}$ (right column) for goal values 17/0.1 (a) (b), 20/0.1 (c) (d), and 22/0.1 (e) (f) in venue 2.

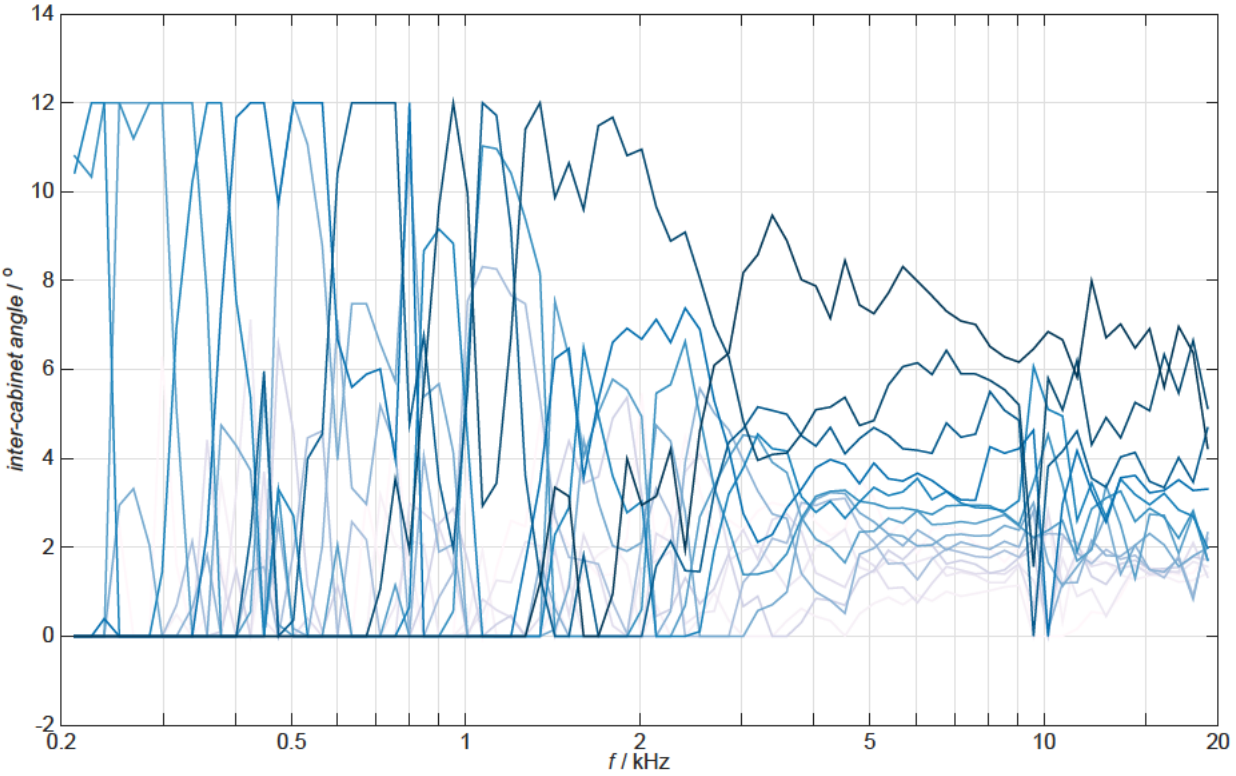
inter-cabinet angle / °
14
12
10
8
6
4
2
0
-2
0.2
0.5
1
2
5
10
20
f / kHz

(a)

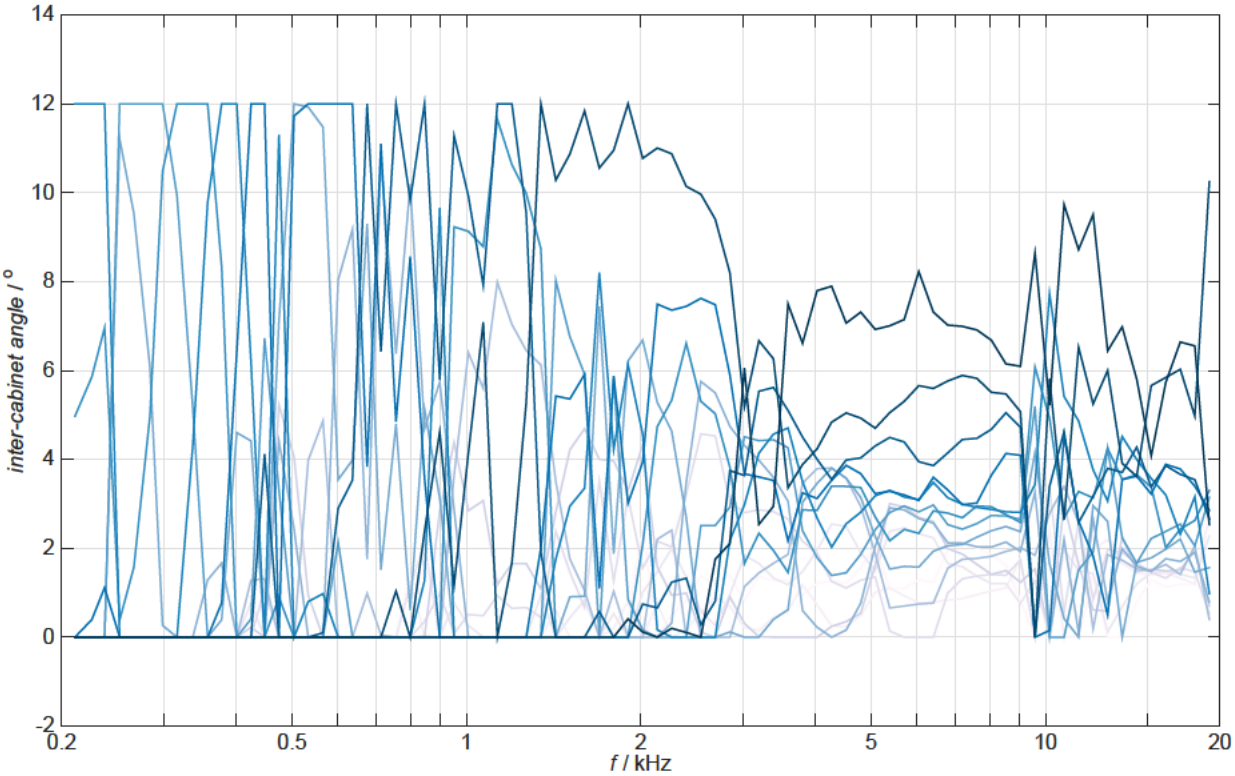
inter-cabinet angle / °
14
12
10
8
6
4
2
0
-2
0.2
0.5
1
2
5
10
20
f / kHz

(b)

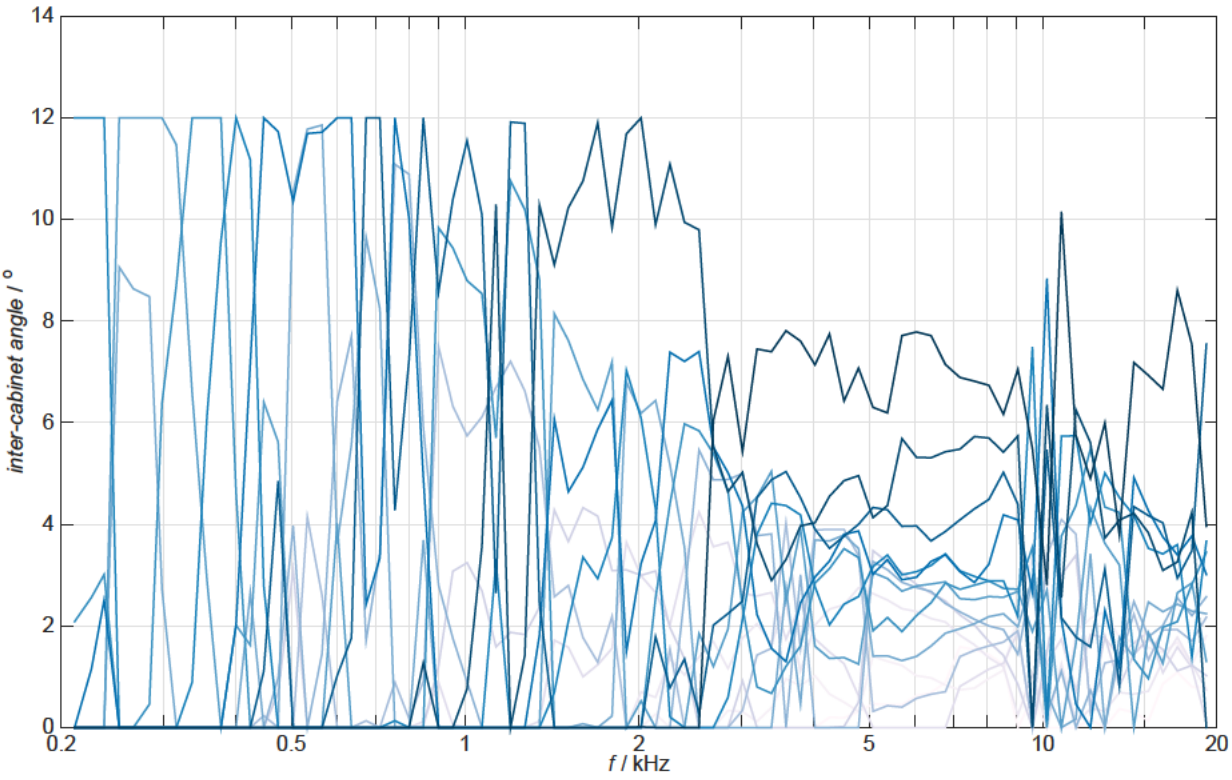

(c)

Figure 25: Tilt angles for all frequency bands when optimising with goal values (a), (b) 20 / 0.1 and (c) 22 / 0.1 for venue 2.

Three frequency bands centred around 0.75, 4.2, and 6 kHz for goal values 17/0.1; 0.65, 1.2, and 9 kHz for goal values 20/0.1; and 0.65, 1 and 5.4 kHz for goal values 22/0.1 are chosen as references for further evaluating the performance of the goal attainment method in venue 2. The resulting sets of tilt angles from the optimisation carried out for each single reference frequency are used to obtain the quality measures throughout the whole frequency range, and are then compared to the quality measures obtained using the PALC algorithm.

Regarding the sound field homogeneity, Fig. 26a shows how for 750 Hz, the sound field homogeneity is notably deteriorated over the 1 kHz mark. Optimising for 4.2 kHz, an improved sound field is obtained except for frequencies over 10 kHz; and for the reference frequency 6 kHz a visible improvement is obtained on most of the frequency range. As the difference between goal values increases, so does the deterioration of the sound field homogeneity, which extends down to 0.9 and 1.5 kHz for the goal values 20/0.1 (Fig. 26c) and reference frequencies 0.65 and 1.2 kHz, while the sound field resulting from reference frequency 9 kHz is more homogeneous throughout most of the frequency range. For the goal values 22/0.1 (Fig. 26e), all results are deteriorated in relation to goal values 20/0.1, especially when optimising for reference frequencies 0.65 and 1 kHz. The reference frequency 5.4 kHz delivers an improved sound field up to 7.5 kHz, where it deteriorates for all high frequencies.

On the other hand, Fig. 26b shows how the goal attainment method yields worse acoustic contrast results than the PALC algorithm for all frequencies for goal values 17/0.1. For the other two goal value combinations, 20/0.1 and 22/0.1 (Fig. 26d and 26f), when optimising for the two lower reference frequencies, namely 0.65 and 1.2 kHz,

and 0.65 and 1 kHz respectively, the results are outstanding, yielding a much better acoustic contrast throughout the whole frequency range. When optimising for 9 kHz and goal values 20/0.1, the acoustic contrast is slightly deteriorated in comparison to the PALC results, and when optimising for 5.4 kHz and goal values 22/0.1, the acoustic contrast improves, but is still slightly worse than the PALC results throughout the whole frequency range.

VENUE 3

When carrying out the optimisation of the tilt angles for the complete frequency range at once with the goal value combinations 17/0.1, 20/0.1 and 20/0.1, it is observed in Fig. 27a how for the goal value combination 17/0.1, the sound field homogeneity resulting from the goal attainment method is similar to that of the PALC algorithm, except for some improvement under 1 kHz and a visible deterioration on frequencies over 1 kHz. The sound field homogeneity visibly deteriorates in most frequencies when using the two other goal value combinations, namely 20/0.1 and 22/0.1 (Fig. 27c and 27e). On the other hand, the acoustic contrast mostly deteriorates when using the goal values 17/0.1 (Fig. 27b) and shows deterioration under 3 kHz and a visible improvement on frequencies over 4 kHz when using the goal values 20/0.1 (Fig. 27d). Regarding the goal value combination 22/0.1, a slight deterioration is observed for frequencies below 1.3 kHz, and a notable improvement on higher frequencies (Fig. 27f).

After evaluating the goal attainment method for all frequencies at the same time, the optimisation is carried out for each frequency band individually, yielding one set of tilt angles each. The chosen goal values are the same three combinations used when optimising for all frequencies. In Fig. 27 we can see the 79 sets of inter cabinet angles across all frequency bands for every one of the three goal value combinations. Each of the LSA cabinets is represented with a single line ranging from light to dark blue, from the uppermost to the bottom LSA cabinet respectively. The first notable characteristic of the three graphics is that all angles remain relatively constant between the frequencies 4 and 9 kHz. Also worth noting is the fact that the value of the inter-cabinet angles appears to decrease throughout the whole frequency range as the difference between goal values increases.

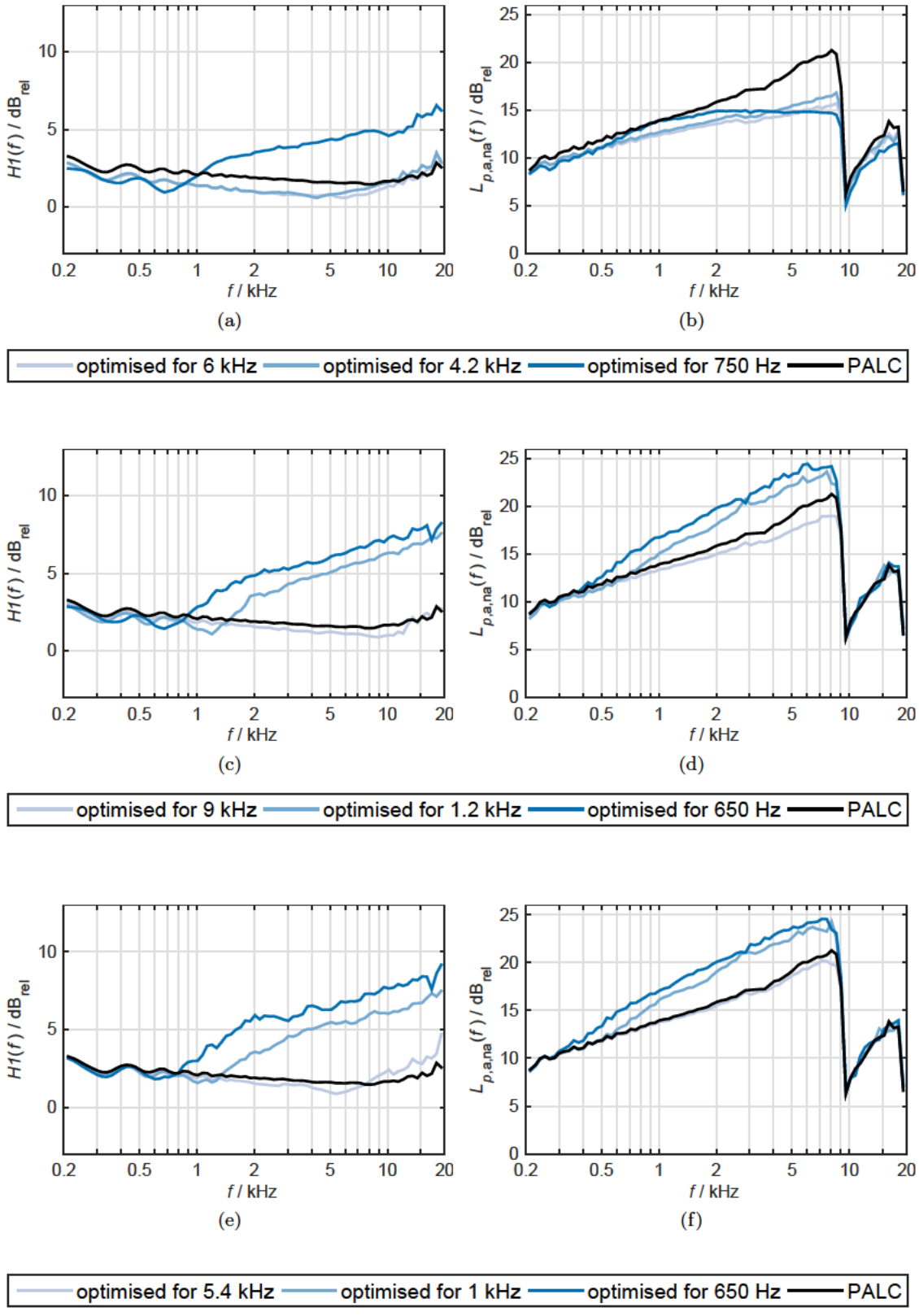

Figure 26: Technical quality measures $H1$ (left column) and $L_{p,\mathrm{a,na}}$ (right column) for goal values 17/0.1 (a) (b), 20/0.1 (c) (d), and 22/0.1 (e) (f) in venue 2.

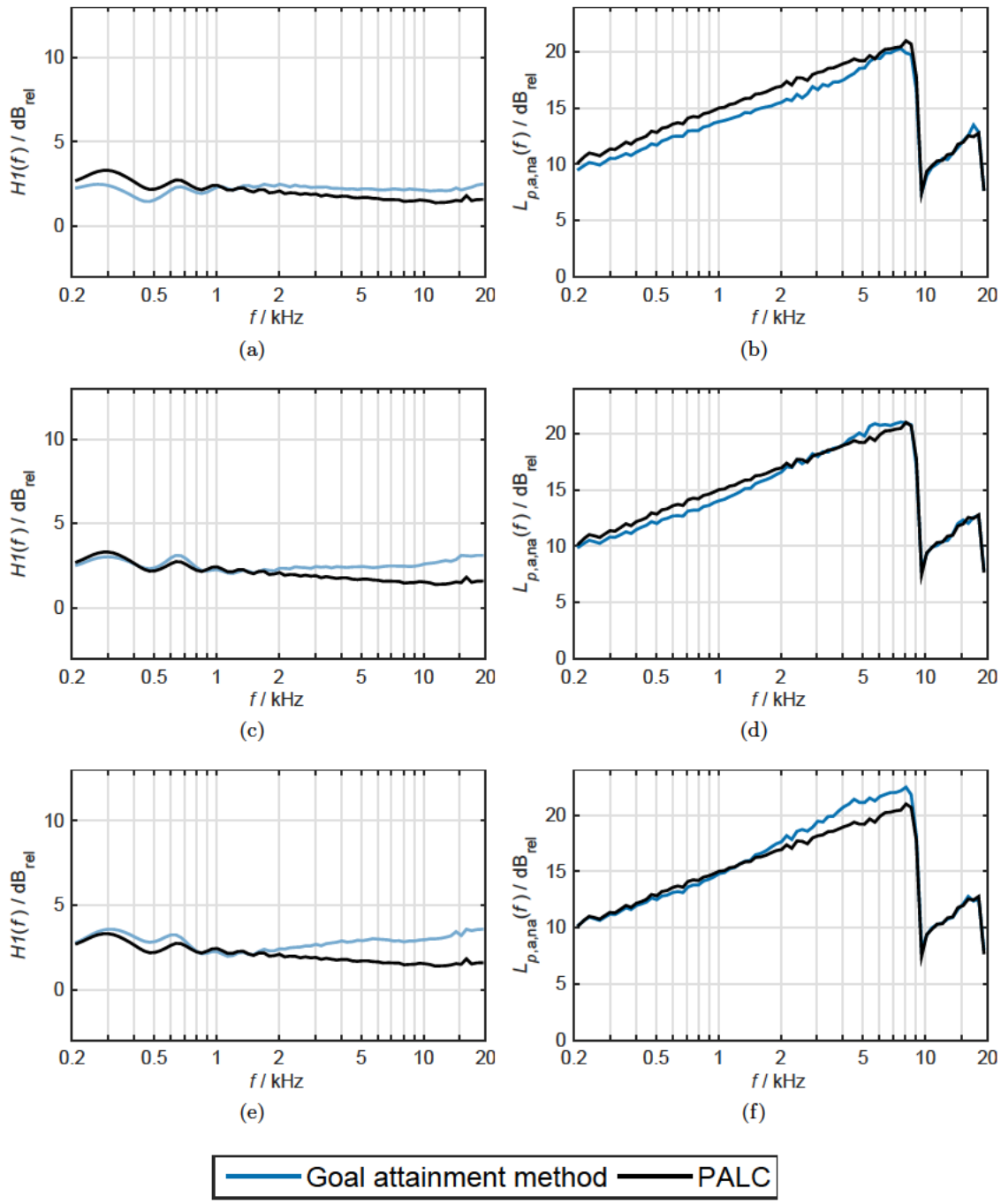

Figure 27: Technical quality measures $H1$ (left column) and $L_{p,\mathrm{a,na}}$ (right column) for goal values 17/0.1 (a) (b), 20/0.1 (c) (d), and 22/0.1 (e) (f) in venue 3.

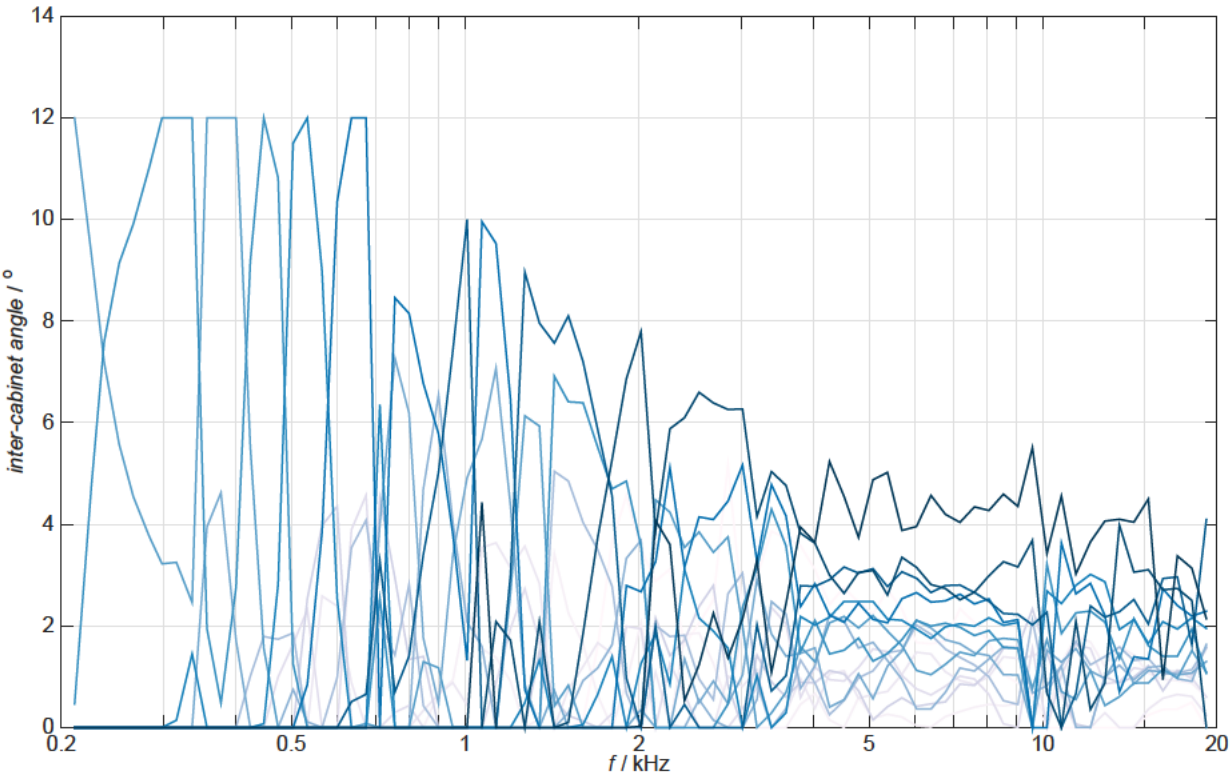
inter-cabinet angle / °
f / kHz
0
2
4
6
8
10
12
14
0.2
0.5
1
2
5
10
20

(a)

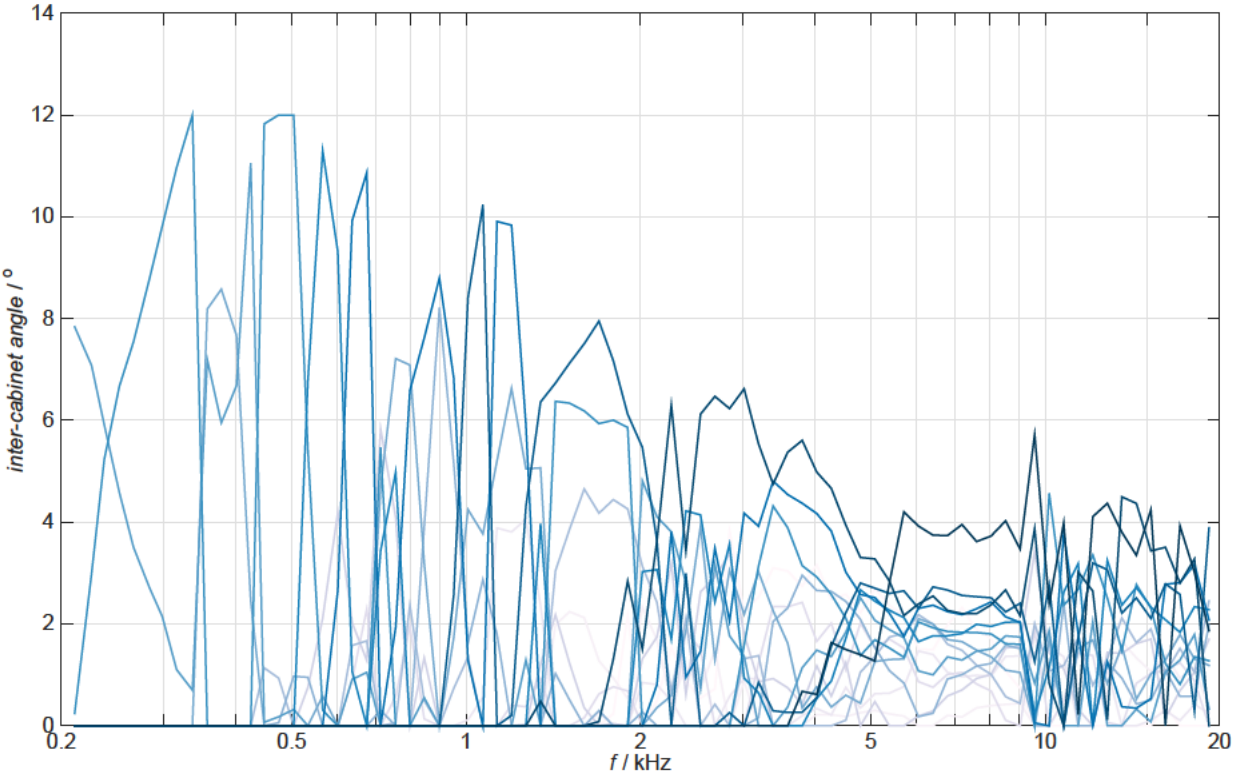
inter-cabinet angle / °
f / kHz
0
2
4
6
8
10
12
14
0.2
0.5
1
2
5
10
20

(b)

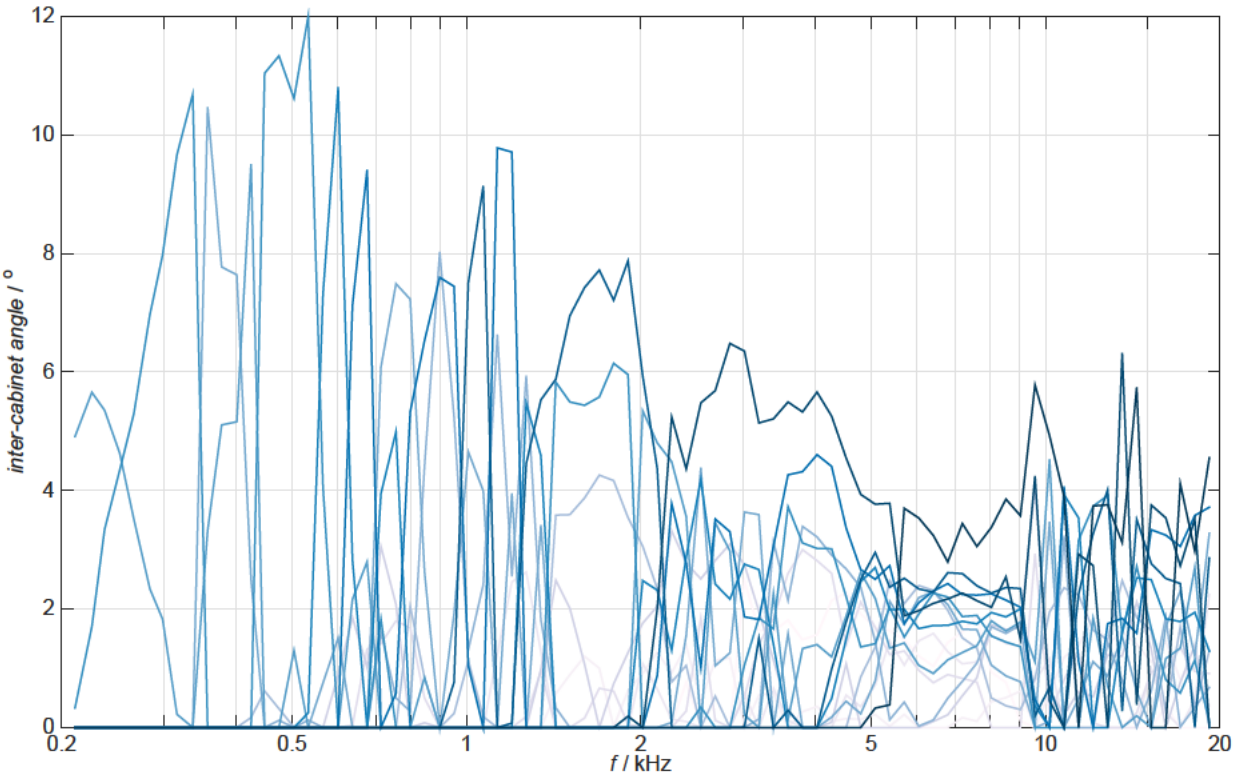

(c)

Figure 27: Tilt angles for all frequency bands when optimising with goal values 17/0.1 (a), 20/0.1 (b), and 22/0.1 (c) for venue 3.

Three frequency bands centred around 0.5, 6 and 9 kHz are chosen as references for further evaluating the performance of the goal attainment method for all three goal value combinations in venue 3. The resulting sets of tilt angles from the optimisation carried out for each single reference frequency are used to obtain the quality measures throughout the whole frequency range, and are then compared to the quality measures obtained from the PALC algorithm.

Regarding the sound field homogeneity, Fig. 28a shows how for the reference frequency 500 Hz and the goal values 17/0.1 a great deterioration is observed for frequencies higher than 750 Hz. As for the other reference frequencies, 6 and 9 kHz, the sound field homogeneity is visibly improved up to 12 kHz and for the whole frequency range respectively. As the difference between goal values increases, so does the deterioration of the sound field homogeneity, which extends down to 0.6 for the reference frequency 500 Hz and goal values 20/0.1 (Fig. 28c). As for the other reference frequencies, 6 and 9 kHz, the sound field deteriorates slightly for frequencies higher than 12 kHz, but is more homogeneous than the one resulting from the PALC algorithm for the rest of the frequency range. Finally, for the goal values 22/0.1, the sound field deteriorates further for all cases, leaving the results for the reference frequencies 6 and 9 kHz deteriorated for frequencies over 10 kHz and 12 kHz respectively, and slightly improved for all lower frequencies.

On the other hand, regarding the acoustic contrast, Fig. 28b, 28d and 28f show how following the principle of non-inferiority, the results that the reference frequencies 6 and 9 kHz yield are in general deteriorated, and the results from the reference frequency 500 Hz are improved in comparison to the PALC algorithm. All three results further

improve as the difference between goal values increases. For the goal values 22/0.1 optimising for the reference frequency 9 kHz, a slightly improved acoustic contrast in comparison to the PALC algorithm is obtained. This case is interesting, since it is the first so far to have an improved acoustic contrast together with an improved sound field homogeneity for all frequencies below 12 kHz.

VENUE 4

When carrying out the optimisation of the tilt angles for the complete frequency range at once with the goal value combinations 17/0.1, 20/0.1 and 22/0.1, it is observed in Fig. 29a how for the goal value combination 17/0.1, the sound field homogeneity resulting from the goal attainment method is very similar to that of the PALC algorithm, except for a minor improvement under 1.5 kHz and a slight punctual deterioration around 9.5 kHz. The sound field homogeneity visibly deteriorates in most frequencies when using the two other goal value combinations, namely 20/0.1 and 22/0.1 (Fig. 29c and 29e).

On the other hand, the acoustic contrast yields very similar yet slightly deteriorated results when using the goal values 17/0.1 (Fig. 29b) and shows visible improvement on frequencies higher than 1 kHz when using the goal values 20/0.1 (Fig. 29d). Regarding the third goal value combination, 22/0.1, a general deterioration is observed for frequencies below 6 kHz, and a visible improvement on higher frequencies (Fig. 29f).

Once again, caused by the principle of non-inferiority, the cases where the acoustic contrast is improved yield a deteriorated sound field, and vice versa.

After evaluating the goal attainment method for all frequencies at the same time, the optimisation is carried out for each frequency band individually, yielding one set of tilt angles each. The chosen goal values are the same three combinations used when optimising for all frequencies. In Fig. 29 we can see the 79 sets of inter-cabinet angles across all frequency bands for every one of the three goal value combinations. Each of the LSA cabinets is represented with a single line ranging from light to dark blue, from the uppermost to the bottom LSA cabinet respectively. It is observed how between 4 and 9 kHz, all angles remain relatively constant, whereas in other frequency bands the variation is more notable. Also worth noting is the fact that, although in this case more subtly than on venue 3, as the difference between goal values increases, the value of inter-cabinet angles decreases throughout all frequencies.

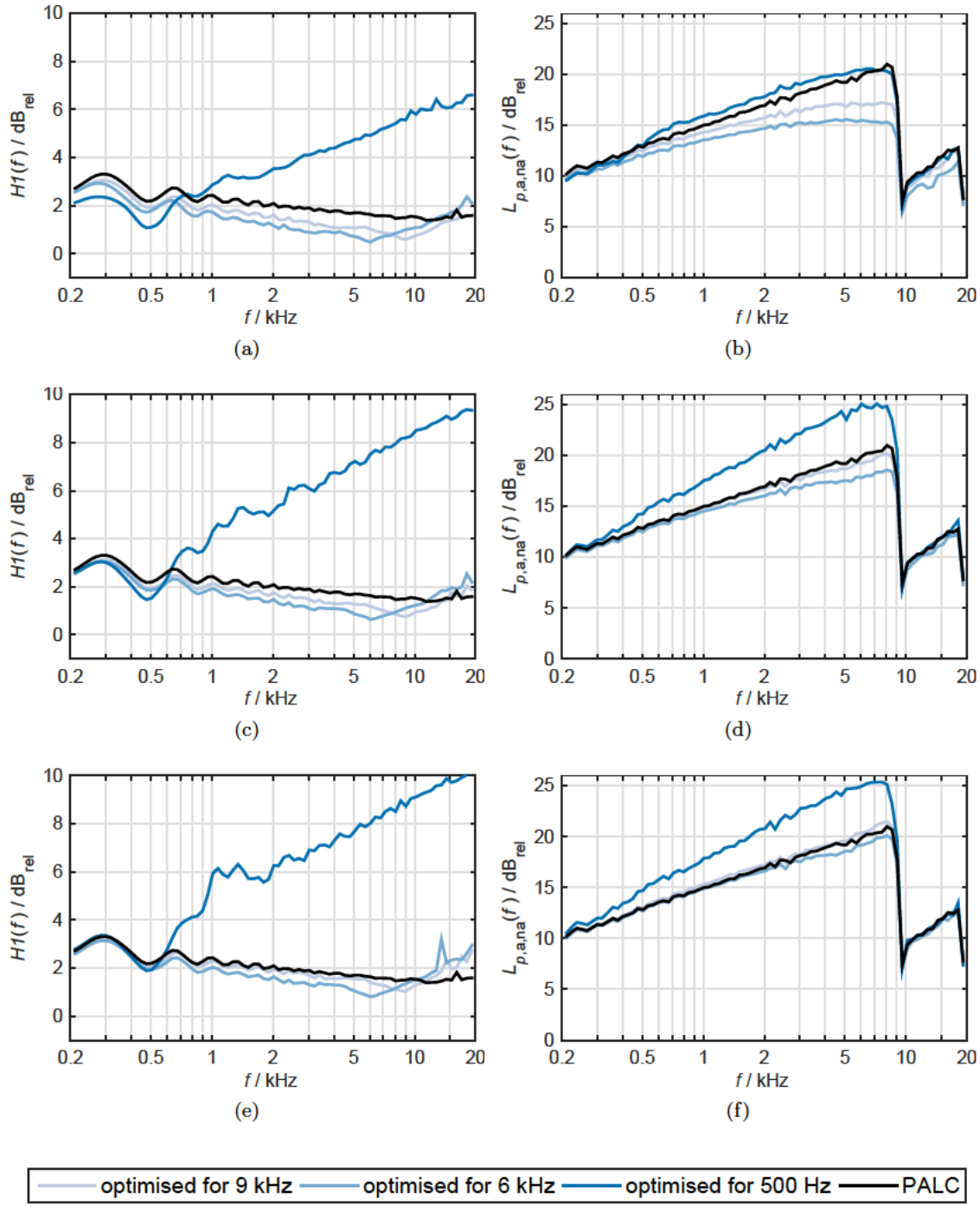

Figure 28: Technical quality measures $H1$ (left column) and $L_{p,\mathrm{a,na}}$ (right column) for goal values 17/0.1 (a) (b), 20/0.1 (c) (d), and 22/0.1 (e) (f) in venue 3.

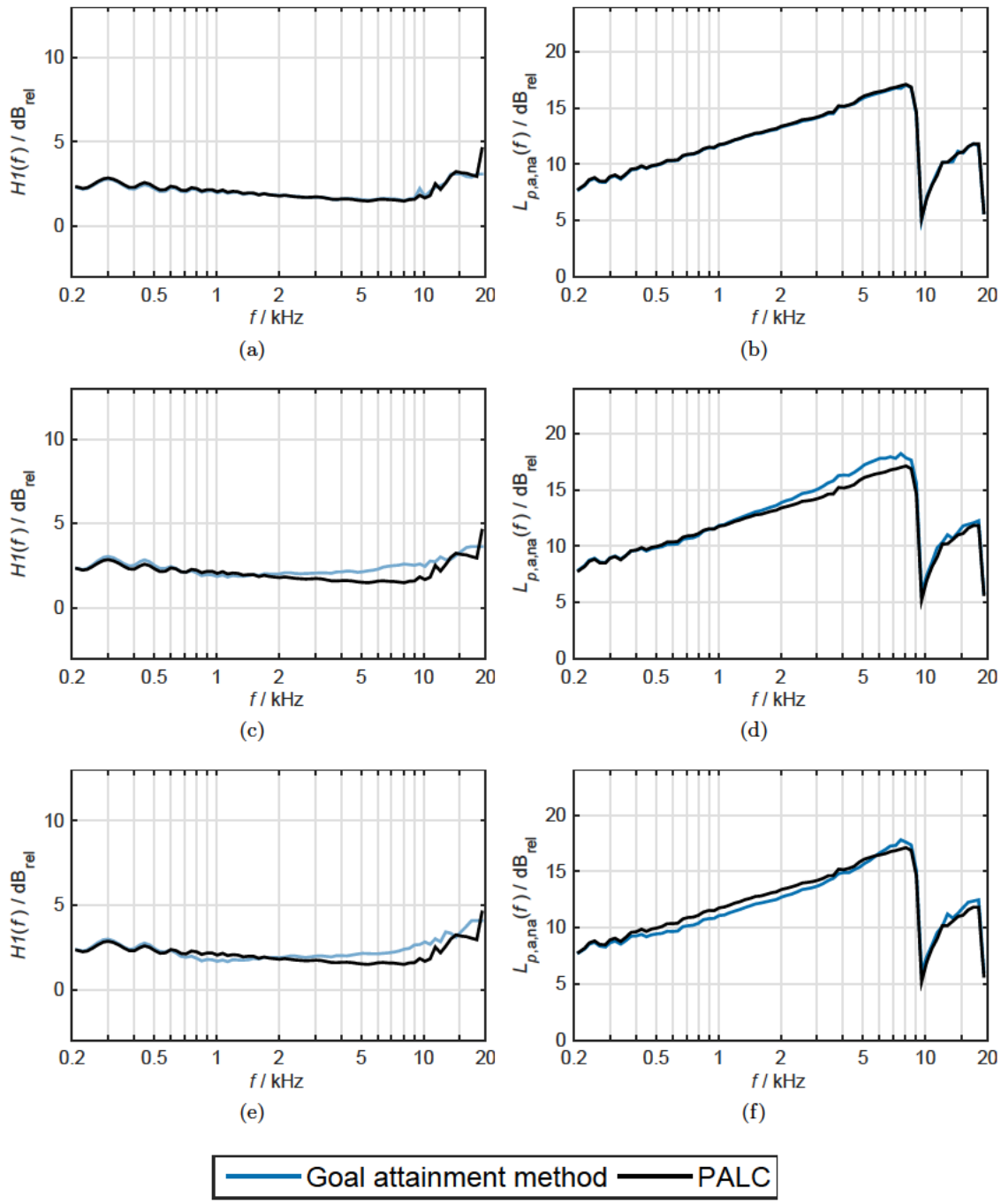

Figure 29: Technical quality measures $H1$ (left column) and $L_{p,\mathrm{a,na}}$ (right column) for goal values 17/0.1 (a) (b), 20/0.1 (c) (d), and 22/0.1 (e) (f) in venue 4.

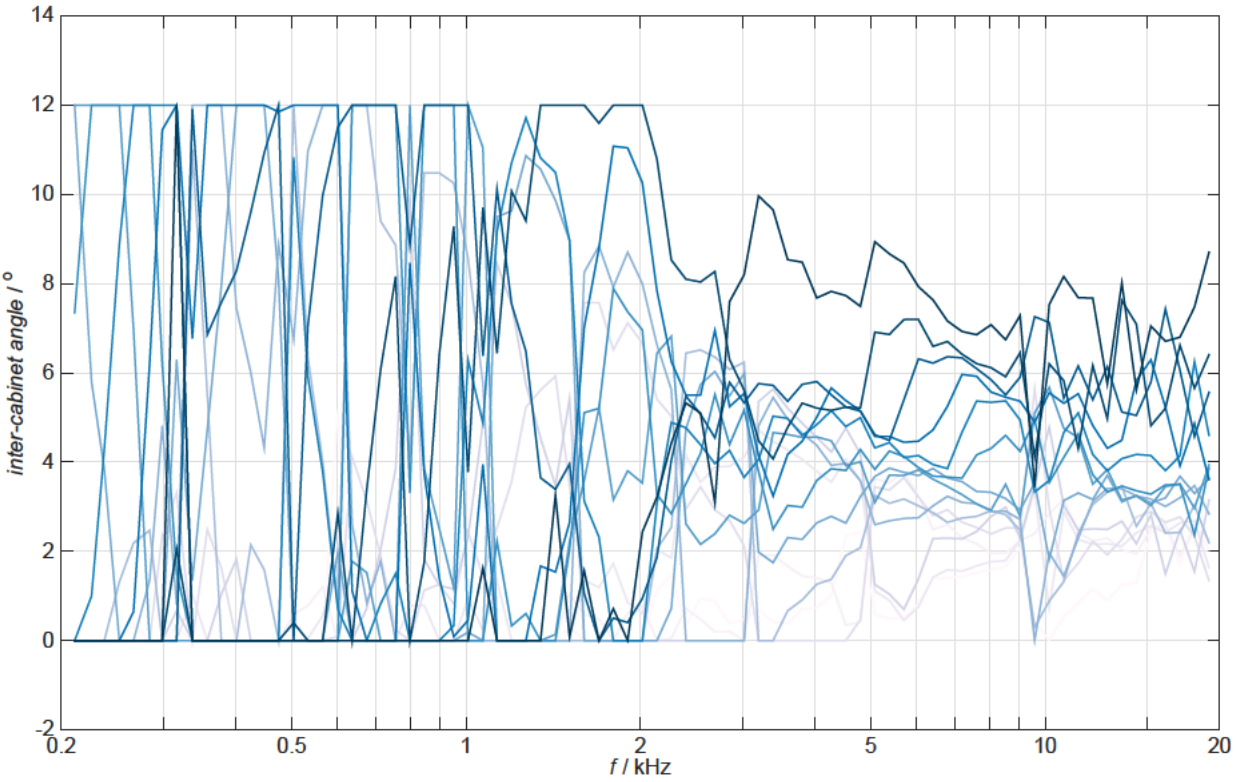
14
12
10
8
6
4
2
0
-2
inter-cabinet angle / °
0.2
0.5
1
2
5
10
20
f / kHz

(a)

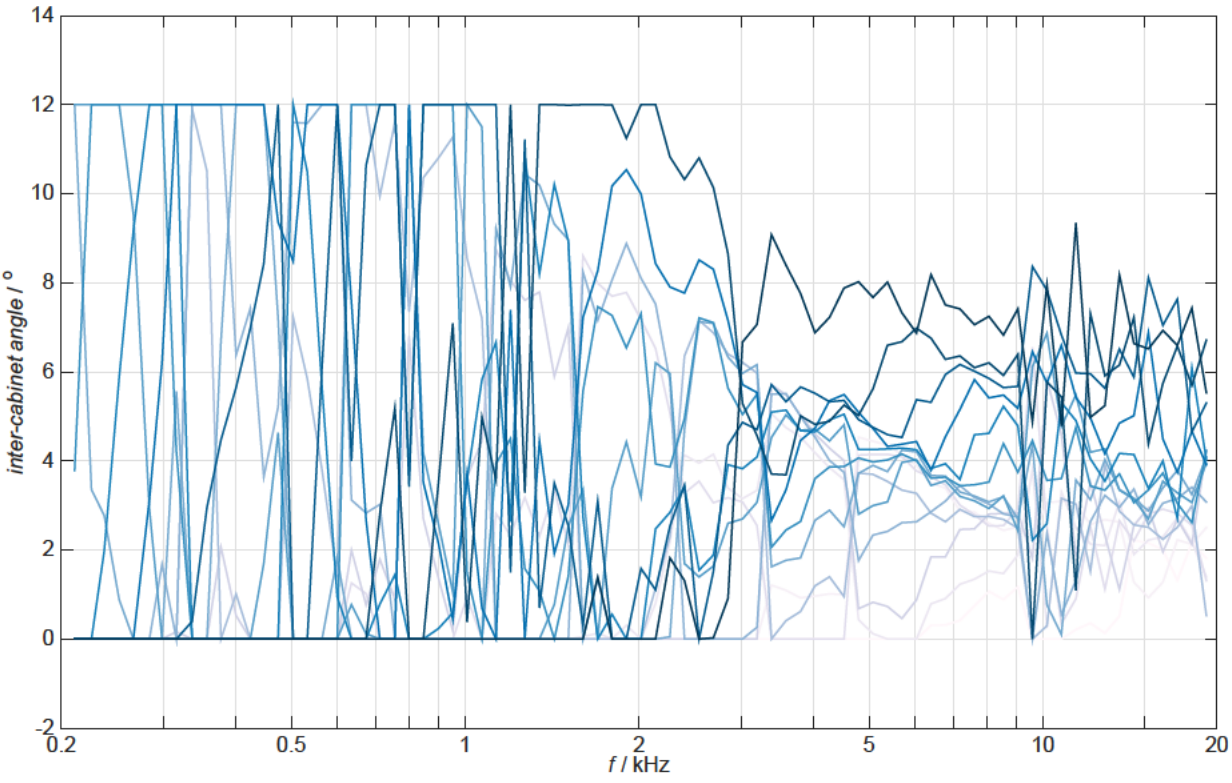
14
12
10
8
6
4
2
0
-2
inter-cabinet angle / °
0.2
0.5
1
2
5
10
20
f / kHz

(b)

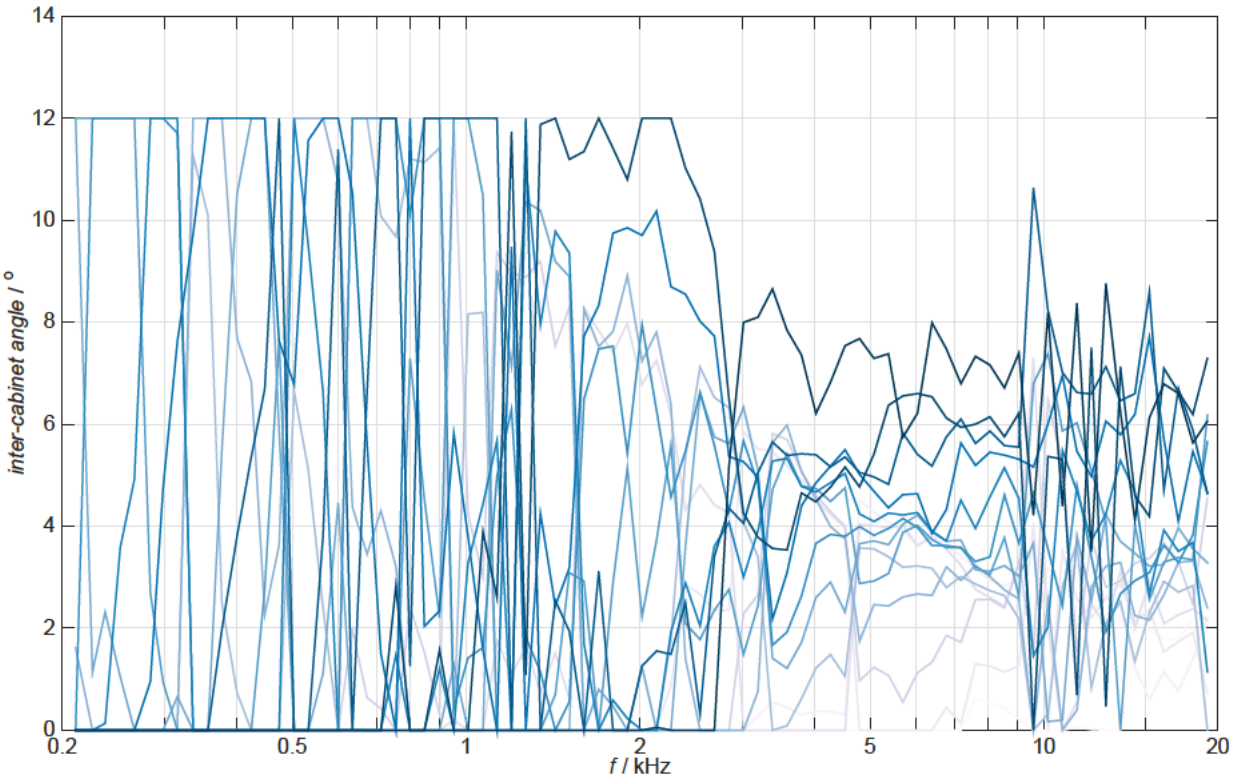

(c)

Figure 29: Tilt angles for all frequency bands when optimising with goal values (a), (b) 20 / 0.1 and (c) 22 / 0.1 for venue 4.

Three frequency bands centred around 0.5, 1 and 4 kHz are chosen as references for further evaluating the performance of the goal attainment method in venue 4. The resulting sets of tilt angles from the optimisation carried out for each single reference frequency are used to obtain the quality measures throughout the whole frequency range, and are then compared to the quality measures obtained using the PALC algorithm.

Regarding the sound field homogeneity, Fig. 30a shows how for 0.5, 1 and 4 kHz a deterioration is observed for all frequencies higher than 0.65, 1.3 and 6 kHz respectively. As the difference between goal values increases, so does the deterioration of the sound field homogeneity, which extends down to 0.55, 1.2 and 5 kHz for the goal values 20/0.1 (Fig. 30c) and down to 0.5, 1.1 and 4.5 kHz for the goal values 22/0.1 (Fig. 30e). On the other hand, Fig. 30b, 30d and 30f show how following the principle of non-inferiority, there are notable improvements observed in the acoustic contrast: for the goal values 17/0.1 (Fig. 30b) the goal attainment method yields better results for all frequencies over 350 and 900 Hz when optimising for 0.5 and 1 kHz, whereas for the 4 kHz reference frequency it is mostly deteriorated except for frequencies higher than 10.5 kHz. For the other two goal value combinations, 20/0.1 and 22/0.1 (Fig. 30d and 30f), the results are outstanding, yielding a much better acoustic contrast throughout the whole frequency range except when optimising for the 4 kHz reference frequency and goal values 20/0.1, where a slight deterioration takes place in frequencies lower than 3.5 kHz.

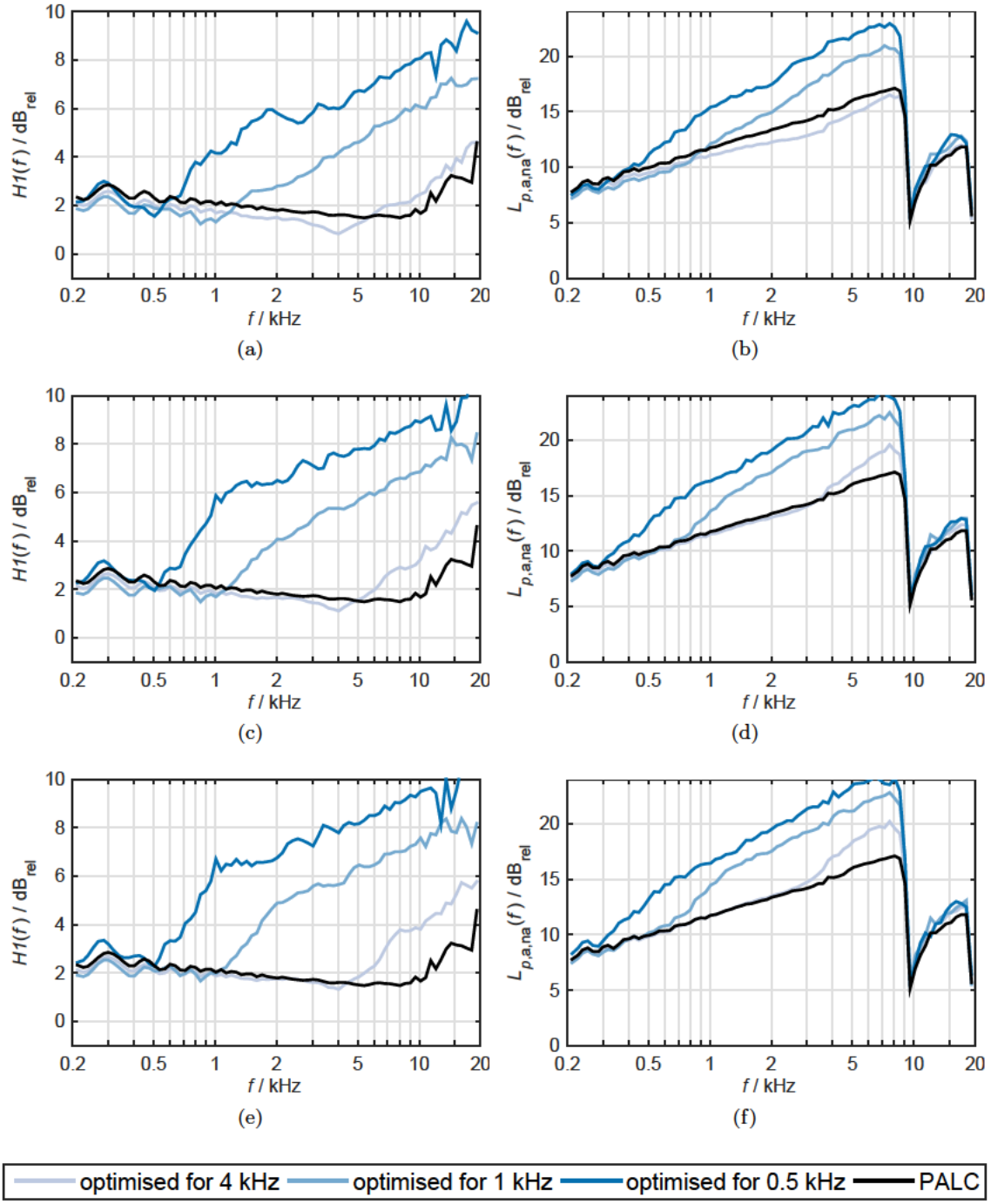

Figure 30: Technical quality measures $H1$ (left column) and $L_{p,\mathrm{a,na}}$ (right column) for goal values 17/0.1 (a) (b), 20/0.1 (c) (d), and 22/0.1 (e) (f) in venue 4.

5 Conclusion

In this thesis, an existing analytical optimisation algorithm (PALC) was adapted for commercially available LSA systems by means of the discretisation of tilt angles resulting from said algorithm. In order to do this, a research into several state of the art LSA systems was carried out, followed by a selection of four LSA systems chosen for the diversity in their sets of available tilt angles. Following the discretisation of the PALC algorithm, a numerical optimisation based on the goal attainment method was applied to the resulting tilt angles.

The results of both the discretised PALC algorithm and the multi objective optimisation based on the goal attainment method were evaluated with the help of two technical quality measures, namely sound field homogeneity and acoustic contrast between audience and non audience zones.

5.1 Discretisation of the inter-cabinet angles

After adapting the resulting tilt angles from the PALC algorithm to the four selected LSA systems with the use of three different rounding methods, and evaluating the results in terms of sound field homogeneity and acoustic contrast between audience and non audience zones in four venues with different grades of geometric complexity using four different LSA systems, there have been cases found which provide more optimal results than others. Let us first analyse the results looking at each venue individually.

VENUE 1

The rounding method "round" provides the most homogeneous sound field and works especially well with the Alcons LR28 system and with the Yamaha NEXO STM system at high frequencies. The "floor" rounding method provides the highest acoustic contrast between audience and non-audience zones and works especially well with the Meyer LYON, and with the Yamaha NEXO STM at high frequencies.

VENUE 2

The rounding method "floor" provides the most homogeneous sound field and the highest acoustic contrast between audience and non-audience zones, working especially well with the Alcons LR28 system.

VENUE 3

The rounding method "floor" provides the most homogeneous sound field and the highest acoustic contrast between audience and non-audience zones, working especially well with the Yamaha NEXO STM system.

VENUE 4

The rounding method "ceil" provides the most homogeneous sound field and works especially well with the Alcons LR28. The highest acoustic contrast between audience and non-audience zones is achieved by the "round" method, which works especially well with the Martin Audio MLA system.

In terms of sound field homogeneity and acoustic contrast between audience and non-audience zones, the "floor" rounding method provides the best general results, outperforming the other two rounding methods for the highest number of venue and LSA system combinations.

Some conclusions can be made from this information:

- The PALC algorithm has been adapted to be used with any commercially available LSA system and tested in four venues with different geometries.
- There is no combination of rounding method and LSA system that works exceptionally well for all the four proposed venues, i.e. no all-around solution to the acoustic irradiation of large audience surfaces using the discretised PALC algorithm presented in this thesis was found, but only tailored solutions for every combination of venue, LSA system and rounding method. However, the "floor" rounding method has shown to deliver good results more often than the other two rounding methods.
- In some cases, the discretised PALC algorithm outperforms the original non-discretised algorithm in terms of sound field homogeneity and acoustical contrast between audience and non-audience zones.

5.2 Optimisation of the curving of LSAs by means of the goal attainment method

After applying the multi objective goal-attainment method for the optimisation of the geometry of LSA systems, i.e. cabinet tilt angles, and evaluating the results in terms of sound field homogeneity and acoustic contrast between audience and non audience zones in four venues with different grades of geometric complexity, several conclusions can be drawn from the obtained results. A conclusion focusing on each one of the venues is in order:

VENUE 1

Initially, the results of the optimisation over the whole frequency range for three combinations of goal values in venue 1 demonstrate the concept of non-inferiority, i.e. any further improvement in one of the quality measures is accompanied by a proportional degradation of the other. In this case, for every goal value combination used, the optimisation improves the acoustic contrast between audience and non audience zones, but degrades the homogeneity of the sound field in equal measure.

After obtaining three sets of tilt angles from optimising the system for three different reference frequencies, and then obtaining the quality measures when using these sets of tilt angles, very similar conclusions are drawn as with the optimisation over the whole frequency range: when the optimisation is focused on middle/low frequencies, i.e. 0.5 and 1 kHz, the acoustic contrast is improved, while the sound field homogeneity notably degraded. When using the tilt angles obtained from the optimisation at 4 kHz, the acoustic contrast shows a slight degradation. On the other hand, in this case the sound field homogeneity shows a slight improvement for frequencies lower than 8 kHz, but again a degradation on higher frequencies. The results obtained when optimising for the reference frequency 4 kHz are thus the best available for this venue, since the sacrifice on acoustic contrast is smaller than the improvement of the sound field homogeneity, although the latter does not apply to the whole frequency range.

VENUE 2

The results of the optimisation over the whole frequency range show how for the goal values 17/0.1, a very slight degradation of the acoustic contrast takes place, while the sound field homogeneity improves for frequencies up to 5 kHz and slightly deteriorates thereafter.

When optimising for the three reference frequencies, two cases stand out: the first is the goal value combination 20/0.1 and reference frequency 9 kHz, where results show

an improved sound field homogeneity over all frequencies while the degradation of the acoustic contrast does not exceed 2 dB on its most extreme point. The second case is for the goal values 22/01 and reference frequency 5.4 kHz, where the improvement of the sound field homogeneity is less prominent and takes place in frequencies below 7.5 kHz, while higher frequencies are deteriorated. The acoustic contrast on the other hand experiences a hardly noticeable deterioration.

VENUE 3

The results of the optimisation over the whole frequency range in venue 3, which is characterised by the simplest geometry of all venues, are quite unremarkable. Only when using the goal values 17/0.1 is there an improvement of the sound field homogeneity, this taking place only for frequencies below 1 kHz, against a greater degradation of the acoustic contrast in comparison.

When optimising for the three reference frequencies, two cases stand out once again: the first is the goal value combination 20/0.1 and reference frequency 6 kHz, where results show a considerably improved sound field homogeneity over all frequencies while the degradation of the acoustic contrast is hardly noticeable. The second case is the goal value combination 22/0.1 and reference frequency 9 kHz, where the improvement of the sound field homogeneity is less prominent and takes place in frequencies below 12 kHz, while higher frequencies are deteriorated, but is accompanied by a slight improvement of the acoustic contrast. This is the only case found where both quality measures experience a general improvement in comparison to the PALC algorithm, partly caused by the simple geometry of the venue.

VENUE 4

The results of the optimisation over the whole frequency range in venue 4 show a degradation of the sound field homogeneity of various levels, accompanied by lesser improvements on the acoustic contrast.

Regarding the optimisation for the three reference frequencies, a clear improvement of the acoustic contrast is observed in most of the cases against a major degradation of the sound field homogeneity. Only when using the goal values 17/0.1 and reference frequency 4 kHz is an improvement of the sound field homogeneity observed, although limited to frequencies below 5.5 kHz, and is accompanied by a deterioration of the acoustic contrast of about 1 dB between 1 and 6 kHz.

Some general conclusions can be drawn when observing the results as a whole:

- As observed in the graphs of the multiple sets of inter-cabinet angles resulting from carrying out the optimisation for each frequency band individually, the values of the resulting angles are very different from one frequency band to the next. The fact that the optimal angles for one frequency band drastically differ from the optimal angles for the next frequency band makes the task of finding an acceptable result for all frequencies complicated. As observed when evaluating the results, the inter cabinet angles remain relatively constant between 4 and 9 kHz in all cases; this was an influencing factor when choosing the reference frequencies for the optimisation in each venue.

- It was only possible to improve both sound field homogeneity and acoustic contrast between audience and non audience zones, if only slightly, in the venue with the most simple geometry. On the other hand, it has been proven how easily achievable it is to drastically improve one quality measure at the cost of degrading the other. This is useful when one of the two quality measures has a higher priority than the other. For example, when taking into account strict noise

regulations in surrounding areas it is possible to increase the acoustic contrast considerably. On the other hand, in the case of a more permissive noise regulation, it is possible to increase the sound field homogeneity considerably.

- The computing time necessary to carry out each optimisation procedure with the equipment available is extremely high compared to other optimisation methods, i.e. the PALC algorithm. This plays an important role when evaluating the feasibility of the method used and the results obtained by these optimisation procedures, not to mention when contemplating the possibility of making such an optimisation tool commercially available.

5.3 Outlook and future research

Regarding the modification of the PALC algorithm, one significant improvement would be to attain a constant SPL throughout the audience line with a predefined tolerance. Another way to make the algorithm more reliable would be to take environmental factors into account, i.e. measuring air temperature, humidity and especially wind speed and direction, and use this data to correct the sound field in real time.

Getting the multi objective optimisation procedure to perform more efficiently, if possible, is paramount to all further research using it. Setting aside the long computing time needed for each optimisation procedure, the goal attainment method itself has turned out to not be very efficient for problems like the one addressed in this thesis, i.e. dealing with complex goals with a high number of interdependent variables.

Aiming at a practical use for this research, the next logical step is to apply the same method of tilt angle discretisation used on the PALC algorithm to the inter cabinet angles obtained by the multi objective optimisation in order to evaluate which method would deliver the best results when applied to commercially available LSA systems.

The fact that the enclosure of each LSA cabinet usually contains three kinds of drivers dedicated to the low, middle and high frequency band respectively is another factor that makes the optimisation of the sound field throughout the whole frequency range so complicated, since each frequency band propagates differently. Therefore, it would be possible to design a LSA system in which not only one set of tilt angles, but different sets of tilt angles for each frequency band were possible, thus making the control of the user over the sound field much more precise.

6 Appendix

6.1 Venue slice coordinates

Table 3: Venue 1

m	$x_m/(\mathrm{m})$	$y_m/(m)$
1	0	-11
15	7	-11
101	50	-11
122	58.15	-4.38
131	58.15	0.12
152	66.3	6.74
165	66.3	13.24
297	0.3	13.24

Table 4: Venue 2

m	$x_m/(\mathrm{m})$	$y_m/(\mathrm{m})$
1	0	-15
21	10	-15
41	20	-15
84	40.5	-7.83
89	40.5	-5.5
121	55.5	-0.33
127	55.5	3
211	93.45	20.5
397	0	20.5

Table 5: Venue 3

m	$x_m/(\mathrm{m})$	$y_m/(\mathrm{m})$
1	0	-10
21	10	-10
62	30.44	-8.47
231	110.04	19.89
246	110.04	27.39
466	0.04	27.39

Table 6: Venue 4

m	$x_m/(\mathrm{m})$	$y_m/(\mathrm{m})$
1	0	-10
21	10	-10
181	90	-10
222	90	10.5
402	0	10.5

Selected slice coordinates for the venues from Fig. 3.

6.2 Tilt angles

LSA cabinet	MLA round	ALCONS round	LYON round	NEXO round
1	-2.45	-2.45	-2.44	-2.45
2	2	1.5	1.5	1.2
3	1	1.5	2	2.5
4	2	2.4	1.5	1.2
5	2	1.5	1.5	1.2
6	1	1.5	2	2.5
7	2	1.5	2	1.2
8	2	2.4	1.5	2.5
9	2	1.5	2	1.2
10	2	2.4	2	2.5
11	3	2.4	3	2.5
12	3	3.8	3	2.5
13	4	3.8	4	5
14	4	3.8	4	5
15	6	6	7	5
16	7	6	7	7

Table 7: Inter-cabinet angles resulting from the discretisation of the PALC algorithm with the "round" rounding type for the different LSA models (MLA, ALCONS LR28, LYON and NEXO STM) in venue 1. The first angle is the tilt angle of the first cabinet and the following angles are the differences between the previous and the current cabinet angle.

LSA cabinet	MLA floor	ALCONS floor	LYON floor	NEXO floor
1	-2.46	-2.53	-2.46	-2.47
2	1	0.95	1.5	1.2
3	2	1.5	1.5	1.2
4	1	1.5	1.5	1.2
5	2	1.5	2	2.5
6	2	1.5	1.5	1.2
7	2	1.5	2	2.5
8	1	2.4	1.5	1.2
9	2	1.5	2	2.5
10	2	2.4	2	1.2
11	3	2.4	2	2.5
12	3	3.8	3	2.5
13	4	3.8	4	5
14	5	6	5	5
15	6	6	5	5
16	7	6	7	7

Table 8: Inter-cabinet angles resulting from the discretisation of the PALC algorithm with the “floor" rounding type for the different LSA models (MLA, ALCONS LR28, LYON and NEXO STM) in venue 1. The first angle is the tilt angle of the first cabinet and the following angles are the differences between the previous and the current cabinet angle.

LSA cabinet	MLA ceil	ALCONS ceil	LYON ceil	NEXO ceil
1	-2.43	-2.43	-2.43	-2.42
2	2	2.4	2	2.5
3	2	0.95	1.5	1.2
4	2	2.4	2	2.5
5	1	1.5	1.5	1.2
6	2	1.5	2	2.5
7	2	2.4	1.5	1.2
8	2	1.5	2	2.5
9	2	2.4	2	1.2
10	2	1.5	2	2.5
11	2	3.8	3	2.5
12	3	2.4	3	2.5
13	4	3.8	4	5
14	5	6	5	5
15	6	3.8	5	5
16	7	6	7	7

Table 9: Inter-cabinet angles resulting from the discretisation of the PALC algorithm with the “ceil" rounding type for the different LSA models (MLA, ALCONS LR28, LYON and NEXO STM) in venue 1. The first angle is the tilt angle of the first cabinet and the following angles are the differences between the previous and the current cabinet angle.

LSA cabinet	MLA round	ALCONS round	LYON round	NEXO round
1	-9.9	-9.9	-9.9	-9.9
2	2	1.5	1.5	1.2
3	1	2.4	2	2.5
4	3	1.5	2	1.2
5	2	2.4	2	2.5
6	2	2.4	3	2.5
7	3	2.4	2	2.5
8	3	3.8	4	2.5
9	3	2.4	3	5
10	4	3.8	3	2.5
11	4	3.8	4	5
12	4	3.8	5	2.5
13	5	6	4	5
14	5	3.8	5	7
15	6	6	7	5
16	7.5	6	7	7

Table 10: Inter-cabinet angles resulting from the discretisation of the PALC algorithm with the "round" rounding type for the different LSA models (MLA, ALCONS LR28, LYON and NEXO STM) in venue 2. The first angle is the tilt angle of the first cabinet and the following angles are the differences between the previous and the current cabinet angle.

LSA cabinet	MLA round	ALCONS round	LYON round	NEXO round
1	-9.9	-9.9	-9.9	-9.9
2	1	1.5	1.5	1.2
3	2	1.5	1.5	1.2
4	2	2.4	2	2.5
5	2	1.5	2	2.5
6	3	2.4	3	2.5
7	3	2.4	2	2.5
8	3	3.8	3	2.5
9	3	2.4	4	2.5
10	3	3.8	3	5
11	4	3.8	4	2.5
12	5	3.8	4	5
13	4	3.8	5	5
14	6	6	5	5
15	6	6	7	7
16	6	6	7	7

Table 11: Inter-cabinet angles resulting from the discretisation of the PALC algorithm with the "floor" rounding type for the different LSA models (MLA, ALCONS LR28, LYON and NEXO STM) in venue 2. The first angle is the tilt angle of the first cabinet and the following angles are the differences between the previous and the current cabinet angle.

LSA cabinet	MLA round	ALCONS round	LYON round	NEXO round
1	-9.9	-9.9	-9.9	-9.9
2	2	2.4	2	2.5
3	2	1.5	1.5	1.2
4	2	2.4	3	2.5
5	2	2.4	1.5	2.5
6	3	2.4	3	2.5
7	2	2.4	2	2.5
8	3	3.8	3	2.5
9	4	2.4	4	5
10	3	3.8	3	2.5
11	4	3.8	4	5
12	5	6	4	2.5
13	4	3.8	5	5
14	6	6	7	5
15	6	6	5	7
16	7.5	6	7	7

Table 12: Inter-cabinet angles resulting from the discretisation of the PALC algorithm with the "ceil" rounding type for the different LSA models (MLA, ALCONS LR28, LYON and NEXO STM) in venue 2. The first angle is the tilt angle of the first cabinet and the following angles are the differences between the previous and the current cabinet angle.

LSA cabinet	MLA round	ALCONS round	LYON round	NEXO round
1	-8.25	-8.25	-8.24	-8.24
2	1	0.95	1	1.2
3	1	0.95	1	1.2
4	1	1.5	1.5	1.2
5	2	1.5	1	1.2
6	1	1.5	2	1.2
7	2	1.5	1.5	2.5
8	2	1.5	2	1.2
9	2	2.4	2	2.5
10	2	2.4	2	2.5
11	3	2.4	3	2.5
12	3	2.4	3	2.5
13	3	3.8	3	2.5
14	4	3.8	4	5
15	5	6	5	5
16	6	6	7	7

Table 13: Inter-cabinet angles resulting from the discretisation of the PALC algorithm with the "round" rounding type for the different LSA models (MLA, ALCONS LR28, LYON and NEXO STM) in venue 3. The first angle is the tilt angle of the first cabinet and the following angles are the differences between the previous and the current cabinet angle.

LSA cabinet	MLA round	ALCONS round	LYON round	NEXO round
1	-8.25	-8.25	-8.25	-8.26
2	0.5	0.95	0.5	0.5
3	1	0.95	1.5	1.2
4	1	0.95	1	1.2
5	2	1.5	1.5	1.2
6	2	1.5	1.5	1.2
7	1	1.5	1.5	2.5
8	3	1.5	2	1.2
9	2	2.4	2	2.5
10	3	2.4	2	2.5
11	3	2.4	3	2.5
12	4	2.4	3	2.5
13	5	3.8	3	2.5
14	5	3.8	4	5
15	3	6	5	5
16	3	6	7	7

Table 14: Inter-cabinet angles resulting from the discretisation of the PALC algorithm with the "floor" rounding type for the different LSA models (MLA, ALCONS LR28, LYON and NEXO STM) in venue 3. The first angle is the tilt angle of the first cabinet and the following angles are the differences between the previous and the current cabinet angle.

LSA cabinet	MLA round	ALCONS round	LYON round	NEXO round
1	-8.22	-8.23	-8.23	-8.23
2	2	1.5	1.5	1.2
3	0.5	0.95	1	1.2
4	1	0.95	1	1.2
5	2	1.5	1.5	2.5
6	1	1.5	1.5	0.2
7	2	2.4	1.5	2.5
8	2	1.5	2	1.2
9	2	2.4	3	2.5
10	2	2.4	1.5	2.5
11	3	2.4	3	2.5
12	3	3.8	3	2.5
13	3	2.4	3	5
14	4	3.8	4	2.5
15	5	6	7	5
16	7.5	6	5	7

Table 15: Inter-cabinet angles resulting from the discretisation of the PALC algorithm with the "ceil" rounding type for the different LSA models (MLA, ALCONS LR28, LYON and NEXO STM) in venue 3. The first angle is the tilt angle of the first cabinet and the following angles are the differences between the previous and the current cabinet angle.

LSA cabinet	MLA round	ALCONS round	LYON round	NEXO round
1	8.5	8.5	8.5	8.5
2	0.5	0.6	0.5	0.5
3	0.5	0.6	1	0.5
4	1	0.6	0.5	1.2
5	1	0.95	1	0.5
6	0.5	0.95	0.5	1.2
7	1	0.95	1	0.5
8	1	0.95	1.5	1.2
9	2	1.5	1	1.2
10	1	0.95	1.5	1.2
11	1	1.5	1.5	2.5
12	2	2.4	2	1.2
13	2	1.5	2	2.5
14	3	2.4	2	1.2
15	2	2.4	3	2.5
16	3	3.8	3	2.5

Table 16: Inter-cabinet angles resulting from the discretisation of the PALC algorithm with the "round" rounding type for the different LSA models (MLA, ALCONS LR28, LYON and NEXO STM) in venue 4. The first angle is the tilt angle of the first cabinet and the following angles are the differences between the previous and the current cabinet angle.

LSA cabinet	MLA round	ALCONS round	LYON round	NEXO round
1	8.5	8.5	8.5	8.5
2	0.5	0.38	0.5	0.5
3	0.5	0.6	0.5	0.5
4	0.5	0.95	0.5	0.5
5	1	0.6	1	0.5
6	1	0.95	1	1.2
7	1	0.95	1	1.2
8	1	0.95	1	1.2
9	1	1.5	1.5	0.5
10	1	0.95	1	1.2
11	2	1.5	1.5	1.2
12	2	1.5	2	2.5
13	2	2.4	2	2.5
14	2	2.4	2	1.2
15	3	2.4	3	2.5
16	3	3.8	3	2.5

Table 17: Inter-cabinet angles resulting from the discretisation of the PALC algorithm with the "floor" rounding type for the different LSA models (MLA, ALCONS LR28, LYON and NEXO STM) in venue 4. The first angle is the tilt angle of the first cabinet and the following angles are the differences between the previous and the current cabinet angle.

LSA cabinet	MLA round	ALCONS round	LYON round	NEXO round
1	8.5	8.5	8.5	8.5
2	1	0.95	1	1.2
3	0.5	0.38	0.5	0.2
4	0.5	0.95	1	1.2
5	1	0.6	0.5	0.2
6	1	0.95	1	1.2
7	1	0.95	1	1.2
8	1	1.5	1.5	1.2
9	1	0.95	1.5	1.2
10	2	1.5	1.5	1.2
11	1	1.5	2	1.2
12	2	2.4	3	2.5
13	2	1.5	2	2.5
14	3	2.4	3	1.2
15	2	2.4	1	5
16	4	3.8	1	0.5

Table 18: Inter-cabinet angles resulting from the discretisation of the PALC algorithm with the "ceil" rounding type for the different LSA models (MLA, ALCONS LR28, LYON and NEXO STM) in venue 4. The first angle is the tilt angle of the first cabinet and the following angles are the differences between the previous and the current cabinet angle.

Bibliography

Audet, C. and Dennis, J. (2000): "Analysis of generalised pattern searches." TR00-07 Department of Computational and Applied Mathematics, Rice University, Houston TX.

Avalos, J.; Sanchez, J.;Velazquez, J. (2011): "Applications of Adaptive Filtering", National Polytechnic Institute, Mexico, Intech, ISBN: 978-953-307-306-4.

Bai, M.R.; Wen, J.C.; Hsu, H.; Hua, Y.H.; Hsieh, Y.H. (2014): "Investigation on the reproduction performance versus acoustic contrast control in sound field synthesis." In: *J. Acoust. Soc. Am.*, 136(4):1591-1600.

CAPS Aiming Software, HK Audio. URL http://hkaudio.com [20.05.2017].

Choi, J.W.; Kim, Y.H. (2002): "Generation of an acoustically bright zone with an illuminated region using multiple sources." In: *J. Acoust. Soc. Am.*, 111(4):1695-1700.

Coleman, P.; Jackson, P.J.B.; Olik, M.; Møller, M.; Olsen, M.; Pedersen, J.A. (2014a): "Acoustic contrast, planarity and robustness of sound zone methods using a circular loudspeaker array." In: *J. Acoust. Soc. Am.*, 135(4):1929-1940.

Coleman, P.; Jackson, P.J.B.; Olik, M.; Pedersen, J.A. (2014b): "Personal audio with a planar bright zone." In: *J. Acoust. Soc. Am.*, 136(4):1725-1735.

Dennis, J.E. and Virginia, J. (1994): "Derivative-free pattern search methods for multidisciplinary problems." American Institute of Aeronautics and Astronautics, pages 922-932.

EASE Software, Acoustic Design Ahnert. URL http://afmg.eu [20.05.2017].

Feistel, S.; Sempf, M.; Köhler, K.; Schmalle, H. (2013): "Adapting loudspeaker array radiation to the venue using numerical optimization of FIR filters." In: *135th Audio Eng. Soc. Convention, New York.*

Feistel, S.; Thompson, A.; Ahnert, W. (2009): "Methods and limitations of line source simulation." In: *J. Audio Eng. Soc., 57(6):379-402.*

Forsythe, K.; Burlingame, G.; Rutkin, A.; Lacas, M. (1994): "New Approaches to Loudspeaker System Control", pp. 58-63. In *Proc. of the AES 13th International Conference.*

G.W.J. van Beuningen, E.W. Start. (2000): "Optimizing directivity properties of DSP controlled loudspeaker arrays." In: *Reproduced Sound 16.*

Gembicki F.W.; Haimes, Y.Y. (1975): "Approach to performance and sensitivity multiobjective optimization: the goal attainment method."

Keele, D.B. (2000): "The Application of Broadband Constant Beamwidth Transducer (CBT) Theory to Loudspeaker Arrays." In: *109th Audio Eng. Soc. Convention, Los Angeles.*

Keele, D.B. (2002): "Implementation of Straight-Line and Flat-Panel Constant Beamwidth Transducer (CBT) Loudspeaker Arrays Using Signal Delays." In: *113th Audio Eng. Soc. Convention, Los Angeles, #5653.*

Meyer, D. (1983): "Digital Control of Loudspeaker Array Directivity." In: *74th Audio Eng. Soc. Convention, New York.*

Meyer, D.G. (1984): "Computer simulation of loudspeaker directivity." In: *J. Audio Eng. Soc., 32(5):294-315.*

Meyer, P.; Schwenke, R. (2003): "Comparison of the directional point source model and BEM model for arrayed loudspeakers." In: *Proc. of the Inst. of Acoustics, 25(4).*

Olver, F.W.J.; Lozier, D.W.; Boisvert, R.F.; Clark, C.W. (2010): "NIST Handbook of Mathematical Functions." Cambridge University Press, 1. ed.

Scheirman, D. (2015): "Large-scale loudspeaker arrays: past, present and future (part two: electroacoustic considerations)." In: *59th Audio Eng. Soc. International Conference, Montreal.*

Schultz, F. (2016): "Sound Field Synthesis for Line Source Array Applications in Large-Scale Sound Reinforcement." Ph.D. thesis, University of Rostock.

Skudrzyk, E. (1971): "The Foundations of Acoustics." New York: Springer.

Straube, F.; Schultz, F.; Albanés Bonillo, D.; Weinzierl, S. (2017): "An analytical approach for optimising the curving of line source arrays." In: *142nd Audio Eng. Soc. Convention, May 2017, Berlin.*

Straube, F.; Schultz, F.; Weinzierl, S. (2015a): "On the effect of spatial discretization of curved Line Source Arrays." In: *Fortschritte der Akustik: Tagungsband d. 41. DAGA, Nuernberg, 459-462.*

Straube, F.; Schultz, F.; Makarski, M.; Spors, S.; Weinzierl, S. (2015b): "Evaluation strategies for the optimization of Line Source Arrays." In: *Proc. of the 59th Audio Eng. Soc. Int. Conf. on Sound Reinforcement, Montreal.*

Thompson, A. (2006): "Line array splay angle optimisation." In: *Proc. Of the Institue of Acoustics, 28 (8).*

Thompson, A. (2008): "Real world line array optimisation." In: *Proc. of the Institute of Acoustics, 30(6).*

Thompson, A. (2009): "Improved Methods for Controlling Touring Loudspeaker Arrays." In: *127th Audio Eng. Soc. Convention, Oct 2009.*

Thompson, A.; Baird, J.; Webb, B. (2011): "Numerically optimised touring loudspeaker arrays - Practical applications." In: *Proc. of the 131st Audio Eng. Soc. Conv., New York, #8511.*

Urban, M.; Heil, C.; Bauman, P. (2003): "Wave- front Sculpture Technology.? In: *J. Audio Eng. Soc., 51(10):912-932.*